Driving the Ocean's Overturning: An Adjoint Sensitivity Study

by

Véronique Bugnion

Diplomierte Naturwissenschaftlerin, Swiss Federal Institute of Technology (1996)

Submitted to the Department of Earth, Atmospheric and Planetary Sciences
in partial fulfillment of the requirements for the degree of

Doctor of Philosophy

at the

MASSACHUSETTS INSTITUTE OF TECHNOLOGY

June 2001

Author .....
Department of Earth, Atmospheric and Planetary Sciences

Certified by .....
Peter H. Stone
Program in Atmospheres, Oceans and Climate
Thesis Supervisor

Accepted by .....
Ronald G. Prinn
Department Head, Department of Earth, Atmospheric and Planetary Sciences

Abstract

The focus of this thesis is the sensitivity of the strength of the meridional overturning circulation to surface forcing and mixing on climatological time scales. An adjoint model is used to gain new insights into the spatial characteristics of the sensitivity patterns.

Adjoint models provide the sensitivity of a diagnostic, often called cost function, to all model parameters in a single integration. In contrast, traditional sensitivity analyses are performed by repeated integrations of the so-called "forward" model, perturbing slightly the value of a single parameter at each integration. The results of the adjoint model allows us to calculate global maps of sensitivity. These maps provide a geographic picture of where on the ocean heat and freshwater flux, wind stress and diapycnal mixing perturbations have the greatest impact on the meridional overturning and its heat transport.

The adjoint model provides clear identification of the physical mechanisms which can influence the meridional overturning on times scales of years to decades. Boundary and equatorial Kelvin waves and equatorially trapped Rossby waves carry information around the boundaries of the basin and across the equator in less than a decade for a basin of the size of the Atlantic. Advection of buoyancy perturbations has an important influence on the meridional overturning on the decadal time scale. Diffusion is important in determining the final equilibrated state of the meridional overturning on the centennial scale.

The role of diapycnal mixing in determining the overturning's strength is confined to regions near the lateral boundaries in the Northern hemisphere and to the tropical region in both hemispheres. The important role played by the tropics in setting the overturning's strength seems to confirm the thermodynamic principles outlined by Sandström (1908), Jeffreys (1925) and Munk and Wunsch (1998): upward advection of heat is balanced by downward diffusion. The strength of the meridional overturning is then determined by the power available to return the fluid to the surface across the ocean's stratification. Because the ocean is most strongly stratified in the tropics, the mixing process is most efficient in that region. Along the eastern boundary in the extratropics, the importance of diapycnal mixing is confined to a shallow layer at the base of the thermocline. The large vertical temperature contrast between the western and deep western boundary currents induces efficient mixing in that region. Surface wind stress has two effects on the ocean's stratification which concentrate the sensitivity in the eastern equatorial region. Ekman suction increases the stratification along the equator while Ekman pumping decreases it in the rest of the tropics. The equatorial easterlies lift the thermocline on the eastern side of the basin, further increasing the stratification and the efficiency of the vertical mixing process in that region. These processes are similar in the results from a coupled model. Atmospheric feedbacks do, however, allow vertical mixing in the Pacific to play a role as important as mixing in the Atlantic in determining the overturning's strength. The large uncertainties in the global value of the diapycnal mixing in the ocean, estimated here at $\kappa_v = 3 \cdot 10^{-5} \pm 2 \cdot 10^{-5}\, m^2 s^{-1}$, translate into an uncertainty of approximately $6\, Sv$ in the maximum value of the meridional overturning streamfunction.

The role of surface buoyancy forcing on the overturning's strength depends on the formulation of the surface boundary conditions. The sensitivities are confined to high latitudes and the vicinity of convection sites when the surface forcing is prescribed as restoring the sea surface salinity or temperature towards observations. When the forcing is prescribed as a flux of heat or freshwater, advection allows buoyancy perturbations in the Atlantic basin to play an important role in determining the evolution of the meridional overturning. For annual and decadal time scales, heat flux perturbations in the North Atlantic are likely to

have the greatest impact on the meridional overturning. On climatological time scales, it is the uncertainty in the precipitation and evaporation fields in the tropics which have the greatest impact on the uncertainty in the streamfunction, the latter can be estimated at: $\psi_{MAX} = 29 \pm 4\,Sv$. Over the intermediate time scale of climate change, the overturning is likely to weaken at first because of warming and freshening in high latitudes. It will, however, eventually recover as positive salinity anomalies are advected northwards from the tropics.

The sensitivity of the overturning to the wind stress forcing is also dependent on the surface boundary conditions. Under restoring boundary conditions, large positive sensitivities are observed in the Antarctic Circumpolar Channel in a pattern reminiscent of the so-called Drake Passage effect. According to that hypothesis, upwelling of North Atlantic Deep Water takes place predominantly in a branch of the Deacon cell in the Drake Passage region. The importance of wind in the Drake Passage vanishes when the surface buoyancy fields are less tightly constrained, for example in the model forced by mixed boundary conditions or in the coupled model. The Agulhas Plateau, the Chilean coastline and the Indonesian throughflow play an important role in setting the overturning's strength in the ocean model forced by mixed boundary conditions. These "gateways" act as a regulator of the salinity of the Atlantic basin. The wind stress determines the balance between the inflow of relatively salty Indian Ocean water through the Agulhas current, the inflow of fresher Benguela current water southwest of Africa and the flow of very cold and fresh water through the Drake Passage. A wind stress perturbation of $\pm 0.03\,N\,m^{-2}$ over the Agulhas Plateau would have a significant impact on the meridional streamfunction's maximum, estimated at $\psi_{MAX} = 29 \pm 0.5\,Sv$. Both Drake Passage and gateway effects disappear almost completely in the coupled version of the model, which shows the strongest positive sensitivities to wind stress in the region of equatorial Ekman upwelling.

Our study shows that, in a climatological ocean model, the choice of air-sea boundary conditions is crucial in determining the sensitivity of the meridional overturning circulation. The climatology of the forward ocean model is credible and quite similar in all scenarios. However, including interactive atmospheric transports of heat and moisture changes the manner in which the ocean model state adjusts to changes in wind stress, heat flux and diapycnal mixing. Considering the role of both the atmosphere and the ocean when studying the climatological behavior of the MOC is, therefore, clearly important. Models which keep one of the components fixed can lead to very different conclusions from models in which both components are represented.

Thesis Supervisor: Peter H. Stone
Title: Professor

Acknowledgements

To my great-grandmother Florence for her sense of humor,
To my grandmother Perle for her sense of dedication,
To my mother Jacqueline for her love.

Without a solid sense of humor, dedication to the task at hand and the love of those around me, I don't know if I would have finished what I set out to do five years ago when I first came to MIT. This thesis is dedicated to three generations of exceptionally bright women who came before me and paved the way.

Like my great-grandmother, I like to smile at most things. Humor at MIT belongs to the students; it's how we manage to laugh at the hoops we are made to jump through. I have been very fortunate to meet some of the best, brightest and nicest people from the four corners of the world. Gerard Roe, who introduced me to MIT, then spent three years trying to convince me that warm beer was actually good; Kerim Nisancioglu and Sussie Dalvin, who every day reminded me that there is life beyond work and Jessica Neu, my favorite training partner, with whom I have shared the joy and tears of being a girl, albeit a tough one, lost in a man's world. Many thanks to my housemates Cindy Kiddoo and Jake Gebbie for allowing me to ramble on late at night on just about anything; I now know more about the brain and the art of skateboarding than I ever thought I would. Much gratitude goes to my officemates over the years, Amy Solomon, Tieh-Yong Koh, Peter Huybers and Baylor Fox-Kemper for having answers to just about anything. To my fellow "staff meteorologists" at the Tech, Greg Lawson, Rob Korty, Bill Ramstrom, it's the best title we will ever have. Thank you to Helen Johnson, Sarah Samuel and Karen Mair for reminding me of the old continent, or at least the island off the old continent, and for many great hiking, kayaking and climbing trips. Francesca Scirre-Scapuzzo and Joe Seidel, thank you for bringing a little bit of home over to Boston. To my classmates, Galen McKinley, Juan Botella, Pablo

Zurita, Yu-Han Chen, Jelena Popovic and Don Lucas for being such a fun and diverse group of people. Thank you Zan Stine and Nili Harnik for being who you are, please don't change. To my favorite skiing, sorry, telemark, buddies Peter Madden, Adam Lorenz and the rest of the 529 gang for teaching me that bruised knees really don't matter.

Without an inordinate amount of dedication, finishing a thesis would be a difficult task. My grandmother taught me from an early age the meaning of that word. I have the greatest respect for my thesis committee, Glenn Flierl, Carl Wunsch, Jochem Marotzke and John Marhsall, for their dedication to science. I am particularly indebted to John Marshall who volunteered to join my committee at the last minute and whose endless enthusiasm for science has made a lasting impression upon me. I would like to thank my advisor, Peter Stone, for his advice and generous support of my academic, and sometimes not-so-academic career; field work in the Canadian Arctic and a summer working on the world's first french windstorm bond were great breaths of fresh air. Without Jane McNabb, Mary Elliff, Maria Raposo and Gail Hickey's dedication to students, the sky would have often been less blue in the morning. I cannot thank enough Linda Meinke for her technical assistance, and for her ability to always recuperate files mistakenly sent to the wastebasket and Will Heres for many great lunchtime conversations and for always keeping the printer working. Thank you to all the people who have contributed to the ocean model and the black box called the adjoint compiler: Alistair Adcroft, Ralf Giering, Patrick Heimbach and the staff of the ECCO project at Scripps and JPL. I am indebted to Xiaoli Wang for laying the groundwork of this project and to Jeff Scott for his patience in teaching me the secrets of ocean mixing. I was very lucky to work with a very bright, but also very nice person, Chris Hill, who insisted on building the world's most complicated computer on the 17^{th} floor of the Green building; he has taught me that research can be fun. I was honored to be involved with two very creative programs. The *Technology and Policy Program* showed me that the word interdisciplinarity really does exist. My thanks go to Jake Jacoby, the heart and soul of the *Joint Program on the Science and Policy of Global Change*, for his endless enthusiasm and for being a role model to so many of us. I am grateful to Mr. "Uncertainty in global warming" - Mort Webster - for all the free lunches, Chris Forest for many interesting discussions and Andrei Sokolov for the data. David Reiner, plasma physicist turned political scientist, thank you for being a great friend, for teaching me about all matters political, and for editing footnote #233.

The love of your family is what remains in the moments when humor and dedication are not quite enough to finish the task at hand. To Andy for his near-infinite patience and wisdom, for being my favorite arctic sidekick and for not falling through the ice in Ross Bay. To my parents, Jacqueline and Jean-Robert, and my brother Edouard, for showing great interest in my work through endless newspaper articles on climate change and other energy problems, and for keeping track of all the funny symbols in my thesis. Without their encouragements, and their constant source of support, I would not be writing this today.

Contents

List of Figures

List of Tables

Chapter 1

Introduction

1.1 Heat Transport in the Atmosphere and the Oceans

Without any transport of heat from the tropics to higher latitudes by the atmosphere and the oceans, the Earth would be approximately forty degrees colder at the poles and warmer by the same amount at the Equator (North et al., 1981). The partitioning of this heat transport between the atmosphere and the ocean changes from basin to basin, between hemispheres and with seasons (Peixoto and Oort, 1992). Only the total heat transport is known accurately, the ratio of oceanic to atmospheric heat transport is poorly known. Observations indicate that neither medium contributes more than two-thirds of the overall heat transport (Peixoto and Oort, 1992). It is also poorly known how efficiently the Earth can compensate an increase in heat transport in one medium by a decrease in the other. Large variations in historical temperature records suggest that this natural compensation mechanism is, at at best, imperfect.

The atmosphere transports heat northward in baroclinically unstable disturbances, primarily in mid-latitude storms, and in stationary waves. The ocean has essentially two methods for transporting heat northward. Considering first the deviations of the flow from its basin wide average, a warm northward anomaly or a cold southward anomaly both achieve a net transport of heat to the North. This is how the wind driven subtropical gyres contribute to the world's heat balance. The basin mean circulation will transport heat towards the pole if there is a polewards warm flow near the surface and a colder equatorwards flow at greater depth. This circulation is referred to as meridional overturning circulation; it advects a large amount of heat from tropical latitudes towards the pole in the Atlantic

basin. The Atlantic ocean has the peculiar feature of transporting heat equatorwards in the Southern Hemisphere, primarily because of heat transport associated with the overturning component. The polewards transport of heat by the gyres in the Pacific and Indian oceans is, however, polewards. Overall, observations indicate that the world's oceans transport heat polewards in both hemispheres (Trenberth and Solomon, 1994; Macdonald and Wunsch, 1996).

1.2 The Stability of the Meridional Overturning Circulation

The meridional overturning circulation, often referred to as thermohaline circulation or popularly as the ocean's conveyor belt, will be the focus of much of this thesis. The heat transported by this circulation is gradually released into the atmosphere, thereby giving Western Europe its comparatively mild climate. The intense cooling of the ocean surface in the Norwegian, Greenland and Labrador Seas leads to a localized convective overturning of the water column in those regions. The pressure gradients, which are thereby generated, drive the southward movement of the North Atlantic Deep Waters.

A seminal paper by Stommel (1961) pointed out that, in a simplified two-box illustration of the meridional overturning circulation, two stable equilibria were possible. Sinking in the northern box corresponds to a thermally dominated circulation, the current situation in the Atlantic. The influence of salinity on the water's density dominates in the reverse circulation which sees sinking near the equator. Rooth (1982) revisited this issue and showed that the pole to pole density gradient can also have a significant influence on the direction and stability of the meridional overturning.

Since the work of Stommel, paleoclimate studies have pointed to disruptions of the thermohaline circulation as a possible explanation for the abrupt changes seen in the temperature records, which are reconstructed from ice and sediment cores (Broecker et al., 1985). A popular theory explains the Younger Dryas cooling event, which took place 11,000-10,000BP, by a massive discharge of icebergs from the Laurentide ice sheet. The freshening of the surface waters in the Atlantic is thought to have led to a temporary shutdown, or at least a significant weakening, of one or several of the branches that form the North Atlantic Deep Water (Keigwin et al., 1992; Lehman and Keigwin, 1992).

Numerical models of the ocean show that the meridional overturning circulation is indeed

sensitive to a large input of freshwater in the Northern North Atlantic (Bryan, 1986; Manabe and Stouffer, 1988; Marotzke and Willebrand, 1991; Rahmstorf, 1995). The simulation of climate change scenarios in coupled atmosphere-ocean general circulation models (GCMs) also show a gradually weakening circulation, attributed to enhanced northward atmospheric moisture transport in a warmer atmosphere and a subsequent freshening of the Atlantic (Manabe and Stouffer, 1994; Wood et al., 1999; Dixon et al., 1999). The dominance of changes in freshwater forcing over changes in the surface heat flux is, however, contested by the results obtained with other models (Mikolajewics and Voss, 2000; Kamenkovich et al., 2000b). Most studies have implicitly assumed that the meridional overturning's sensitivity to the surface fluxes of heat and water is geographically co-located with the sites of convection and downwelling, where the deep water is formed. The role played by the geographic distribution of the changes in forcing, the relative importance of changes in the tropics vs. high latitudes or of changes in the Atlantic vs. the Pacific are largely unknown. The role of pole to pole dynamics has received more attention. The work of Wang et al. (1999a,b), Scott et al. (1999) and Rahmstorf (1996) points to the freshwater flux in the South Atlantic as a possible regulator of the intensity of the meridional overturning circulation. The relative importance of oceanic and atmospheric transport mechanisms in determining the sensitivity of the meridional overturning circulation is also poorly known, although theoretical studies have shown that the atmosphere adds a number of positive feedback mechanisms, which tend to amplify disturbances in the overturning's strength (Nakamura et al., 1994; Marotzke, 1995). Other outstanding issues include the role played by the rate of warming on the evolution of the overturning (Stocker and Schmittner, 1997; Wood et al., 1999), and the presence of stability thresholds beyond which changes in the circulation become difficult to reverse (Rahmstorf, 1995; Zhang et al., 1999).

Past discussions have often implicitly or explicitly assumed that the mechanism responsible for controlling the intensity of the meridional overturning circulation was convective mixing and the downwelling branch of the circulation. While this may be true for short-term changes in the circulation, the energy required to return abyssal waters to the surface is thermodynamically the factor limiting the intensity of the steady-state meridional overturning circulation (Sandström, 1908; Jeffreys, 1925). A number of mechanisms have been suggested to provide this source of energy. The first focuses on vertical mixing of heat, particularly along coastal boundaries and mid-oceanic ridges, as the true driving force of

the circulation (Marotzke and Scott, 1999; Zhang et al., 1999; Huang, 1999). This mixing would realistically be the product of wind or tidally induced gravity wave breaking (Munk and Wunsch, 1998). Such small scale processes are not resolved by the coarse resolution ocean general circulation models of the type used in this thesis, which therefore parameterize mixing as a diffusive process. The second hypothesis has the Southern Oceans playing a crucial role in determining the intensity of the overturning. Because of the absence of continental barriers, there can be no net East-West pressure gradient and, therefore, no net geostrophically balanced North-South flow in the Antarctic circumpolar channel. The westerlies drive a northward Ekman drift in the near surface layers that does not need to be in geostrophic balance. To satisfy geostrophy, the return flow must take place below the depth of the topographic ridges, notably below the sill located between the southern tip of South America and Antarctica. The divergence of the Ekman transport south of the Drake Passage can thereby draw up an estimated $15\,Sv$ of deep water from below the level of the topographic ridges. This, theoretically, provides the source of energy required to convert the cold and salty North Atlantic Deep Water, which is observed below the top of topographic ridges, into fresher surface water (Toggweiler and Samuels, 1995, 1998). This Deacon cell, and its associated upwelling, is largely eliminated from the meridional overturning circulation, when the eddy induced transport velocity is added to the Eulerian mean velocity (Danabasoglu and McWilliams, 1995). This additional "bolus" velocity is linked to the Gent-McWilliams parameterization. By adding a down-gradient diffusion of the thickness between isopycnal surfaces, this parameterization produces an effect that can be expressed as an additional tracer advection.

Only a sensitivity study, which includes all the elements forcing and constraining the ocean's circulation, has the potential to determine the relative influence of freshwater, heat fluxes, dia- and isopycnal mixing, thickness diffusion and wind stress on the intensity and stability properties of the meridional overturning circulation.

1.3 Sensitivity Studies

Traditional sensitivity studies are performed by adding small perturbations to the variables or parameters presumed to be important, and comparing the perturbed integrations to the control run. This method has the advantage of giving information about the impact of

the perturbation on all model variables during the integration period, its drawback is the limit to the number of parameters or input variables that can be examined. This constraint is imposed by the necessity to run one simulation for each perturbed parameter or initial condition, and the associated large computational requirement of the method.

Adjoint methods have the advantage of providing the sensitivity of a scalar function of the model state at a given time, often called cost function in optimization problems, to all model parameters and initial conditions in a single integration of the adjoint model. The use of adjoint methods to perform sensitivity studies in climate models was pioneered by Hall & Cacuci in a sequence of papers in the early 80s (Hall et al., 1982; Hall and Cacuci, 1983; Hall, 1986). They first applied it to a radiative-convective model of the atmosphere, demonstrating that the method was successful in deriving useful sensitivities, even though that model contained complex non-linear processes of the general type found in atmospheric and oceanic GCM's, notably episodic convective adjustment. The method was then tested on a greatly simplified atmospheric GCM showing that, within the limitations imposed by computational costs, deriving sensitivities useful to the interpretation of the results of climate models was a feasible task. In spite of their computational advantage over traditional perturbation methods, sensitivity studies using adjoint methods have largely been abandoned since Hall & Cacuci's efforts, primarily because of the necessity to write manually the code of the adjoint model. This daunting task has recently been greatly simplified by the advent of adjoint compilers which use automatic differentiation methods to generate the adjoint code (Giering, 1997). More recently, Marotzke et al. (1999) used automatic differentiation to derive the adjoint model of an ocean GCM, these authors examined the sensitivity of the heat transport in the Atlantic to the temperature and salinity distribution throughout the basin one year earlier.

Because they provide information about the gradient of a diagnostic with respect to the model state, adjoint methods have been used in data assimilation problems in atmosphere and ocean GCMs (Wunsch, 1996; Talagrand, 1997). The matrix composed of these gradients allows for the solution of the minimization problem that is required to constrain the flow to best correspond to observations.

Within the uncertainty in the model parameters, adjoint methods allow a ranking of the impact of changes in various model inputs on a given cost function. The adjoint method therefore provides the tool that allows to determine which of the competing influences on the

stability and intensity of the meridional overturning circulation plays the greatest role. A quantitative comparison of the effect of perturbations in the parameters on the overturning's intensity requires the multiplication of the sensitivities obtained with the adjoint model with a perturbation in the field or parameter. While the uncertainty in fields such as wind stress is quantifiable, other fields are much less precisely known. The globally averaged value of the diapycnal mixing is, for example, unknown to a factor of three or more (Gregg, 1987). Because of the linearization, which underlies the adjoint model, the validity of the comparative analysis if furthermore limited to small perturbations in the underlying fields.

Adjoint methods are, however, no substitute for traditional perturbation methods when the objective is to determine how these parameters affect the physical characteristics of the general circulation within the ocean model.

1.4 Climate Predictability

Adjoints have also been used in ensemble forecasting by the European Center for Medium Range Weather Forecasting (ECMWF) (Mureau et al., 1993; Palmer et al., 1994; Buizza et al., 1993; Buizza and Palmer, 1995; Molteni et al., 1996). In that scheme, the "singular vectors", provide the geographic locations where disturbances are most likely to grow over the time span of the weather forecast. The operator, which maps small perturbations in the atmosphere along the weather forecast's trajectory from the initial state to a future time is known as the forward tangent propagator. Singular vectors are the product of the forward tangent propagator with its adjoint with respect to an energy norm.

The suitability of this method is, however, limited to the time scale over which the perturbation growth remains linear, approximately three to four days in the atmosphere (Molteni and Palmer, 1993; Palmer, 1993a). It is unclear whether an equivalent time scale exists for slower ocean processes. The results of Wang et al. (1999b) suggest that the evolution of the thermohaline circulation, when forced by increasing fluxes of freshwater in high latitudes, is dependent on the sequence of random wind stress fluctuations. This result would imply that there exists a limit to the predictability of the evolution of the climate system. These results have, however, not been reproduced by other coupled climate models. Reconstructions of historical temperatures from ice cores or other paleoclimate data sources do, however, show important fluctuations on a number of time scales. It is unknown which

of these variations are predictable and which are not (Palmer, 1996). Addressing these questions requires climate models, which are sufficiently simple to be integrated over long time scales. It is also important that these models parameterize the transport of tracers such as heat, moisture or salinity by turbulent eddies. This requirement is due to the difficulty in obtaining useful adjoint sensitivities beyond the limit of predictability of the behavior of the individual eddy (Lea et al., 2000; Köhl and Willebrand, 2001). The use of non eddy resolving ocean models, such as the one used in the present analysis, may, however, limit the generalization of the results to more complicated eddy resolving systems. Provided that climate models show adequate intrinsic climate variability when forced by changes in orbital parameters, solar cycles, aerosol or greenhouse forcing, the singular vector method used for ensemble forecasting by the ECMWF could be used to gauge the predictability of the response of the climate system to these various types of forcing (Palmer, 1993b, 1999).

1.5 Outline of the Thesis

Chapter 2 gives a brief overview of the dynamics of the adjoint model. This chapter is provided to familiarize the reader with the mechanisms and time scales over which information is communicated around the basin in the adjoint model. This overview will include the dynamics of adjoint Kelvin and Rossby waves, as well as advection in the adjoint space. The focus of this chapter is entirely on time dependent processes.

Chapter 3 will provide a suite of experiments in an idealized single basin setting to develop an understanding of the steady-state sensitivity patterns provided by the adjoint model. Complexity is gradually built up by focusing first on the forcing by temperature and precipitation alone, while omitting the forcing of the momentum terms by the wind stress. The effect of wind is analyzed in a second series of experiments. The role played by the formulation of the surface buoyancy forcing terms is examined in a third set of calculations, highlighting the dependency of the model's response on how the surface forcing terms are calculated. The analysis will focus on the role of mixing, surface buoyancy forcing and when appropriate, wind stress forcing on the meridional overturning circulation.

Chapter 4 briefly presents the structure and flow characteristics of the simplified coupled ocean, energy and moisture balance atmosphere model. This model will be used to analyze, in chapter 5, the sensitivity of the meridional overturning circulation to surface forcing and

mixing in a realistic geography configuration. This chapter is structured by theme, and focuses on using the adjoint model to gain insight and provide support for the theories, which seek to explain the intensity of the overturning in terms of mixing, wind stress and buoyancy forcing. This chapter also outlines how uncertainty in the heat, freshwater and momentum fluxes can be used to provide a range of uncertainty in the model's estimates of the overturning's intensity and polewards heat transport in the Atlantic basin.

Chapter 6 reviews the major results of this thesis, but also emphasizes the limitations of the adjoint method. This chapter also outlines the direction of future research.

Chapter 2

Adjoint Dynamics

2.1 Introduction

The analysis of the sensitivity of the output of a climate model integration to the model's parameters can provide valuable help in interpreting the model results. It can, for example, allow a quantitative estimate of the impact of uncertainties in these parameters on the state of the model at the end of the integration. By 'parameter' is meant here the combination of the model's initial conditions as well as the constant physical parameters, which determine the model's evolution. The sea surface temperature at the time when the integration starts is an example of an initial condition, the model's viscosity or gravity are physical parameters. Sensitivities to initial conditions will be referred to as "initial value" sensitivities, the terminology will be "parametric" sensitivity in the case of constant parameters.

Traditional sensitivity analysis is performed by repeated integrations of the ocean or coupled general circulation model model, perturbing slightly the value of a single parameter at each integration. Sensitivities are obtained by dividing the difference between the perturbed integration and the reference, unperturbed, run with the magnitude of the perturbation itself. For complex models such as the one presented in this chapter, any extensive analysis using such a procedure is computationally unfeasible because of the number of parameters involved. In practice, this means that only the few parameters judged *a priori* as being the most important can be investigated.

Adjoint methods express the response of the model as a diagnostic or *cost function* of the model variables. The system of adjoint equations, developed from a differentiated form of the original model equations, allows the computation of the sensitivity of the diagnostic

to all model parameters in a single calculation. In contrast, the traditional approach gives the sensitivity of all the model variables to a single parameter.

The terminology "forward" model will be used when referring to the numerical ocean or coupled general circulation model. The numerical code derived from the forward model, which calculates the sensitivity of the cost function to the model parameters will be referred to as "adjoint" model.

2.2 Theoretical Background

The output of an adjoint model calculation gives the sensitivity of the *cost function* to the initial conditions as well as to the model's physical parameters. The cost function can be any scalar function of the model output, as long as it remains differentiable. This can, for example, be the sea surface temperature at one geographic location, the intensity of the meridional overturning circulation at a given time or the change in the amount of heat transported by the ocean over time.

The adjoint problem is easiest to pose for discrete time intervals, $n = 0...N$, which conveniently represents time stepping in numerical oceanic and atmospheric models (see for example Talagrand (1997)). The evolution of the state vector $\mathbf{y_n}$ between time steps 0 and $n+1$ can be represented from the composition of the mapping of the state at one time step onto the next:

$$\mathbf{y_{n+1}} = \mathbf{C_n}(\mathbf{y_n}) = \mathbf{C_n} \circ \mathbf{C_{n-1}} \circ \cdots \mathbf{C_1}(\mathbf{y_0}) \tag{2.1}$$

where

$$\mathbf{y_0} = (T_0, S_0, \vec{u}_0, p_0, \rho_0, \alpha)$$

In the ocean model described later in this chapter, $\mathbf{y_n}$ is comprised of the prognostic variables: temperature (T), salinity (S) and the three-dimensional velocity vector ($\vec{u}$), the diagnostic variables pressure (p) and density (ρ) as well as the model's physical parameters (α). The variables are represented by three-dimensional arrays of the dimensions of the model grid, α is a vector of the same dimension as the number of independent parameters in the model.

The evolution of a perturbation of the state vector $\delta\mathbf{y_n}$ at time $n+1$ can be represented

as:

$$\delta \mathbf{y_{n+1}} = \mathbf{C'_n} \delta \mathbf{y_n} \tag{2.2}$$

$$\mathbf{C'_{n_{ij}}} = \frac{\partial \delta \mathbf{y_{(i;n)}}}{\partial \delta \mathbf{y_{(j;n-1)}}}$$

$\mathbf{C'}$ is often called the *linear propagator*, the index n represents time, ij are spatial indices. $\mathbf{C'}$ exists only if the mapping is differentiable. $\delta \mathbf{y_n}$ is in turn related to the initial perturbation $\delta \mathbf{y_0}$ at time $t = 0$ through the repeated application of the rules of derivation for the composition of functions:

$$\delta \mathbf{y_{n+1}} = \mathbf{C'_n} \delta \mathbf{y_n} = \mathbf{C'_n C'_{n-1}} ... \mathbf{C'_1} \delta \mathbf{y_0} = \mathbf{C'} \delta \mathbf{y_0} \tag{2.3}$$

$$\mathbf{C'_{ij}} = \frac{\partial \delta \mathbf{y_{(i;n)}}}{\partial \delta \mathbf{y_{(j;0)}}}$$

Equations 2.2 and 2.3 are a compact representation of the so-called *tangent linear* system of equations.

The gradient of the cost function, a response functional of the output state vector $J(\mathbf{y_N})$ at final time $t = N$, with respect to the model input obeys the following equation:

$$\frac{\partial J}{\partial y_{(i;0)}} = \sum_{j=1}^{r} \frac{\partial y_{(j;N)}}{\partial y_{(i;0)}} \frac{\partial J}{\partial y_{(j;N)}} \quad i = 1...q \tag{2.4}$$

or in more compact notation:

$$\nabla_{\mathbf{y_0}} J = \mathbf{C'^*_1 C'^*_2} ... \mathbf{C^*_N} \nabla_{\mathbf{y_N}} \mathbf{J} = \mathbf{C'^*} \nabla_{\mathbf{y_N}} \mathbf{J} \tag{2.5}$$

where the superscript * indicates the use of the adjoint matrix. This follows from the properties of the inner product $\langle\ ,\ \rangle$:

$$\delta J = \langle \nabla_{\mathbf{y_N}} J, \delta \mathbf{y_N} \rangle = \langle \nabla_{\mathbf{y_N}} J, \mathbf{C'} \delta \mathbf{y_0} \rangle = \left\langle \mathbf{C'^*} \nabla_{\mathbf{y_N}} \mathbf{J}, \delta \mathbf{y_0} \right\rangle = \langle \nabla_{\mathbf{y_0}} J, \delta \mathbf{y_0} \rangle \tag{2.6}$$

Equation 2.5 illustrates the fact that the adjoint model is integrated backwards in time: $\nabla_{\mathbf{y_N}} J$ is calculated first before being multiplied with $\mathbf{C^*_N}$, $\mathbf{C^*_{N-1}}$ back to $\mathbf{C^*_1}$.

The adjoint concept can be generalized to any time step, $\nabla_{\mathbf{y_n}} J$ gives the sensitivity of the cost function to a perturbation of the state variables or parameters applied on day n and maintained until day N.

The system of adjoint equations can be derived independently of any cost function. The cost function J allows to relate the variations in the initial state or in model parameters to the corresponding variations in a diagnostic, which has interesting physical properties.

The system of adjoint equations in the continuous time domain will be derived on a case by case basis for the examples chosen to illustrate the model's adjoint dynamics later in this chapter. The reader is referred to Morse and Feshbach (1953), Lanczos (1961) and Hall et al. (1982) for a derivation of the general principles of adjoint construction.

2.3 Implementation

The automatic derivation of the adjoint of the ocean model is performed by the Tangent Linear and Adjoint Model Compiler (TAMC) (Giering, 1997). A detailed description of the construction of the adjoint code as well as an example of its implementation can be found in Marotzke et al. (1999). Three approaches can be used to derive adjoint code. In the terminology of Sirkes and Tziperman (1997) the "adjoint of finite difference" approach derives the adjoint equations directly from the finite-difference equations of the forward model. The "finite difference of adjoint" approach derives the adjoint equations to the linearized continuous model, and subsequently determines an appropriate finite-difference formulation. The approach used by the TAMC is to derive the adjoint of the numerical code itself. Numerical stability issues related to discretization of the adjoint equations set aside, all approaches should give the same result.

No stability problems related to the discretization of the equations in the adjoint model were noticed during this analysis. This is due to the fact that the Adams-Bashford time stepping scheme used by the forward model has no computational mode, and none can therefore exist in the adjoint model. The issues related to the discretization of adjoint equations mentioned by Sirkes and Tziperman (1997) were related to the use of the Leapfrog scheme, which has a computational mode that needs to be damped in both the forward and the adjoint model.

The procedure used by the TAMC is to perform first an integration of the *forward* model

while storing the variables required by the adjoint model to calculate the derivative terms. The latter model makes use of this information while working its way backward in time and calculating the derivatives according to equation 2.5.

The following one-dimensional advection problem illustrates the methodology. The temperature at point A is specified and grows by 1 at each time step, it is advected by a specified flow velocity to point B.

$$T_A(i+1) = T_A(i) + 1 \tag{2.7}$$

$$T_B(i+1) = T_B(i) + \frac{u\Delta t}{\Delta x}(T_A(i) - T_B(i)) \tag{2.8}$$

The model state is described by $\mathbf{y}= (T_A, T_B, u, \Delta t, \Delta x)$, while the initial conditions and model parameters are: $\mathbf{y_0}= (T_A(0), T_B(0), u, \Delta t, \Delta x)$.

If the cost function is defined as:

$$J = T_B^2(N) \tag{2.9}$$

the adjoint model answers the question of how J depends on $\mathbf{y_0}$. For two time steps:

$$\nabla_{\mathbf{y_0}} J = \mathbf{C_1'}^* \mathbf{C_2'}^* \nabla_{\mathbf{y_2}} J \tag{2.10}$$

If the initial state is described by $\mathbf{y_0}= (1.5, 1, 1, 1, 2)$, the model is solved by calculating:

$$\begin{pmatrix} \frac{\partial J}{\partial T_A(0)} \\ \frac{\partial J}{\partial T_B(0)} \\ \frac{\partial J}{\partial u} \\ \frac{\partial J}{\partial \Delta t} \\ \frac{\partial J}{\partial \Delta x} \end{pmatrix} =$$

$$\begin{bmatrix} 1 & \frac{u\Delta t}{\Delta x} & 0 & 0 & 0 \\ 0 & 1 - \frac{u\Delta t}{\Delta x} & 0 & 0 & 0 \\ 0 & \frac{\Delta t}{\Delta x}(T_A(0) - T_B(0)) & 1 & 0 & 0 \\ 0 & \frac{u}{\Delta x}(T_A(0) - T_B(0)) & 0 & 1 & 0 \\ 0 & -\frac{u\Delta t}{\Delta x^2}(T_A(0) - T_B(0)) & 0 & 0 & 1 \end{bmatrix} \cdot \begin{bmatrix} 1 & \frac{u\Delta t}{\Delta x} & 0 & 0 & 0 \\ 0 & 1 - \frac{u\Delta t}{\Delta x} & 0 & 0 & 0 \\ 0 & \frac{\Delta t}{\Delta x}(T_A(1) - T_B(1)) & 1 & 0 & 0 \\ 0 & \frac{u}{\Delta x}(T_A(1) - T_B(1)) & 0 & 1 & 0 \\ 0 & -\frac{u\Delta t}{\Delta x^2}(T_A(1) - T_B(1)) & 0 & 0 & 1 \end{bmatrix} \begin{pmatrix} 0 \\ 2T_B(2) \\ 0 \\ 0 \\ 0 \end{pmatrix} =$$

$$\begin{pmatrix} 2T_B(2)\left(\frac{u\Delta t}{\Delta x}+\left(1-\frac{u\Delta t}{\Delta x}\right)^2\right) \\ 2T_B(2)\left(1-\frac{u\Delta t}{\Delta x}\right)^2 \\ 2T_B(2)\frac{\Delta t}{\Delta x}\left(T_A(1)-T_B(1)+\left(1-\frac{u\Delta t}{\Delta x}\right)(T_A(0)-T_B(0))\right) \\ 2T_B(2)\frac{u}{\Delta x}\left(T_A(1)-T_B(1)+\left(1-\frac{u\Delta t}{\Delta x}\right)(T_A(0)-T_B(0))\right) \\ -2T_B(2)\frac{u\Delta t}{\Delta x^2}\left(T_A(1)-T_B(1)+\left(1-\frac{u\Delta t}{\Delta x}\right)(T_A(0)-T_B(0))\right) \end{pmatrix} = 2T_B(2)\begin{pmatrix} 1.5 \\ 0.5 \\ 1.5 \\ 1.5 \\ -0.75 \end{pmatrix}$$

For a 10% perturbation in each of the components in $\mathbf{y_0}$, the impact on the cost function of a generic parameter α can be estimated as: $\Delta J = \frac{\partial J}{\partial \alpha}\Delta\alpha$. Even after two time steps, the initial value of T_A plays a greater role in determining J than $T_B(0)$. Increasing the advective velocity or the time step, or decreasing the grid spacing all have the same impact.

The computational cost of an adjoint time step involves the multiplication of a 5×1 vector by a 5×5 matrix. This is much cheaper than the equivalent tangent linear version which requires matrix by matrix multiplications until the final step. This reduced computational load is one of the major advantages of the adjoint model. The drawback is the prerequisite knowledge of the T_A and T_B sequence of numbers.

When using a model of the size of a coupled atmosphere-ocean GCM for multi-year runs, the storage requirements necessary during the forward run rapidly exceeds the capacity of any computer. A procedure called *checkpointing* (Griewank and Corliss, 1991) is therefore introduced to reduce the storage requirements to a manageable size. This procedure consists in splitting the model's time stepping into multiple embedded loops. For the two level checkpointing system shown in Fig. 2-1, time stepping is split into an outer and an inner loop. Obtaining sensitivities requires two runs of the forward model, the first integration stores the model state at every call of the outer loop, N times. This information is then used for the integration of each individual segment of the inner loop, starting at $n = N - 1$. A second forward run stores the state M times, this information is used during the adjoint run. After finishing the $N - 1$ segment, the model reads the state stored at $N - 2$ before proceeding with the integration of that segment.

Three level checkpointing is required in the implementation of the ocean model in order to obtain sensitivities on climatological time scales. The innermost loop stores the model state to the computer's active memory. The middle and outer loops use storage to files. When optimized to minimize storage requirements (Griewank and Corliss, 1991), a 400 year adjoint calculation of a 4 degree resolution global ocean model requires approximately 1.4GB of disk space. The storage of multiple files can theoretically be avoided if the model

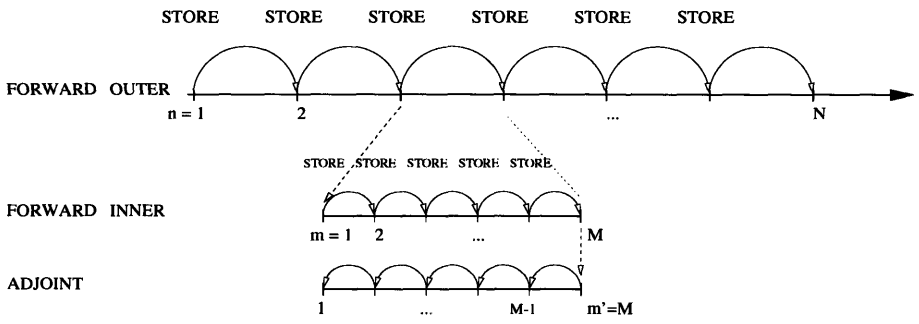

Figure 2-1: Illustration of a two-level checkpointing sequence. This scheme requires two integrations of the forward model and one integration of the adjoint code. Information is stored at the N outer checkpoints, and picked up as starting points for the inner nested loop of the forward and adjoint models, which has M time steps.

is in an exact steady state, a single file should then suffice. Although the present model has little internal variability and most of the results presented here are linearizations about a steady-state, this solution was avoided. The objective was to develop a methodology, which could be applied to a linearization about a time dependent trajectory.

Because of the necessity to perform three forward calculations before proceeding with the adjoint calculation, and because the adjoint code itself contains more terms than the original code, the complete sensitivity calculation takes approximately 4.6 times the time of an equivalent forward run.

2.4 Description of the Forward Model

The ocean model used in this project is the MIT OGCM; it is described in detail in Marshall et al. (1997a,b). This model is designed to study ocean processes ranging from the non-hydrostatic scale of convection to the hydrostatic global scale. The version used here consists of a single rectangular basin 64° wide in the zonal direction, which extends from 66° S to 70° N. A continuous channel is added in southern latitudes to represent the Antarctic Circumpolar current, this "ACC" is 80° wide and extends from 66° S to 46° S. The resolution of the model is 4° × 4° and the model has 15 layers in the vertical, with thicknesses ranging from $50\,m$ near the surface to $690\,m$. at the bottom. The depth of the basin is uniform ($4200\,m$) except between the "continent" and "Antarctica" where a $2500\,m$ deep sill is added. The time stepping procedure is asynchronous (Bryan, 1984), the momentum

equations have a time step of 40 minutes while tracers are advected with a time step of one day. The Redi isopycnal diffusion scheme is used in all model runs, it allows for the diffusion of tracers along three-dimensional isopycnal surfaces instead of the horizontal and vertical directions. The Gent Mc-Williams scheme parameterizes the advective effect of the geostrophic eddies with a "bolus velocity", which is added to the Eulerian-mean velocity (Danabasoglu and McWilliams, 1995). A table summarizing the value of key model parameters is provided in Appendix A. By idealizing the domain geometry and restricting its size, the objective was to allow an extensive exploration of the sensitivity of the circulation to various surface forcing configurations.

The forcing fields are derived from the zonal average of the wind stress, sea surface temperature and salinity, heat flux and net precipitation fields over the Atlantic basin (Jiang et al., 1999; Levitus and T.P.Boyer, 1994a,b). The zonal mean sea surface temperature in the North Atlantic was, however, lowered by a few degrees from observations in order to maintain convection and the overturning. The heat flux and freshwater forcing fields are adjusted to ensure zero net input of energy or mass into the system. The net precipitation field (evaporation-precipitation) is imposed as a virtual salt flux.

The steady-state sea surface temperature, sea surface salinity, circulation and meridional streamfunction are shown in Fig.2-2, 2-3 and 2-4. In these illustrations, the surface boundary conditions were "mixed". The boundary condition on temperature combines the observed zonally averaged heat flux with a term relaxing temperatures to the observed zonal mean temperature on a sixty day time scale. The meridional overturning peaks in high latitudes at a value of $11.5\,Sv$ and the heat transported northward in the basin amounts to $0.7\,PW$, nearly all transported by the meridional overturning circulation. Although the basin has a width similar to the Atlantic, both the volume and heat transport are significantly smaller than in alternate runs with more realistic geographic boundaries (see chapter 4 or Jiang et al. (1999)). The reason for the reduction in overturning strength is likely to be related to the zonally averaged nature of the boundary conditions imposed in the single basin model which do not allow the locally intense cooling observed in the North Atlantic. The greater longitudinal extent of the rectangular basin in high latitudes, when compared to a more realistic geometry, also prevents the ocean's heat loss from being concentrated over a few small regions.

As is often the case in similar models (Colin De Verdière, 1988; Marotzke and Scott,

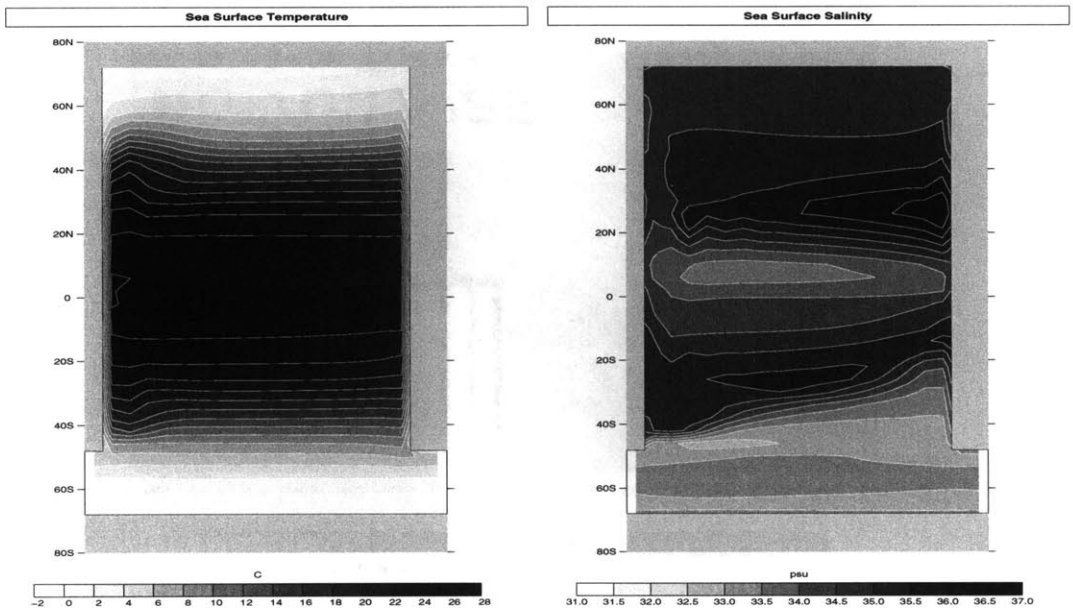

Figure 2-2: State of the single basin model when forced with mixed boundary conditions: $Q = \overline{Q}_{obs} + \lambda_s(T - \overline{T}_{obs})$, $E - P - R = (\overline{E - P - R})_{obs}$. The overline refers to the use of forcing fields, averaged over the Atlantic basin. Left: Sea surface temperature in $°C$. Right: Sea surface salinity.

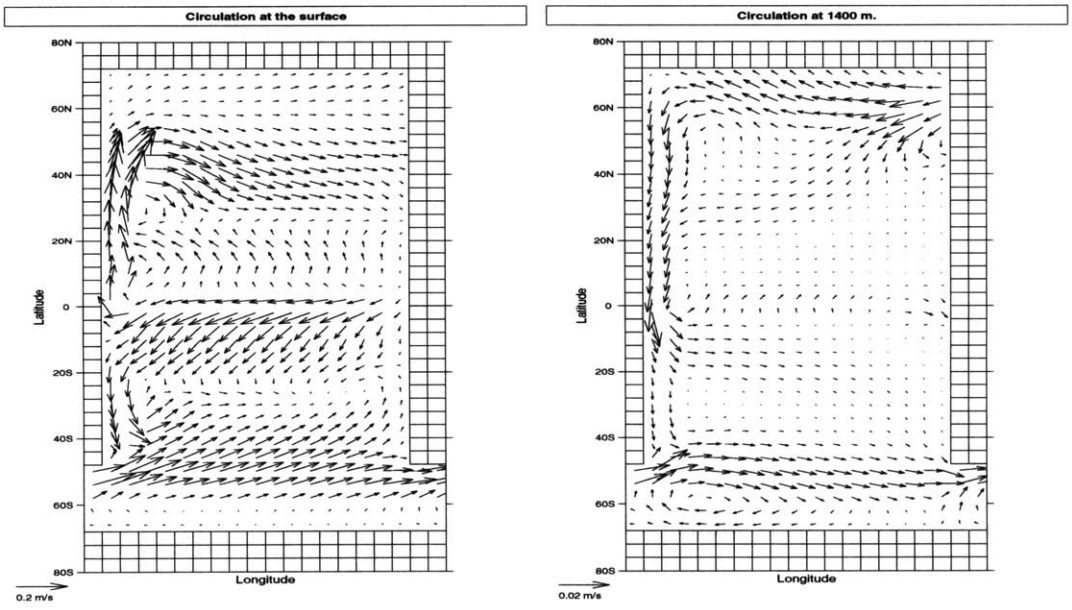

Figure 2-3: Circulation in the single basin model when forced with mixed boundary conditions. Left: Flow at the surface. Right: Flow at $1400\,m$ depth.

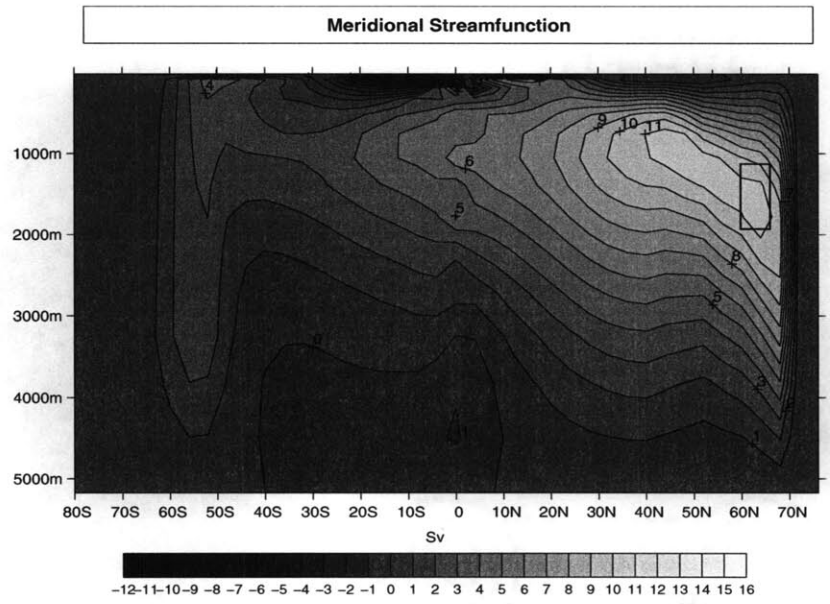

Figure 2-4: Meridional overturning streamfunction, in Sv, in the single basin model, when forced with mixed boundary conditions. The rectangular box encloses the area used as cost function for some of the calculations.

1999), the actual downward mass transport signature of the MOC is taking place along the eastern wall from 40° to 68° N, with peak downwelling velocity in the northeast corner. The "convective mixing", which contributes to setting up the up- and downwelling patterns that balance of the overturning, takes place in northwest corner in the basin's coldest spot. The separation of the western boundary current from the coast near 50° N, which is clearly visible in the surface velocity plot in Fig.2-3 plays an important role in isolating the northwest corner and allowing it to cool while warming the northeast corner.

Convective mixing was kept in quotes above because the model ceases to become statically unstable anywhere in the domain after the first 500 years of the spinup integration. While the neutral stratification is initially set up by convection in the northwest corner, the mixing induced by the projection of the isopycnal diffusion onto the vertical in regions of steeply sloping isopycnals is sufficient to keep the column's stratification homogeneous after year 500. Since the Gent-McWilliams scheme caps the maximum slope of the isopycnals at 10^{-3}, the projection onto the vertical can reach $\kappa_i \cdot 10^{-3} = 1000 \cdot 10^{-3} = 1\, m^2/s$, which is sufficient to homogenize a kilometer thick layer over ten days. This efficient adiabatic diffusion effectively substitutes itself for convection and plays a similar role. For clarity, the

neutrally buoyant column in the northwest will still be referred to as the site of convection in subsequent discussions.

2.5 Equilibration Process

By restricting the domain size to a single basin, the objective was to allow a clear determination of the time scales over which information propagates in the basin. By simplifying the geometry, the goal was to identify how information propagates in the adjoint model. The following sections illustrate the pathways and time scales over which the model equilibrates and adjusts to perturbations.

2.5.1 Time Scales of Equilibration

The equilibration process can follow two basic paths. For parameters that are time invariant such as the wind stress or the diapycnal mixing coefficient, the sensitivities can be interpreted as the equivalent of adding a small perturbation at one point or column, maintaining this perturbation throughout the integration and calculating the sensitivity by dividing the difference between the value of the cost function in the perturbed integration (J_{pert}) to the unperturbed one (J_{ref}) by the magnitude of the perturbation (e.g. $\Delta\tau_x$):

$$\frac{J_{pert} - J_{ref}}{\Delta\tau_x}$$

These parametric sensitivities can be expected to asymptote to a constant value over time scales sufficiently long to include all the processes likely to influence the cost function. For time dependent variables such as temperature, the sensitivity to the initial condition can be expected to asymptote towards zero with time as the model loses memory of the perturbation. If the model was chaotic, the initial value sensitivities would, however, initially grow exponentially with time and cease to grow once the limit cycle is reached (Frøyland and Alfsen, 1984; Tanguay et al., 1995; Lea et al., 2000). The time taken to reach a steady value should be similar for parametric and initial value sensitivities; it represents the time needed by diffusion effects to erase any impact of a perturbation before it reaches the cost function. Fig. 2-5 illustrates the difference between parametric (right) and initial value (left) sensitivities, these figures are best analyzed with time going backwards from right to

left. The cost function is calculated by averaging the meridional streamfunction where it reaches its maximum, between $\phi = 60$ and $68° N$ and and $[1055 - 1785\,m.]$, λ_1 and λ_2 are the longitudes at the western and eastern sides of the basin, z_B is the depth of the basin (see Fig.2-4 and the enclosed box):

$$\psi(\phi, z) = r \cdot \cos(\phi) \cdot \int_{\lambda_1}^{\lambda_2} \int_{z}^{z_B} v \, dz \, d\lambda \tag{2.12}$$

The sensitivity of the cost function, here the maximum intensity of the meridional overturning streamfunction to a temperature perturbation imposed 800 years earlier at $2° N$ (bottom left) is zero; it is, however, 5.5 $Sv°C^{-1}$ if the perturbation is imposed 50 years before the diagnostic is calculated. The equilibrium sensitivity to a constant wind stress perturbation imposed at $18° N$ is (top right) 0.8 $Sv\,N^{-1}m^2$. It is clear from these figures that most of the information, which will be obtained with the adjoint model, is present after approximately 400 years. This will, therefore, be the total integration time chosen for the simulations described in later chapters. The "steady-state" sensitivity patterns are in fact the patterns at year 400.

All four curves share a common shape with a primary (for the parametric sensitivities) or secondary (for the initial value sensitivities) peak between years -200 and -100. Initial value sensitivities obviously have their greatest value over much shorter time scales. The timing of this secondary peak is linked to the latitude where the perturbation is imposed; it appears later for locations further away from the diagnostic, in this case further South. This indicates that this peak is related to two competing influences. Advection tends to increase the radius over which perturbations can influence the cost function while diffusion tends to reduce the magnitude of the perturbation for increasing distances from the diagnostic.

The exact value towards which the parametric sensitivities asymptote can take close to 400 years to equilibrate, the geographic maps or patterns of sensitivity are, however, set more rapidly. These patterns then decrease in intensity but do not change shape. This "rapid" equilibration time scale is on the order of $\sim$ 200 years for most parameters, sometimes more rapid when the surface boundary conditions includes a restoring term, which forces a rapid loss of information. This indicates that the maximum radius, over which advective processes are effective, is reached after 200 years.

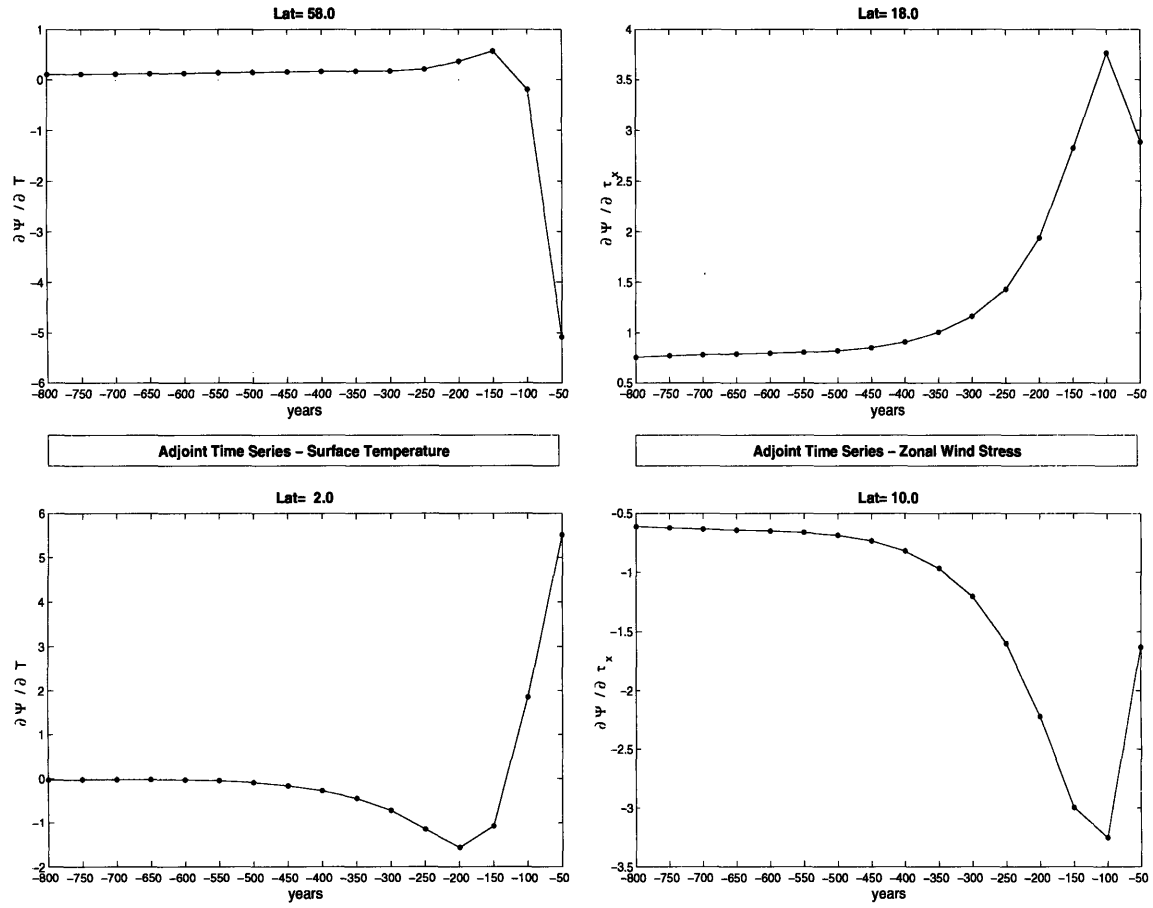

Figure 2-5: Time series of the sensitivity of the meridional overturning's maximum streamfunction ψ_{MAX} to the initial surface temperature distribution $\frac{\partial \psi_{MAX}}{\partial T}$ in $\frac{Sv}{^{\circ}C}$ (left) and to the zonal wind stress field $\frac{\partial \psi_{MAX}}{\partial \tau_x}$ in $\frac{Sv}{N\,m^{-2}}$ (right) for points at different latitudes in the model

2.5.2 Adjoint Kelvin Waves

Kelvin waves are one the fundamental processes, which carry perturbations around the basin (Kawase, 1987). This has been noted in relation to the adjustment of the thermocline in response to changes in deep water formation (Huang et al., 2000), as well as to explain how changes in wind stress forcing over the Southern Oceans relate to changes in overturning strength (McDermott, 1996). In both studies, coastal and equatorial Kelvin waves transport the perturbation signal rapidly along the boundaries of the basin and along the equator. The interior flow adjusts through the radiation of Rossby waves from the boundaries.

Theory

Equatorial Kelvin waves in a shallow framework obey the following equations:

$$\begin{aligned} u_t \quad & -g\eta_x \quad = 0 \\ \eta_t \quad & +Hu_x \quad = 0 \end{aligned} \tag{2.13}$$

where u is the zonal velocity, η is the perturbation to the sea surface height and H is the mean depth of the layer. This linear equatorial Kelvin wave operator can be written succinctly as:

$$\mathcal{A}\psi = 0 \tag{2.14}$$

with $\psi = \begin{bmatrix} \eta \\ u \end{bmatrix}$ and:

$$\mathcal{A} = \begin{bmatrix} \frac{\partial}{\partial t} & H\frac{\partial}{\partial x} \\ -g\frac{\partial}{\partial x} & \frac{\partial}{\partial t} \end{bmatrix} \tag{2.15}$$

The derivation of the adjoint Kelvin wave operator requires the use of Green's generalized theorem. The derivation of that theorem is drawn from Morse and Feshbach (1953). Gauss' theorem states that the integral over the surface A of a vector is equal to the integral of the divergence of that vector over the volume V enclosed by the surface A

$$\oint U \cdot d\mathbf{A} = \int\int\int \operatorname{div} U dv$$

Constructing vectors $U\operatorname{grad} V$ and $V\operatorname{grad} U$ from two "reasonable" scalar functions,

applying Gauss' theorem to both vectors and substracting one from the other yields:

$$\oint [U\text{grad}\, V - V\text{grad}\, U] \cdot d\mathbf{A} = \int\int\int \left[U\nabla^2 V - V\nabla^2 U\right] dv \tag{2.16}$$

A generalization of this equation in terms of an abstract operator $\mathcal{A}$ is:

$$\mathbf{u}\mathcal{A}\mathbf{v} - \mathbf{v}\mathcal{A}\mathbf{u} = \nabla \cdot \mathcal{P}(\mathbf{u}, \mathbf{v}) \tag{2.17}$$

where $\mathcal{P}$ is a generalized vector and ∇ is the corresponding gradient operator. For example, in Green's theorem:

$$\mathbf{u}\nabla^2\mathbf{v} - \mathbf{v}\nabla^2\mathbf{u} = \nabla \cdot (\mathbf{u}\nabla\mathbf{v} - \mathbf{v}\nabla\mathbf{u})$$

$$\mathcal{A} = \nabla^2$$

$$\mathcal{P} = \mathbf{u}\nabla\mathbf{v} - \mathbf{v}\nabla\mathbf{u}$$

Relation 2.17 is not satisfied by all operators $\mathcal{A}$, generalizing it requires the use of the adjoint operator $\tilde{\mathcal{A}}$. Green's generalized theorem states that:

$$\mathbf{u}\mathcal{A}\mathbf{v} - \mathbf{v}\tilde{\mathcal{A}}\mathbf{u} = \nabla \cdot \mathcal{P}(\mathbf{u}, \mathbf{v}) \tag{2.18}$$

If the operator $\mathcal{A}$ satisfies $\mathcal{A}\psi = 0$, the adjoint operator satisfies the adjoint equation:

$$\tilde{\mathcal{A}}\tilde{\psi} = 0 \tag{2.19}$$

The adjoint operator is derived by integrating the first part of equation 2.18 by parts:

$$\begin{aligned}
\int\int \mathbf{u}\mathcal{A}\mathbf{v}\, dx\, dt = \quad & \int\int u_1 \left(v_{1t} + H v_{2x}\right) + u_2 \left(-g v_{1x} + v_{2t}\right) dx\, dt = \\
& \int\int \left(-v_1 u_{1t} - v_2 u_{2t} + g v_1 u_{2x} - H v_2 u_{1x}\right) dx\, dt + \\
& \int \left[u_1 v_1 + u_2 v_2\right]\Big|_{ta}^{tb} dx + \int \left[H u_1 v_2 - g u_2 v_1\right]\Big|_{xa}^{xb} dt = \\
& \int\int v_1 \left(-u_{1t} + g u_{2x}\right) + v_2 \left(-H u_{1x} - u_{2t}\right) dx\, dt + \ldots = \\
& \int\int \mathbf{v}\tilde{\mathcal{A}}\mathbf{u}\, dx\, dt + \ldots
\end{aligned} \tag{2.20}$$

The adjoint equatorial Kelvin wave operator is:

$$\tilde{\mathcal{A}} = \begin{bmatrix} -\frac{\partial}{\partial t} & g\frac{\partial}{\partial x} \\ -H\frac{\partial}{\partial x} & -\frac{\partial}{\partial t} \end{bmatrix} \tag{2.21}$$

which indeed satisfied Green's generalized theorem:

$$\mathbf{u}\mathcal{A}\mathbf{v} - \mathbf{v}\tilde{\mathcal{A}}\mathbf{u} = \begin{bmatrix} \frac{\partial}{\partial t} & \frac{\partial}{\partial x} \end{bmatrix} \cdot \begin{bmatrix} u_1 v_1 + u_2 v_2 \\ H u_1 v_2 - g u_2 v_1 \end{bmatrix} = \nabla \cdot \mathcal{P}(\mathbf{u}, \mathbf{v}) \tag{2.22}$$

$\tilde{\psi}$ therefore satisfies the equatorial Kelvin wave equation with time and space reversed:

$$\tilde{\psi}(x,t) = \psi(-x,-t) \tag{2.23}$$

The zonal velocity of the equatorial Kelvin wave is furthermore in balance with the meridional pressure gradient on the equatorial beta plane:

$$\beta y u = -g\frac{\partial \eta}{\partial y} \tag{2.24}$$

The adjoint operator implies that a reversal of space in the meridional direction is sufficient to satisfy the equation: $\tilde{\psi}(y) = \psi(-y)$.

The general solution to the classic shallow water equatorial Kelvin wave problem is a wave of the form:

$$\eta(x,y,t) = e^{y^2/4a^2} F(x+ct) + e^{-y^2/4a^2} G(x-ct) \tag{2.25}$$

where $a = \frac{c}{\sqrt{2\beta}}$ is the equatorial radius of deformation, $c = \sqrt{gH}$ is the phase speed of the wave. The solution, which decays exponentially away from the equator in the meridional direction, is an eastward propagating wave:

$$\eta(x,y,t) = e^{-y^2/4a^2} G(x-ct) \tag{2.26}$$

The adjoint equatorial Kelvin wave has the general form:

$$\tilde{\eta}(x,y,t) = \eta(-x,-y,-t) = e^{-y^2/4a^2} F(-x-ct) + e^{y^2/4a^2} G(-x+ct) \tag{2.27}$$

Retaining only the component that decays away from the equator, the solution represents a wave, which also propagates from West to East. However, it makes little sense to analyze these adjoint waves with time going in the normal "forward" direction since this would be tantamount to observing a wave that is moving toward the impulse that causes it and not away from the it. It would furthermore represent a wave moving towards an impulse that will take place later in time, as shown on the left-hand side in Fig.2-6. The model results are therefore more intuitive when analyzed with time reversed ($\eta(-x,-y,t)$). The wave then propagates away from the impulse that causes it, as shown on the right-hand side of Fig.2-6. In that case, the adjoint equatorial Kelvin wave can be expected to propagate from East to West.

$$\tilde{\eta}(x,y,-t) = \eta(-x,-y,t) = e^{-y^2/4a^2} F(-x+ct) \tag{2.28}$$

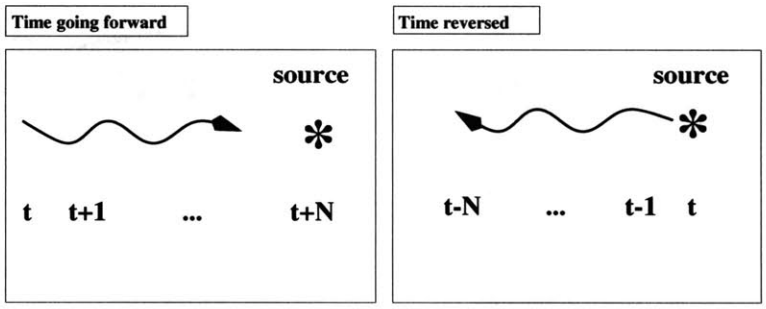

Figure 2-6: Illustration of the adjoint model's response to a perturbation source. Left: time runs in the normal "forward" direction and the wave propagates towards the source that causes it. Right: with time reversed, the wave propagates away from the source.

A similar analysis of the mathematics of adjoint coastal Kelvin waves indicates that, when viewed with time going backwards, they can be anticipated to propagate with the boundary to their left in the Northern hemisphere and to their right in the Southern hemisphere.

Model Results

The example chosen to illustrate the dynamics of adjoint boundary Kelvin waves, in Fig.2-7, is the sensitivity of the sea surface temperature at 58° N along the eastern boundary to the forcing by a perturbation in the zonal flow $t-N$ months earlier at any point in the basin. Many other dynamical variables could have been chosen in place of T and u.

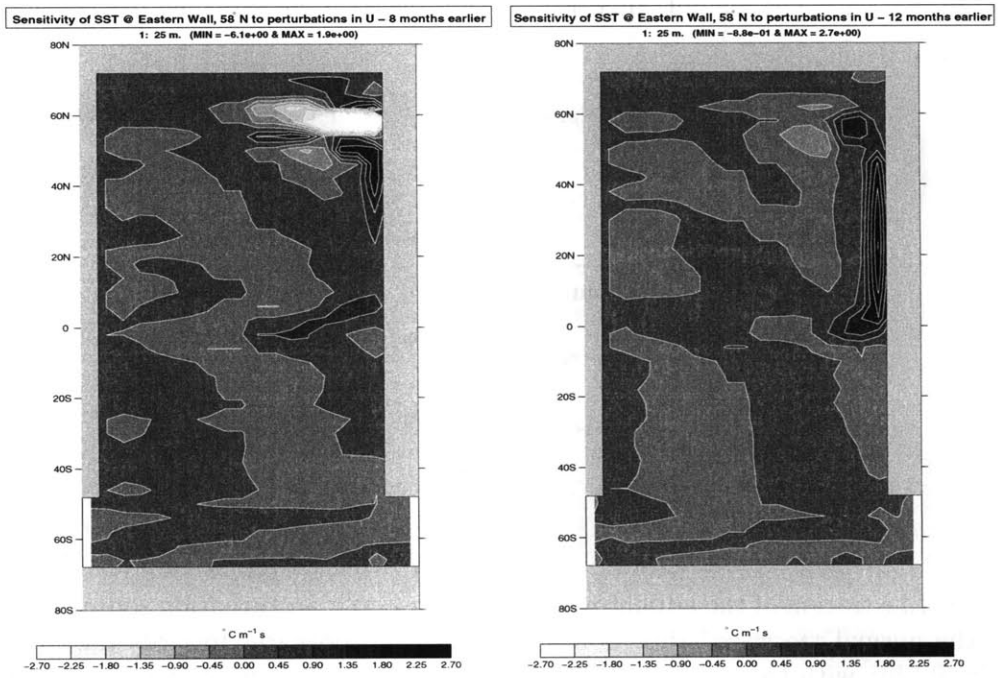

Figure 2-7: Sensitivity of the sea surface temperature at $58° N$ along the eastern boundary to a perturbation in the zonal velocity imposed 8 (left), respectively 12 (right) months earlier: $\frac{\partial T}{\partial u}$ in $°C\, m^{-1}\, s$. Note that both figures are plotted on the same scale.

After eight months, the pattern begins to show an adjoint boundary Kelvin wave propagating southward from $58°\,N$ along the eastern boundary. This implies that a velocity perturbation added along the eastern wall at $40°\,N$ would induce a boundary Kelvin wave which, eight months later, would influence the temperature at the site of diagnosis of the cost function. For $\frac{\partial T}{\partial u} \sim 1\,°C\,m^{-1}\,s$, the impact of a $\Delta u = 0.01\,m\,s^{-1}$ perturbation would be a $\Delta T = 0.01\,°C$ change in temperature. While Kelvin waves propagate indeed with the boundary on their right in the northern hemisphere, adjoint Kelvin waves propagate with the boundary on their left when viewed with time reversed. The adjoint boundary Kelvin wave takes approximately one year to reach the equator; its phase velocity can thus be estimated as $\frac{58°}{12\,months} \sim 0.20\,ms^{-1}$.

The second example, Fig.2-8, illustrates the dynamics and vertical structure of adjoint equatorial Kelvin waves. It shows the response of the sea surface temperature in the eastern equatorial region to perturbations in the zonal velocity.

The wave crosses the basin from east to west in a little less than one year. Given that the basin is 60° wide, its phase speed can be estimated at $0.2\,ms^{-1}$, which is slower than the first baroclinic mode in the world's ocean, which travels at an estimated $2.8\,ms^{-1}$ (Gill, 1982). This slow phase speed is not due to the model's coarse resolution, since the C-grid that is used does not distort the phase speed of Kelvin waves (Davey et al., 1983). The propagation speed of equatorial Kelvin waves is reduced by a factor $\frac{1}{\sqrt{\alpha}}$ because of the asynchronous time stepping used to accelerate the model's convergence (Bryan, 1984). α is the model's "time stretching" factor, or the ratio between the tracer and momentum time steps: $\alpha = \frac{1\,\mathrm{day}}{40\,\mathrm{min}} = 36$. The effective velocity of the Kelvin wave in an equivalent model with synchronous time stepping should therefore be six times larger, or approximately $1.2\,ms^{-1}$, closer to observations yet still too slow.

The comparison between the top and bottom rows in Fig.2-8 shows a reversal in the sign of the sensitivity, this change takes place between $765\,m$ and $2225\,m$ depth. This indicates that we are in the presence of the first baroclinic mode of the wave, and not the barotropic mode. The latter mode propagates faster ($c \sim 200\,ms^{-1}$ in the ocean, (Gill, 1982)), decays more rapidly and is also weaker than the first baroclinic mode. The slower, higher order modes are quite certainly also present. They are, however, difficult to identify because of the additional structure in the flow field, which stems from the reflection of the baroclinic mode at the western boundary. The cost function is much more sensitive to the adjoint

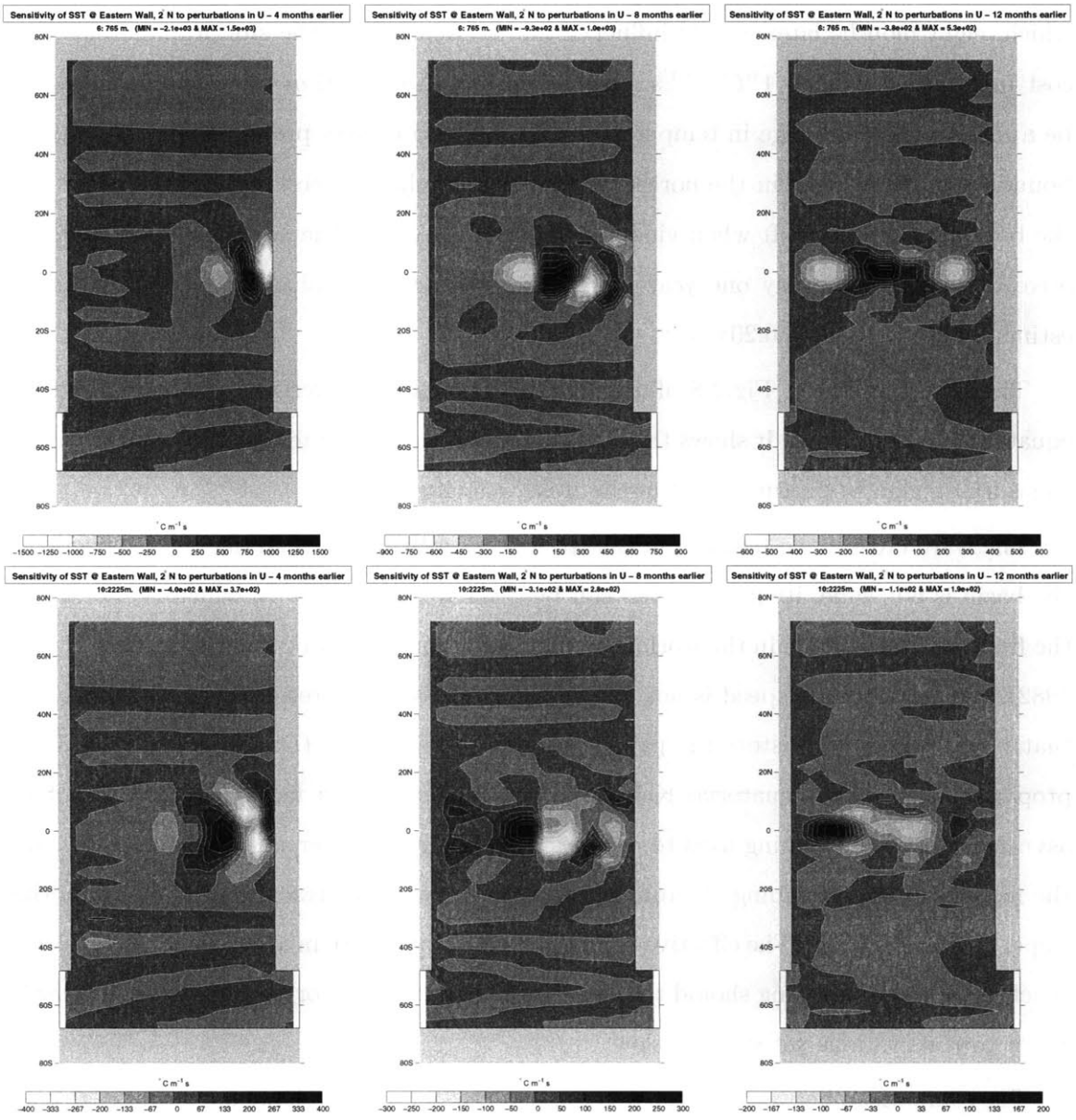

Figure 2-8: Sensitivity of the sea surface temperature at $2°$ N along the eastern boundary to a perturbation in the zonal velocity imposed 4 (left), respectively 8 (middle) and 12 (right) months earlier: $\frac{\partial T}{\partial u}$ in $°C\,m^{-1}\,s$. Top panels: sensitivity to perturbations added at $765\,m$ depth. Bottom panels: sensitivity to perturbations imposed at $2225\,m$ depth. Note that the scale is different on each plot.

equatorial Kelvin wave than it was to the boundary wave. This sensitivity does, however, decay rapidly with time and depth. The wavelength of the adjoint equatorial Kelvin wave can be estimated at around $2000\,km$.

After impinging on the western boundary, the adjoint Kelvin wave will be reflected eastward as an adjoint Rossby wave, and refracted north- and southward as adjoint boundary Kelvin waves.

2.5.3 Adjoint Rossby Waves

The mathematics of adjoint Rossby waves can be analyzed with the same method used for adjoint Kelvin waves. The baroclinic Rossby wave for a fluid with constant stratification can be written as:

$$\partial_{txx}p + \partial_{tyy}p + \frac{f^2}{N^2}\partial_{tzz} + \beta\partial_x p = 0 \tag{2.29}$$

is the stratification parameterThe adjoint operator is:

$$\tilde{A} = -\partial_{txx} - \partial_{tyy} - \frac{f^2}{N^2}\partial_{tzz} - \beta\partial_x \tag{2.30}$$

If $p(x,y,z,t)$ is a solution of the barotropic Rossby wave equation, $\tilde{p}(x,y,z,t) = p(-x,y,-z,-t)$ will satisfy the adjoint barotropic Rossby wave. It is interesting to point out that Rossby waves are invariant to a change in meridional direction, but not to changes in the zonal direction and in time. For reasons already mentioned, the evolution of these waves is more sensible when observed with time reversed. Figure 2-9 shows the eastward propagation of an equatorially trapped Rossby wave. This represents the sensitivity of the sea surface temperature along the western boundary at the equator to a zonal flow perturbation.

The speed of propagation of the first baroclinic mode of the equatorially trapped Rossby wave should be a third of speed of the equivalent mode of the Kelvin wave (Gill, 1982). It takes the adjoint Rossby wave three to four years to cross the basin, giving it a phase speed of $0.05\,ms^{-1}$. It is again clearly the first baroclinic component of the wave, the barotropic mode propagates much more rapidly. Imposing Green's function perturbations to the flow field, Stammer and Wunsch (1996) observed that the barotropic Rossby wave field took less than 50 days to decay.

The sensitivity of the sea surface temperature to adjoint Rossby waves is substantially

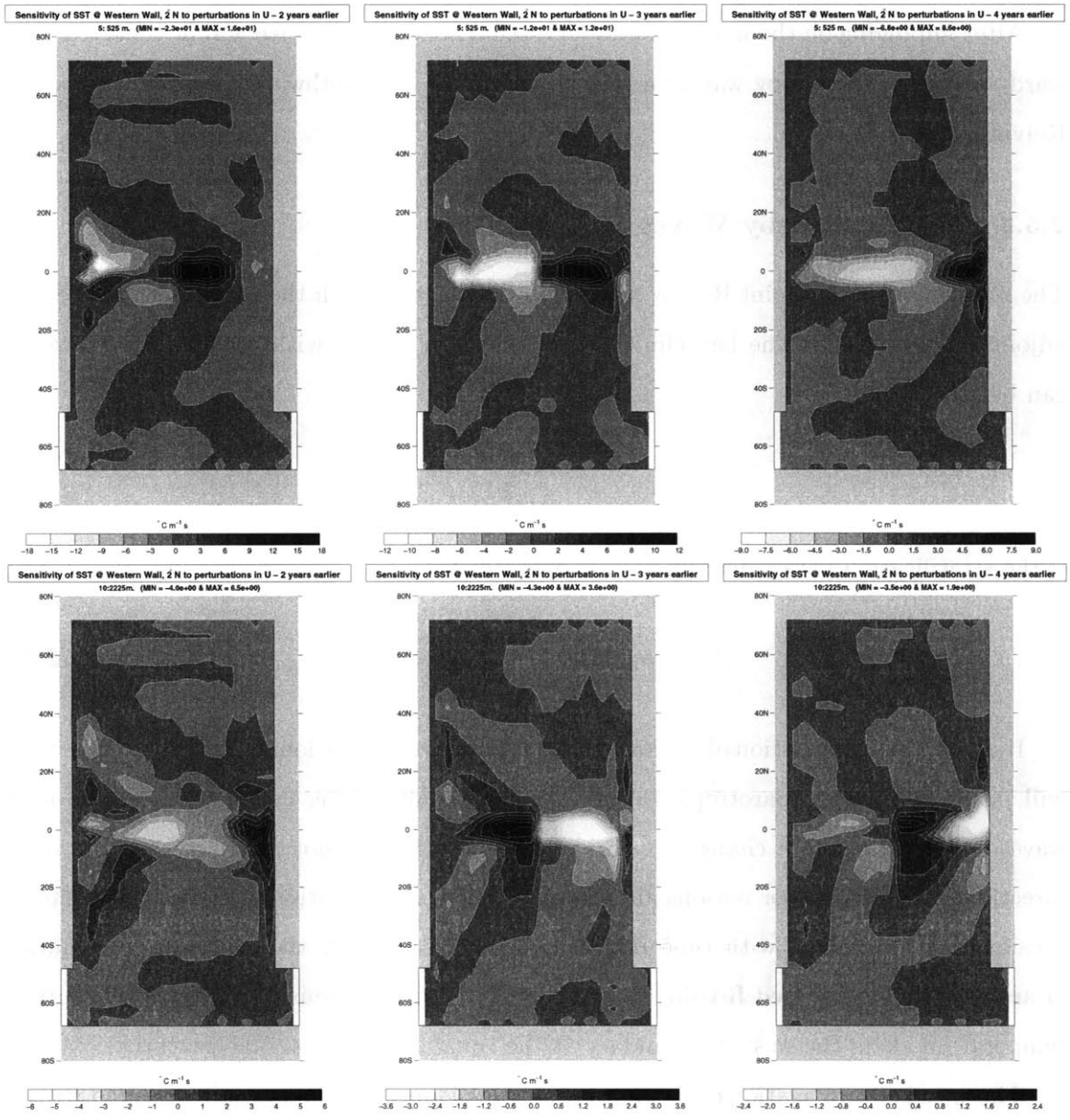

Figure 2-9: Sensitivity of the sea surface temperature at $2° N$ along the western boundary to a perturbation in the zonal velocity imposed 2 (left), respectively 3 (middle) and 4 (right) years earlier: $\frac{\partial T}{\partial u}$ in $°C\, m^{-1}\, s$. Top panels: sensitivity to perturbations at $525\, m$ depth. Bottom panels: sensitivity to perturbations at $2225\, m$ depth. Note that the scale is different on each plot.

smaller than it was to the adjoint equatorial Kelvin waves, primarily because the wave is slower to take shape. The wavelength of the adjoint equatorially trapped Rossby wave is close to the size of the basin, $\sim 6600\,km$.

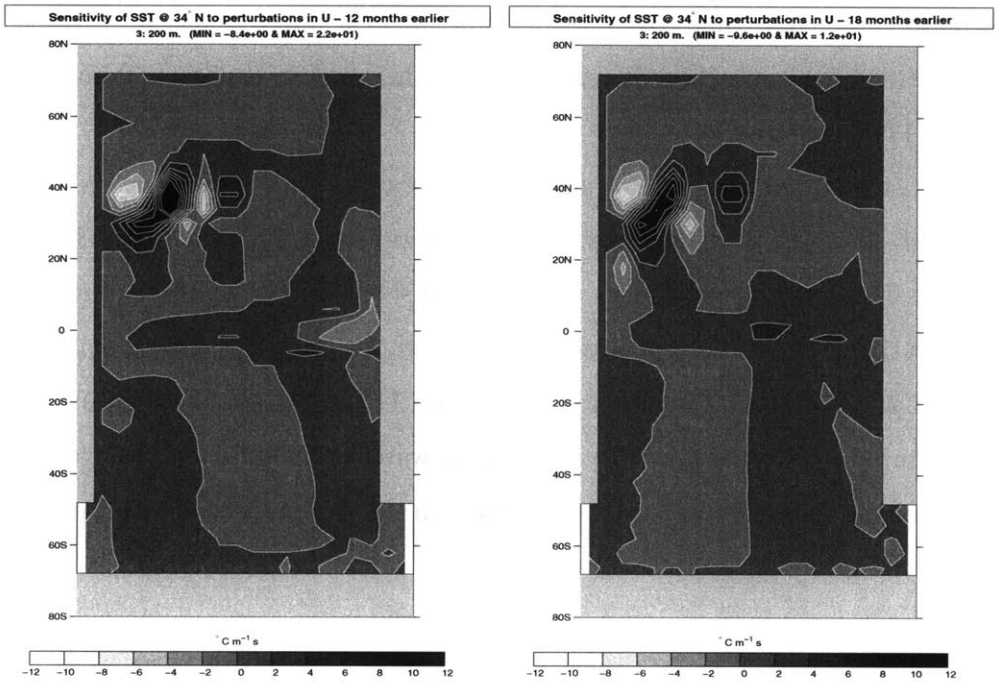

Figure 2-10: Sensitivity of the sea surface at 34° N, 12° East of the western boundary, to a perturbation in the zonal velocity imposed 12 (left), respectively 18 (right) months earlier: $\frac{\partial T}{\partial u}$ in $^{\circ}C\,m^{-1}\,s$ at $200\,m$ depth. Note that both plots are on the same scale.

Figure 2-10 gives an indication of the structure of the adjoint mid-latitude Rossby waves, which play a large role in the equilibration of the flow (see for example (Huang et al., 2000)). The plots show the sensitivity of the sea surface temperature at 34° N, 12° east of the western boundary, to the zonal velocity. The wave train is propagating primarily in the eastward direction, this could have been anticipated since planetary waves propagate primarily westward in mid-latitudes (Stammer and Wunsch, 1996). This implies that the interior flow in the adjoint model equilibrates, in the northern hemisphere, through the radiation of planetary waves from the western boundary. In the forward model, the interior responds to the radiation of waves from the eastern boundary. Westward propagating Rossby waves also exist, and could be observed more clearly in a larger basin with a higher resolution model.

2.5.4 Summary of the Role of Waves in the Equilibration Process

The step by step evolution of the equilibration process is shown in Fig. 2-11 for the response of the maximum meridional streamfunction ψ_{MAX} to a mechanic perturbation by the zonal wind stress forcing. Each plot refers to the effect on the overturning at time t of a perturbation applied at time t-N. The cost function is, again, calculated by averaging the meridional streamfunction where it reaches its maximum, between $\phi = 60$ and $68° N$ and and $[1055 - 1785\, m.]$.

These sensitivity patterns will be slightly different from those described above. Unlike the velocity field which is re-calculated at every time step, the wind stress is a constant forcing field. The sensitivity patterns are therefore showing the cumulative impact of perturbations in the wind stress, applied and maintained throughout the integration from time $t - N$ to time t when the cost function is calculated. This explains the absence of any wavelength signature in the adjoint Kelvin and Rossby waves, which display the overall effect of the passage of the wave. The absence of wavelength signature gives a clearer picture of the wave reflection and refraction processes.

- *t - {1 month - 1 year}*

  The band of high sensitivities is located directly over the latitudes where the cost function is calculated $[60 - 68° N]$. The sign is such that a westerly wind perturbation induces a southward Ekman transport, which is compensated at depth by a northward geostrophic return flow. This induced cell opposes the overturning streamfunction, and would thus tend to locally weaken it.

  The adjoint boundary Kelvin wave propagates along the eastern boundary, taking approximately one year to reach the equator.

- *t - {1-5 years}*

  The adjoint equatorial Kelvin wave reaches the western equatorial boundary after about two years, at which point it is reflected and refracted in three directions: as adjoint boundary Kelvin waves that propagate toward the poles in both hemispheres and as an adjoint equatorial Rossby wave.

  As suggested by McDermott (1996) the Kelvin waves, which advance by depressing isopycnals ahead of their route, most likely get halted in their journey around the

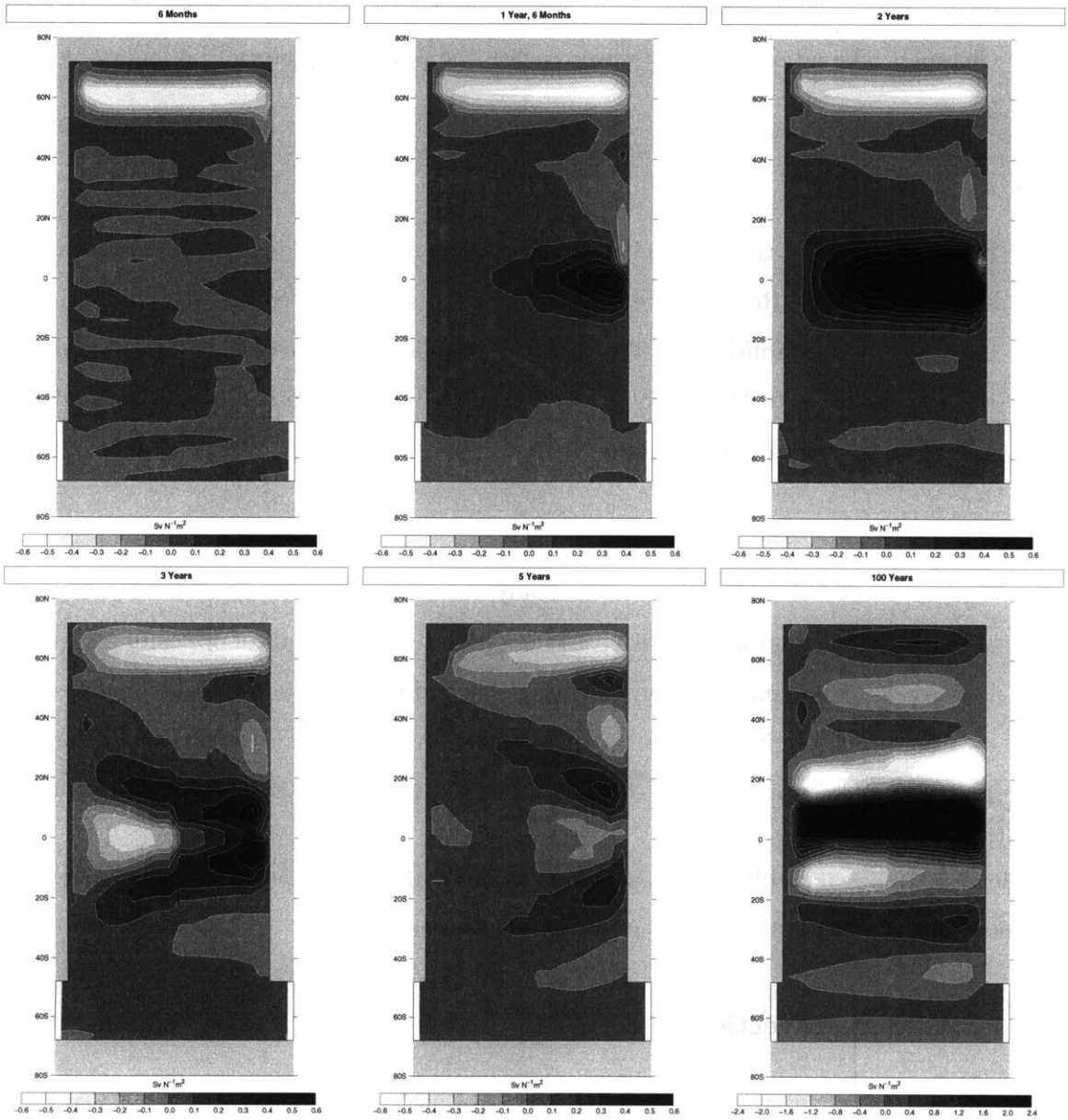

Figure 2-11: Sensitivity of the meridional overturning streamfunction maximum ψ_{MAX} to the zonal wind stress forcing: $\frac{\partial \psi_{MAX}}{\partial \tau_x}$ in $Sv\, N^{-1}\, m^2$ for 6 months, 1.5 years, 2 years, 3 years, 5 years and 100 years. All plots are on the same scale except for the last one which is on a scale four times larger.

basin at the neutrally buoyant column in the northwest corner where the isopycnals are near vertical. At year 5, a perturbation can be observed in the northwest corner as the wave locks on to the site of convection and perturbs it. Meanwhile, the boundary waves have communicated information as far south as the Antarctic Circumpolar Channel. The adjoint Rossby wave reaches the eastern equatorial boundary at year 5.

- *t - {5–50 years}*

  Beyond five years, the sensitivity pattern begins to show added complications as the adjoint equatorial Rossby wave is again reflected and refracted and the circulation in the interior is established by the radiation of planetary waves from the boundaries (Huang et al., 2000; McDermott, 1996). It is also over those time scales that adjoint advection begins to play an important role.

- *t - {50–800 years}*

  The patterns, which are observed in steady-state, begin to emerge after 50–100 years: a band of high equatorial sensitivities surrounded by two bands of opposite polarity in the tropics. This time scale suggests that, beyond wave motions, advection also plays an important role in determining the sensitivity of the ocean to the surface forcing. It is also after approximately one hundred years that peak sensitivities are reached.

Beyond 100 years, diffusion as well advection both play important roles. The final pattern (shown in Fig. 3-19) is set after about 400 years.

2.5.5 Adjoint Advection

Theory

The advection operator can only be considered linear for a passive tracer. The advection and adjoint advection operators are respectively:

$$\mathcal{A} = \frac{\partial}{\partial t} + u\frac{\partial}{\partial x} + v\frac{\partial}{\partial y} + w\frac{\partial}{\partial z} = \frac{d}{dt} \tag{2.31}$$

$$\tilde{\mathcal{A}} = -\frac{\partial}{\partial t} - u\frac{\partial}{\partial x} - v\frac{\partial}{\partial y} - w\frac{\partial}{\partial z} = -\frac{d}{dt} \tag{2.32}$$

The adjoint advection of a tracer, for example temperature, in a constant velocity field with no temperature sources or sinks ($\mathcal{A}T = 0$), is $\tilde{\mathcal{A}}\tilde{T} = 0$. $\tilde{T}$ satisfies the tracer advection equation with time and space reversed: $\tilde{T}(x, y, z, t) = T(-x, -y, -z, -t)$. In a Lagrangian sense, information is advected backwards in time.

Model Results

The patterns of sensitivity of the maximum value of the meridional streamfunction to the wind stress forcing have provided an interesting picture of the ways in which mechanically induced perturbations travel around the basin. The advective pathways are best observed when a perturbation in the buoyancy field is imposed. The example shown in Fig. 2-12 is a time series of the sensitivity of the streamfunction maximum to the heat flux forcing field. The model is forced at the surface with constant heat and freshwater fluxes. The boundary condition imposed on the surface temperature may be less "realistic" than a mixed boundary condition, which includes a term restoring the sea surface temperature towards observations on a relatively short time scale. This example was, however, chosen as a good illustration of the advective pathways in the adjoint model. Other buoyancy perturbations, such as changes in the net precipitation field have a similar impact. The explanation of the physical mechanisms that drive the development of these patterns, will be delayed until chapter 3. The focus is here entirely on the pathways used by the perturbations use to influence the cost function.

- t - $\{$*1 month - 1 year*$\}$: On short time scales, the mechanisms that can influence the overturning are convection, or alternatively strong vertical mixing, rapid vertical advection and the response at depth to a surface perturbation. The slope of the isopycnals is capped by the Gent-McWilliams scheme (Danabasoglu and McWilliams, 1995) at 10^{-3}, the projection of the isopycnal mixing ($\kappa_i = 10^3\, m^2 s^{-1}$) onto the vertical can therefore reach $1\, m^2\, s^{-1}$ near the northwest corner. This is sufficient to communicate information from the surface to the depth where the cost function is calculated in approximately two weeks. This is the mechanism, which substitutes itself for convection, responsible for conveying information downwards on the western boundary. Along the eastern boundary, the vertical advection is sufficiently strong to communicate a perturbation to $1000\, m$ in just about one year. Elsewhere, the sensitivity is most likely

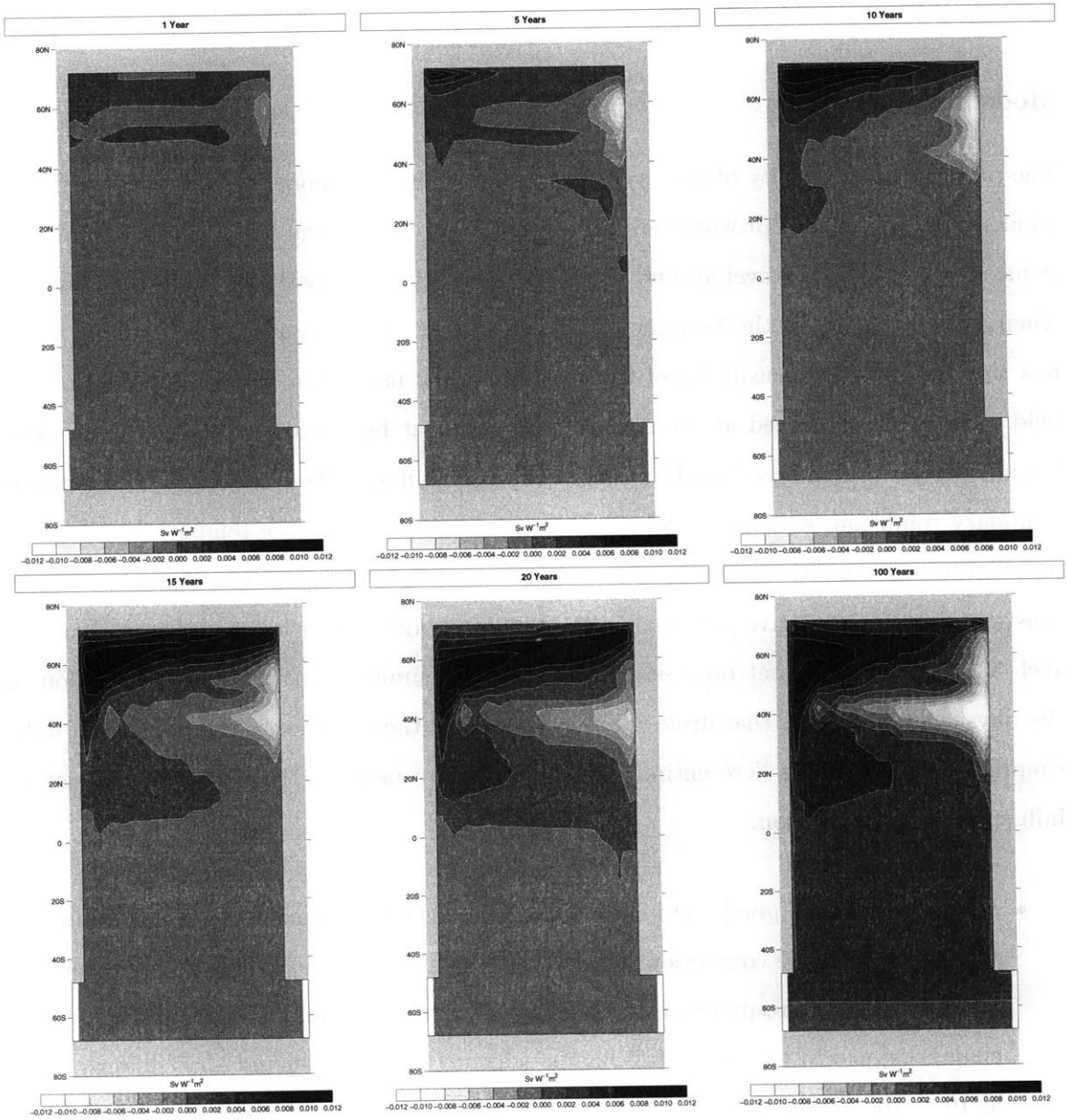

Figure 2-12: Sensitivity of the streamfunction maximum ψ_{MAX} to the imposed heat flux under flux boundary conditions: $\frac{\partial \psi_{MAX}}{\partial Q}$ in $Sv\,W^{-1}\,m^2$. The figures show the sensitivity after 1, 5, 10, 15, 20 and 100 years. All figures are plotted on the same scale

related to the effect of a surface thermal, or equivalently vorticity perturbation. For a perturbation of 400 km radius and an average stratification $N \sim 10^{-3}s^{-1}$, the Rossby depth or scale over which the perturbation will decay, is close to 4 km. This means that a surface perturbation can influence the circulation at the depth at which the cost function is diagnosed. This explains the generally positive, yet weak, sensitivity observed over short time scales between 60 and 68° N.

- t - {*1–10 years*}: The source of the positive sensitivity spreads eastward along the northern wall and southward along the western boundary. This is, in both cases, due to adjoint advection by the sum of Eulerian velocity and eddy-induced bolus transport, which is an eastward flow directed away from the site of convection. Note that without the bolus transport, the adjoint advection would be westward along the northern boundary, and advection would be ruled out as the mechanism responsible for the sensitivity pattern. By year 10, the signal reaches the northern extent of the subtropical gyre, and is rapidly advected southward by the adjoint western boundary current. The pattern also shows the role played by the recirculation of water along the northern boundary of the subtropical gyre. Along the eastern boundary, the negative sensitivities extend to 35° N and westward from there, again in agreement with advection by the flow field.

- t - {*10–20 years*}: By year 20, the northern boundary of the subtropical gyre in the northern hemisphere and the equatorial boundary are clearly outlined. One can also notice that signals from the southern hemisphere are first communicated northward through an eastern equatorial passage. After catching on to the western boundary current, the signal travels around the subtropical gyre down to the Equator in approximately 10 years, which translates into what is the observed average flow velocity of $3 - 4\,cm\,s^{-1}$. The negative signal is meanwhile also clearly being advected westward by the strong adjoint East to West current in that region. The zero contour separates the water that is advected towards the northern part of the basin from that which reaches the eastern boundary directly.

- t - {*20–400 years*}: The signal begins to spread in the southern hemisphere after approximately 20 years, by year 100 it has filled the basin. Most of the features of the steady-state pattern of sensitivity are set after one hundred years.

2.5.6 Adjoint Diffusion

The diffusion operator in cartesian space is $\mathcal{A} = -\frac{\partial}{\partial t} + \kappa_i \left(\frac{\partial^2}{\partial x^2} + \frac{\partial^2}{\partial x^2} \right) + \kappa_d \frac{\partial^2}{\partial z^2}$. The adjoint operator, which satisfies Green's theorem (see equation 2.33) is $\tilde{\mathcal{A}} = \frac{\partial}{\partial t} + \kappa_i \left(\frac{\partial^2}{\partial x^2} + \frac{\partial^2}{\partial x^2} \right) + \kappa_d \frac{\partial^2}{\partial z^2}$.

$$u\mathcal{A}v - v\tilde{\mathcal{A}}u = \frac{\partial (uv)}{\partial t} + \kappa_i \frac{\partial (uv_x - vu_x)}{\partial x} + \kappa_i \frac{\partial (uv_y - vu_y)}{\partial y} + \kappa_d \frac{\partial (uv_z - vu_z)}{\partial z} = \nabla \cdot P(\mathbf{u}, \mathbf{v}) \tag{2.33}$$

Note that the ocean model calculates diffusion along and across isopycnals, not in the vertical and horizontal directions.

Diffusion is invariant against a change in spatial direction, but not against a change in the sense of time: $\tilde{\psi}(x, y, z, t) = \psi(x, y, z, -t)$. Diffusion plays a crucial role in determining the equilibrated state of the ocean model. It is, however, also the slowest of the important dynamical processes. Because of the presence of waves and advection, it is difficult to isolate and illustrate its effects in the adjoint model because the more.

2.6 Summary and Discussion

An attempt is made, in Fig. 2-13, to summarize the pathways over which information propagates away from the cost function in the adjoint model. These processes are numbered by the order in which they appear. The effect of a dynamic perturbation is shown on the left, that of a buoyancy perturbation on the right. This is an idealization, dynamic and kinematic effects cannot be separated quite as clearly.

Adjoint Kelvin waves take approximately three years to go around the basin in the northern hemisphere or to reach the Antarctic circumpolar channel in the southern hemisphere. This phase velocity is at least six times slower than what would be obtained in a model with synchronous time stepping. The waves in the northern hemisphere are stopped in their progress around the basin by the neutral stratification at the site of convection. Adjoint Rossby waves are slower by a factor of three or four, and so take a number of years to equilibrate the interior portion of the circulation. Adjoint advection is still slower, it takes twenty years for a perturbation in the subtropical gyre to be advected to the northern part of the basin, and over half a century for the southern hemisphere to have any influence.

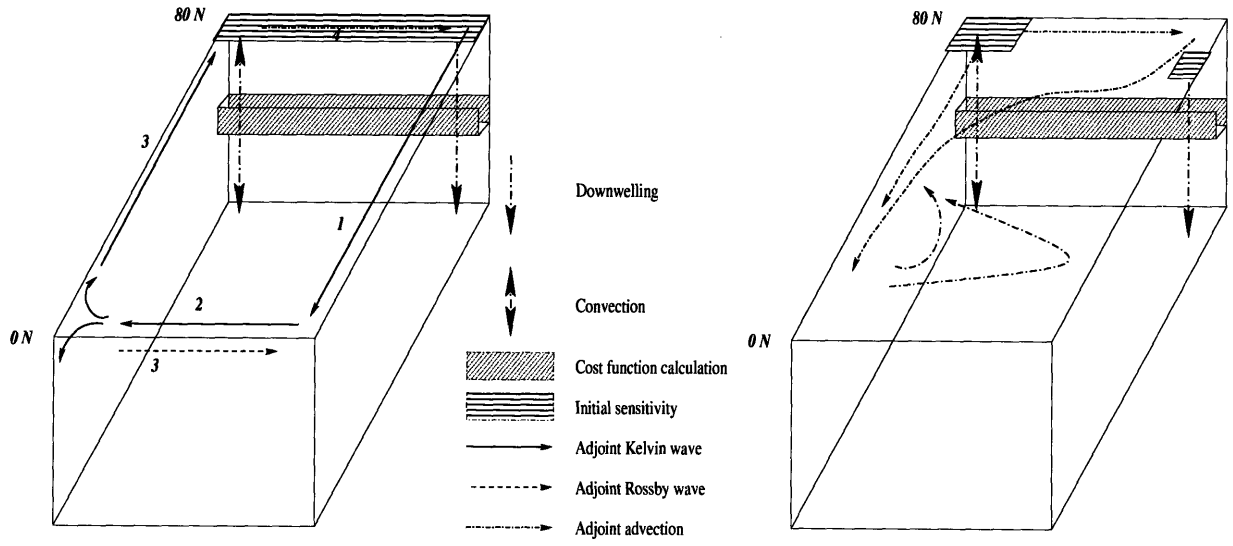

Figure 2-13: Illustration of the pathways over which information is communicated around the basin in the adjoint model. Left: Sensitivity to a mechanical perturbation. Right: Sensitivity to a buoyancy perturbation.

Adjoint diffusion is slowest, and difficult to observe.

The steady-state patterns, which will be described in chapters 3 and 5, take approximately 400 years to equilibrate and are the product of all the physical mechanisms described above.

This analysis has shown that the adjoint model behaves in a reasonable way over a number of time scales. It reproduces the physical behavior, which was anticipated from the mathematical analysis of simplified systems. It also shows quite clearly how perturbations can have an impact on a given cost function over a range of time scales.

The sensitivity patterns obtained with the adjoint model outline clearly what regions can have an influence on the meridional overturning circulation on short time scales. For example, inter-annual variability in the wind stress in coastal and equatorial regions is more likely to influence the overturning than the variability in the interior of the basin. Similarly, the influence of changes in the buoyancy forcing in the southern hemisphere on the overturning will take several decades to be felt. For time scales up to a decade, the influence of perturbations in heat and freshwater fluxes is confined to the polar region. The region of influence extends to include the northern hemisphere subtropical gyre over the second decade. Equivalent patterns would have been very difficult to generate with traditional

perturbation methods. The model was discretized on a $20 \times 40 = 800$ point grid in this single basin experiment. Imposing a perturbation in the freshwater flux at each point would have required 800 "forward" perturbation experiments. The efficiency of the adjoint method is even more evident when considering the number of perturbation experiments required to reproduce the sensitivity to the zonal velocity field: $20 \times 40 \times 15 = 12000$. Furthermore, the adjoint model calculates the sensitivity to all initial conditions and parameters in a single integration, there is no need to run separate experiments to obtain the sensitivity to, for example, wind stress and velocity.

Chapter 3

Adjoint Sensitivities and Surface Forcing

3.1 Introduction

The objective of this chapter is to use a single basin model to explore the influence of the surface boundary conditions on the sensitivity fields obtained with the adjoint model. The first set of simulations neglects wind stress forcing and includes only buoyancy as the direct forcing of the thermodynamic fields. The changes induced when wind stress is included will be analyzed in the second series of calculations. The role played by the formulation of the surface buoyancy forcing, from restoring the sea surface temperature and salinity toward observations to imposing fixed heat and freshwater fluxes will be examined third. The objective of the analysis will, in all cases, be the sensitivity of the meridional overturning streamfunction, diagnosed where it reaches its maximum, to the relaxation sea surface temperature or salinity, or alternatively the heat and freshwater fluxes. To obtain a more complete picture of the relevant physical mechanisms, this analysis will be complemented by examining the sensitivity of the overturning's strength to the zonal wind stress and to iso- and diapycnal mixing, and to the thickness diffusion parameter of the Gent Mc-Williams scheme.

The forward model and the construction of its adjoint were described in chapter 2. Changes in circulation from the reference case obtained under mixed boundary conditions and shown in Fig.2-2, 2-3, 2-4 will be noted in the preamble to each section.

3.2 Diagnostic Analysis using Green's Functions

Diagnostic analyses were performed by choosing the points that exhibited the largest or most interesting sensitivities, and perturbing the relevant parameter at those points. The Green's function $G(\mathbf{x}|\mathbf{x_0})$ is the field at the observer's point $\mathbf{x}$ caused by a unit point source at the source point $\mathbf{x_0}$. The Green's function for an abstract operator $\mathcal{A}$ is:

$$\mathcal{A}G(\mathbf{x}|\mathbf{x_0}) = -4\pi\delta(\mathbf{x} - \mathbf{x_0}) \tag{3.1}$$

The corresponding Green's function for the adjoint operator is:

$$\tilde{\mathcal{A}}\tilde{G}(\mathbf{x}|\mathbf{x_0}) = -4\pi\delta(\mathbf{x} - \mathbf{x_0}) \tag{3.2}$$

The two Green's functions are directly related:

$$G(\mathbf{x}|\mathbf{x_0}) = \tilde{G}(\mathbf{x_0}|\mathbf{x}) \tag{3.3}$$

The left-hand side describes the effect at location $\mathbf{x}$ of a point source at $\mathbf{x_0}$, the propagation from $\mathbf{x}$ to $\mathbf{x_0}$ being governed by the operator $\mathcal{A}$. On the right-hand side, the source is at $\mathbf{x}$ and the effect is measured at $\mathbf{x_0}$, the propagation is governed by the adjoint operator $\tilde{\mathcal{A}}$. In other words, the effect of point source on a diagnostic calculated with the forward model is, in theory, the same as the sensitivity at that location calculated with the adjoint model.

The use of this traditional Green's function approach has three advantages:

- It allows one to observe the details effects of a perturbation on all model variables.
- Provided that the direct perturbation is small, it allows a verification of the accuracy of the sensitivities derived with the adjoint method.
- If both adjoint and finite difference sensitivities are equivalent for a small finite perturbation, the limits of the linearity assumption, which underlies the construction of the adjoint code, can be tested by increasing the perturbation until the finite difference sensitivity is no longer accurate. This avenue was, however, not extensively pursued.

The accuracy of the adjoint model was estimated by comparing adjoint and finite different sensitivities. For a 400 year integration of the single basin model, the difference between

the two methods, using 1% or 10% perturbations in the parameter value was on average 2.6% and never worse than 8.2%. The distribution of the percentage difference between the finite difference estimation and the adjoint sensitivity is shown in Fig.3-1.

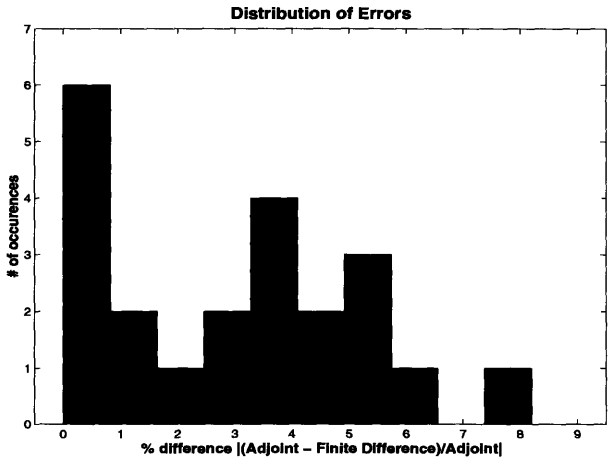

Figure 3-1: Distribution of the difference between the finite difference and the adjoint estimate of the sensitivity for 22 randomly sampled points and variables.

Because of its coarse resolution, this model does not contain any of the obviously non-linear processes such as eddy formation, shedding and re-absorption, which would limit the time scale over which the adjoint sensitivity would remain accurate. All remaining non-linear processes, notably advection and convection, appear easily linearized in this particular framework.

3.3 Adjoint Sensitivities under Pure Buoyancy Forcing

The first set of simulations relied on buoyancy alone to drive the overturning, the wind stress was set to zero. Both the sea surface temperature and the sea surface salinity were relaxed towards climatological values (Levitus and T.P.Boyer, 1994a,b) on a sixty day time scale.

$$BC_T = \lambda_T \left(T - \overline{T}_{obs} \right)$$

$$BC_S = \lambda_S \left(S - \overline{S}_{obs} \right)$$

where $\lambda_T = \lambda_S = \frac{1}{60 \text{ days}}$, $\overline{T}_{obs}$ and $\overline{S}_{obs}$ are zonally averaged observed sea surface temperatures and salinities.

3.3.1 Circulation

The flow exhibits many features that are qualitatively more symmetric with respect to the equator than the circulation when wind is included. A strong surface western boundary current exists in both hemispheres. Because of the absence of wind, these currents extend to the northern boundary in the northern hemisphere and to the northern limit of the circumpolar channel in the southern hemisphere. The flow then converges to two primary areas of downwelling: the northeast corner and the southernmost point along the eastern boundary. While the former point is the source of the abyssal waters of the basin and the southwestward return flow takes place below $1500\,m$, the latter is the source of a shallow overturning cell, which returns towards the western boundary no deeper than $500 - 700\,m$. The $3\,Sv$ of northern hemisphere deep water that penetrate into the southern hemisphere are forced to upwell underneath this shallow cell and return to the surface north of the equator. This flow pattern is overall quite similar to what was obtained by Klinger and Marotzke (1999) and Marotzke and Klinger (2000) in double hemisphere studies of the buoyancy driven circulation with no open channel.

The maximum intensity of the meridional streamfunction is $10.5\,Sv$, close to what was obtained when the wind stress is turned on ($11.5\,Sv$).

3.3.2 Cost Function

The cost function is the average value of the meridional overturning streamfunction, calculated over six points between $\phi = 60 - 64^\circ\,N$ and $1055 - 1785\,m$ where it peaks (z_B is the depth of the basin, λ is longitude):

$$\psi(\phi, z) = r \cdot \cos(\phi) \cdot \int_{\lambda_1}^{\lambda_2} \int_{z}^{z_B} v\, dz\, d\lambda \tag{3.4}$$

$$\psi_{MAX} = \overline{\psi}(60 - 64^\circ\,N; 1055 - 1785\,m) \tag{3.5}$$

Under relaxation boundary conditions, the sensitivity of the cost function, J, to the surface boundary conditions can be estimated from the following equations:

$$\frac{\partial J}{\partial BC_T} = \frac{\partial J}{\partial T_0}\frac{\partial T_0}{\partial BC_T} + \frac{\partial J}{\partial T_{obs}}\frac{\partial T_{obs}}{\partial BC_T} = \lambda\left(\frac{\partial J}{\partial T_0} - \frac{\partial J}{\partial T_{obs}}\right) \tag{3.6}$$

$$\frac{\partial J}{\partial BC_S} = \lambda \left(\frac{\partial J}{\partial S_0} - \frac{\partial J}{\partial S_{obs}} \right) \tag{3.7}$$

These equations contain two terms. The first is the sensitivity to the *initial value* of the sea surface temperature or salinity, a term that will naturally decay over the course of the integration as information about the initial state becomes less and less relevant. The second term is the parametric sensitivity to the restoring sea surface temperature and salinity. This term asymptotes to a constant value over time and will rapidly dominate the sensitivity pattern.

The other parameters, which will be examined, are the dia- and isopycnal mixing coefficients and the thickness diffusion. These parameters are three-dimensional arrays with the same value at every point ($\kappa_d = 3 \cdot 10^{-5}\ m^2\, s^{-1}$; $\kappa_i; \kappa_{td} = 1000\ m^2\, s^{-1}$). This allows a determination of the response of the cost function to a perturbation in these parameters at any point in the model. The linearization provided by the adjoint model allows a representation of the sensitivity as a two-dimensional map, latitude vs. longitude, by simply adding the sensitivities in the vertical direction. The response to a global perturbation in the mixing coefficient can be estimated by adding the sensitivities in all three directions.

3.3.3 Diapycnal Mixing

Figure 3-2 shows the two-dimensional pattern of sensitivity to diapycnal mixing, it represents the response of a perturbation applied throughout each individual water column. Three regions play an important role: the eastern and western boundaries and the tropics.

Tropical Dynamics

The pattern in Fig.3-2 shows clearly that the sensitivity of the overturning to mixing increases from the poles towards the tropics and peaks at $6 - 10^\circ\, N$. The only region of negative sensitivity is found north of $60^\circ\, N$.

Scott and Marotzke (2001) anticipated this result and explain it in terms of an advective-diffusive balance (equation 3.8); the energy supplied to mixing allows to return to the surface the abyssal waters formed in the northern part of the basin.

$$w \frac{\partial \rho}{\partial z'} = \frac{\partial}{\partial z'} \kappa_d \frac{\partial \rho}{\partial z'} \tag{3.8}$$

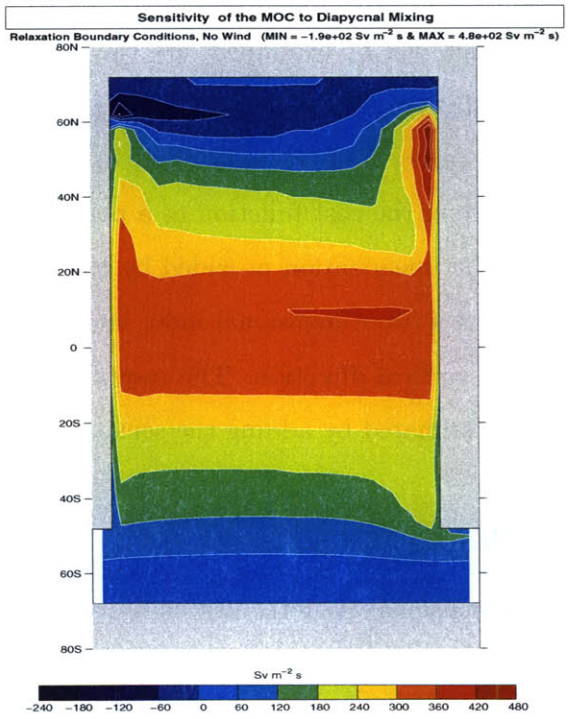

Figure 3-2: Sensitivity of the maximum value of the streamfunction ψ_{MAX} to the diapycnal mixing: $\frac{\partial \psi_{MAX}}{\partial \kappa_d}$ in $Sv\, m^{-2}\, s$; Relaxation boundary conditions, no wind. This figure represents the response of a perturbation applied throughout each water column.

z' is the direction perpendicular to the surfaces of constant density. In the tropics, this is very nearly the vertical direction.

The vertical temperature gradient is everywhere positive (temperatures increase upwards) and the diapycnal mixing coefficient is constant in the vertical direction. This leaves only two possible scenarios: the downward mixing of heat ($T_{zz} > 0$) must be balanced by upward motion ($w \cdot T_z > 0$) and the upward mixing of heat ($T_{zz} < 0$) by downward motion ($w \cdot T_z < 0$). One can a priori expect the sensitivity to diapycnal mixing to be positive where it induces upward motion and negative where it induces downward motion. Scaling the advection-diffusion equation yields an upwelling velocity proportional to the diapycnal mixing and inversely proportional to the thermocline depth δ, ($W \propto \frac{\kappa_d}{\delta}$). Diapycnal mixing is most efficient in the tropics because of the greater stratification in that region and the greater amount of heat, which diffuses into the thermocline. There is no ventilated thermocline in this setup but only a vertical structure where advection and diffusion largely balance one another, at least in the interior (Fig.3-3).

Without wind forcing, upwelling takes place in the entire tropical region, with only a narrow region of downwelling near the surface driven by mass convergence along the equator. This allows each point in a broad region from 10° S to 20° N to have an almost equally large impact on the overturning. The maximum sensitivity is found in a band at 10° N where the relaxation temperatures, and hence the surface temperatures, are the warmest. The eastern half of the basin exhibits greater sensitivities because vertical advection balances a larger fraction of the local heat gain by the ocean, horizontal heat advection is more important in the western half of the basin.

The depth dependency of the sensitivity pattern, shown for a sample column at 14° N in the middle of the basin (right-hand panel in figure 3-3), indicates that the overturning will respond most vigorously to perturbations applied between 200 and 500 m depth. An analysis of the vertical heat budget, the left-hand panel of the same figure, confirms that the maximum diffusive heat flux is taking place at the depths where the maximum sensitivities are observed. Two- to three hundred meters is the depth where the transition between the relatively uniform near-surface temperature gradients and the very small abyssal gradients takes place.

The magnitude of the perturbation in the overturning, which could be induced by perturbing the diapycnal mixing over the equatorial and tropical regions, can easily be esti-

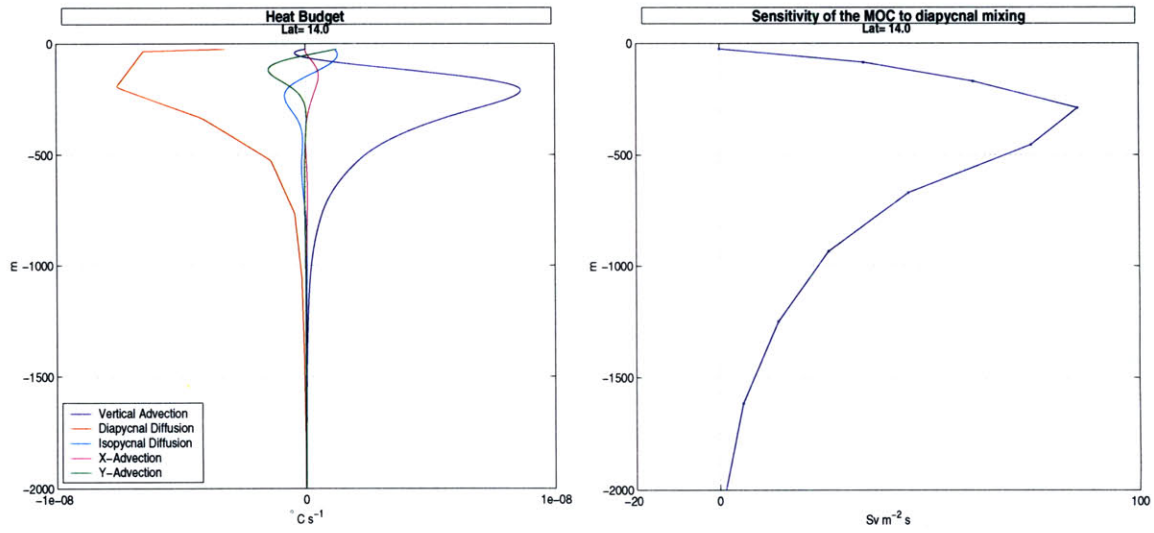

Figure 3-3: Left: Vertical profile of the heat budget at $14^\circ\ N$ in the the middle of the basin, all curves are in $^\circ C\, m^{-1}\, s$. The blue line represents vertical heat advection: wT_z; the red line represents diapycnal heat diffusion: $\sim \kappa_d T_{zz}$;the light blue line represents isopycnal heat diffusion: $\sim \kappa_i(T_{xx} + Tyy)$ the pink and green lines represents respectively heat advection in the x- and y- directions: uT_x, vT_y; Right Vertical profile of the sensitivity to diapycnal mixing $\frac{\partial \psi_{MAX}}{\partial \kappa_d}$ in $Sv\, m^{-2}\, s$ at $14^\circ\ N$ in the middle of the basin. Both plots represent the flow under relaxation boundary conditions with no wind forcing.

mated by summing the sensitivities over that region:

$$\Delta\psi = \left(\sum_{20^\circ S}^{20^\circ N} \frac{\partial \psi}{\partial \kappa_d} \right) \Delta\kappa_d$$

For a perturbation of 10% of the value of the mixing coefficient, $\Delta\kappa_d = 3 \cdot 10^{-6}\, m^2 s^{-1}$, the impact on the overturning is $\Delta\psi_{MAX} = 0.16\, Sv$. If the mixing was doubled, the overturning would increase by $1.6\, Sv$ due to that region alone. This may, however, be stretching the limits of the linearization, which underlies the adjoint model.

Eastern Boundary Dynamics

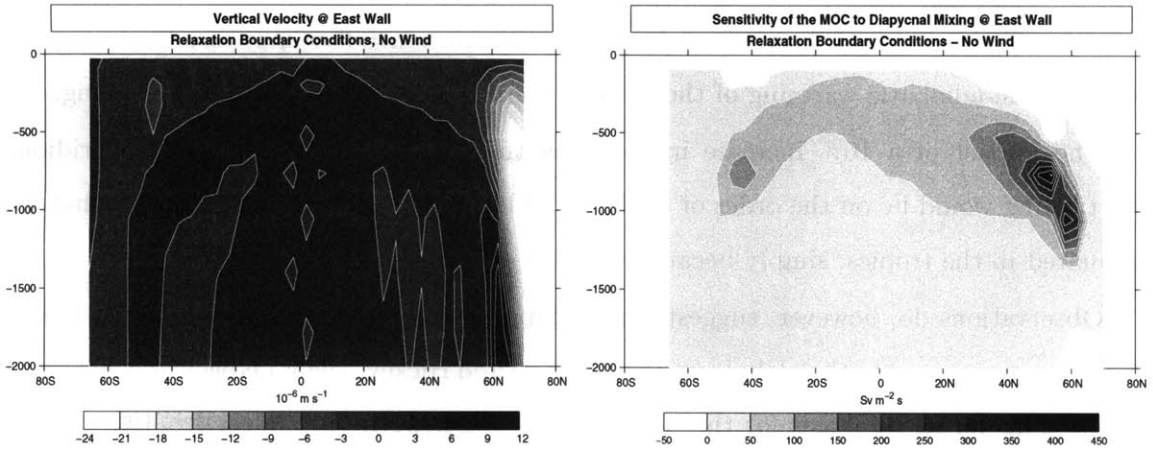

Figure 3-4: Left: North-South cross-section along the eastern wall of the vertical velocity, in $10^{-6}\, m\, s^{-1}$ Right: North-South cross-section along the eastern wall of the sensitivity to diapycnal mixing $\left(\frac{\partial \psi_{MAX}}{\partial \kappa_d}\right)$ in $Sv\, m^{-2}\, s$. Both plots were calculated under relaxation boundary conditions with no wind forcing

The source of the sensitivity to diapycnal mixing along the eastern boundary, shown in the right panel in Fig.3-4, follows the boundary between the "subduction zone" and the upwelling which lies beneath it (left-hand panel). This is where comparatively large temperature gradients and curvatures are created. This process is most efficient between $45^\circ\, N$ and $60^\circ\, N$ where large vertical velocities are observed. Vertical diffusion peaks just below the depth of the zero-crossing of the vertical velocity, it balances part of the upward advection below this region. A similar process can be observed along the downwelling region in the southern hemisphere.

Above this subduction zone lies an area of small negative sensitivities where the vertical heat flux is divergent ($T_{zz} < 0$). This process is, however, minor compared to the dominant balance between the advection of the zonal and vertical temperature gradients and horizontal diffusion:

$$uT_x + wT_z \approx \kappa_i \left(T_{xx} + T_{yy}\right)$$

The role played by the eastern boundary in determining the intensity of the meridional overturning was outlined by Scott and Marotzke (2001): downward diffusion of heat along the eastern wall increases the zonal temperature gradient, which in thermal wind balance equilibrates with a northward flow at the surface and a deep southward return flow.

The results obtained with the adjoint model suggest that the role of mixing in setting the East-West temperature contrast is limited to the region located at the base of the thermocline. The strength of the vertical shear in the North-South flow may also be determined by the quasi-adiabatic warming of the eastern boundary associated with downwelling.

The impact of a 10% increase in κ_d along the eastern boundary on the meridional overturning would be on the order of $+0.02\,Sv$. This is significantly smaller than what was estimated in the tropics, simply because the area of high sensitivities is smaller.

Observations do, however, suggest that mixing may be greatly enhanced along boundaries when compared to the global average (Ledwell and Hickey, 1995; Ledwell and Bratkovich, 1995). This forms the basis for the boundary mixing hypothesis (Marotzke, 1997), which would justify choosing a larger perturbation $\Delta\kappa_d$ in that region. This issue will be addressed more thoroughly in a more realistic setting (chapter 5).

Western Boundary Dynamics

The contrast between the warm waters, which are advected northward by the western boundary current, and the upwelling of cold water leads to large vertical temperature and density gradients. The shallow thermocline increases the efficiency of the diapycnal mixing of heat in that region. Note that the heat budget along the western boundary is by no means in vertical advective-diffusive balance, it is largely a balance between northward and vertical heat advection: $vT_y \approx -wT_z$, with the diabatic terms playing a smaller, yet not insignificant role (not shown).

The sensitivity of the overturning to diapycnal mixing along the western boundary,

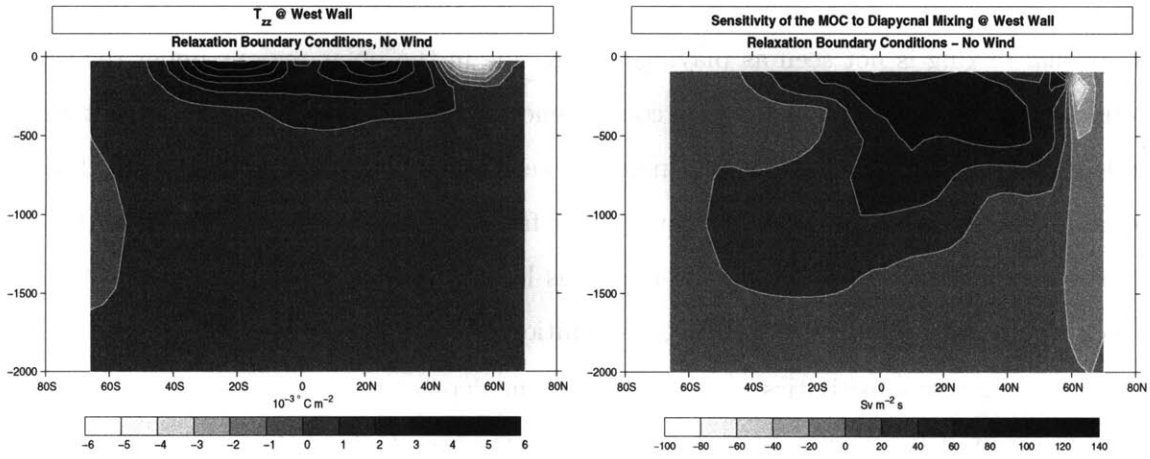

Figure 3-5: Left: North-South cross-section along the eastern wall of the vertical gradient of the vertical temperature gradient (T_{zz}), in $°Cm^{-2}$. Right: North-South cross-section along the western wall of the sensitivity to diapycnal mixing $\left(\frac{\partial \psi_{MAX}}{\partial \kappa_d}\right)$ in $Sv\,m^{-2}\,s$. Both plots were calculated under relaxation boundary conditions with no wind forcing

right-hand panel in Fig. 3-5, is significant down to a depth of $500\,m$, which corresponds to the base of the thermocline, but positive throughout the water column. A localized increase in diapycnal mixing induces upward motion and cooling throughout the depth of the water column below the level of the perturbation. This upwelling is partially compensated locally, but a substantial fraction is compensated by increased downwelling along the eastern boundary. Much of the associated mass transport is in the zonal direction, but a small fraction projects onto the meridional plane and contributes to enhancing the overturning. This meridional transport is also a necessary consequence of the warming associated with enhanced downwelling along the eastern boundary and cooling associated with upwelling along the western boundary. The increase in the zonal temperature gradient must, namely, be compensated by an increase in the meridional shear of the flow.

A localized maximum in sensitivity can be observed at $60°\ N$ along the western boundary. This is a very shallow process driven by a local surface temperature inversion. This inversion allows the upward advection of colder water to be balanced by upward heat diffusion This feature is not observed in most of the other simulations and is not deemed important.

Polar Dynamics

Diapycnal mixing is not seen as playing a large role in the polar regions under relaxation boundary conditions. This is a logical consequence of the small stratification in that region and of the fact that convection is a much more efficient way of mixing a vertical water column than diapycnal mixing. It is quite clear from Fig.3-5 that the definition of the cost function over the $60 - 64^{\circ}\,N$ latitude band has locally a large impact on the sensitivities, which would not be robust to a different definition of the diagnostic.

Small negative sensitivities are generated at the depth where the water exits the downwelling region of the Northeast to form a westward current along the northern boundary. This current then feeds into the northerly deep western boundary current. It is plausible that this cold current could be weakened by increased diapycnal mixing by increasing the mass loss out of the current ($\kappa_d' T_{zz} = w' T_z - \kappa_d T_{zz}'$). It is, however, difficult to imagine how this could be an important process overall since the stratification is small in high latitudes.

3.3.4 Isopycnal Mixing and Thickness Diffusion

In the version of the MIT OGCM that was used for this project, the same parameter represents both isopycnal mixing and the thickness diffusion and its associated tracer transport.

The Redi scheme diffuses tracers, temperature and salinity (here referred to generically as τ), along isopycnals (Adcroft and Hill, 2000):

$$\nabla \cdot \kappa_d \mathbf{K_{Redi}} \nabla \tau \tag{3.9}$$

This term is added to the tracer tendency equation. κ_d is the diffusivity in the along isopycnal direction. $\mathbf{K_{Redi}}$ is a tensor, which projects the gradient of τ onto the isopycnal surface.

The thickness diffusion (κ_{td}) is used, in the Gent Mc-Williams scheme, to parameterize the role played by geostrophic eddies in transporting tracers. This term is also added to the tracer tendency equation:

$$\nabla \cdot \tau \mathbf{u}^{\star} \tag{3.10}$$

The effect of eddies is represented by a "bolus" velocity $\mathbf{u}^{\star}$. The latter is defined as:

$$(u^\star, v^\star, w^\star) = \left(-\kappa_{td} \frac{\partial S_x}{\partial z}, -\kappa_{td} \frac{\partial S_y}{\partial z}, \kappa_{td} \left(\frac{\partial S_x}{\partial x} + \frac{\partial S_y}{\partial y} \right) \right) \tag{3.11}$$

S_x and S_y are the components of the isopycnal slope in the zonal and meridional directions.

Fig.3-6 represents the sensitivity of the meridional streamfunction's maximum to the sum of both processes.

Contrary to diapycnal mixing, which exhibits predominantly positive sensitivities, the sign of the sensitivity to isopycnal mixing and bolus transport changes throughout the domain. The overall effect of perturbations in κ_i and κ_{td} on the overturning is, therefore, much smaller than was the case for diapycnal mixing.

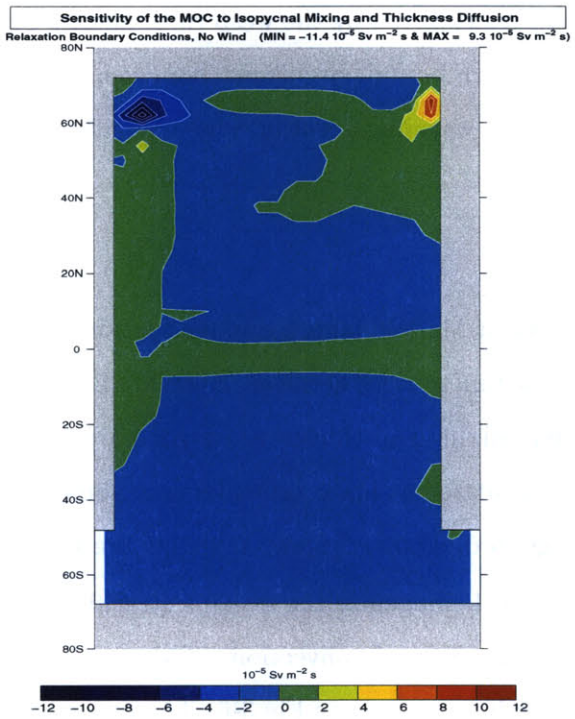

Figure 3-6: Sensitivity of the maximum value of the streamfunction ψ_{MAX} to the isopycnal mixing and thickness diffusion: $\frac{\partial \psi_{MAX}}{\partial \kappa_d} + \frac{\partial \psi_{MAX}}{\partial \kappa_{td}}$ in $Sv\, m^{-2}\, s$; Relaxation boundary conditions, no wind. This figure represents the response of a perturbation applied throughout each water column.

The sensitivity to isopycnal mixing and thickness diffusion is quite small in the tropics, a logical consequence of the small slope of the density contours in that region when compared to higher latitudes.

Western Boundary Dynamics

The sensitivity of the overturning to isopycnal mixing and thickness diffusion is positive in the western boundary current to a depth of $500\,m$ and negative in the deep western boundary current between 700 and $1400\,m$ (not shown here, but Fig.3-13 shows the depth dependency of the sensitivity to thickness diffusion for a case that includes wind) . A uniform 10% increase in κ_i in the western boundary current would increase the overturning's strength by approximately $0.02\,Sv$. A similar increase in the deep western boundary current would, however, weaken the overturning by approximately $0.015\,Sv$. The effect of a near surface increase in the thickness diffusion would be to draw heat laterally out of the current, thereby flattening the isopycnals and locally cooling the current. This cooling will tend to increase the east to west temperature contrast and enhance the overturning. It will also reduce the amount of heat transported by the western boundary current and cool the polar region. In the cold deep western boundary current, homogenizing isopycnals requires a flow of heat into the current. This warming eventually weakens the overturning.

Polar Dynamics

Isopycnal mixing and the Gent Mc-Williams parameterization undoubtedly play a large role in high latitudes. The cost function is, however, calculated between 60° and 64° N where the sensitivies to isopycnal mixing and thickness diffusion are the largest. An analysis with a different cost function calculated at lower latitudes (not shown) indicates that the results are not robust to a change in diagnostic. Some thoughts are nonetheless warranted.

By constantly working to homogenize the ocean's stratification, the GM parameterization is trying to counter the effect of convection. This would explain the large negative sensitivities around the northwest corner in Fig.3-6. The projection of the isopycnal mixing onto the vertical maintains the small stratification in that region. By removing potential energy, this "convection" weakens the meridional overturning, this effect is, however, small (Marotzke and Scott, 1999).

Sensitivities are also high, but positive along the eastern boundary near 60° N. This patch represents a sensitivity to isopycnal mixing in the 1000 to $2000\,m$ depth range. The large slope gradients present in that region are due to the adjacency of strong down- and upwelling (see Fig.3-4).

3.3.5 Relaxation Temperature and Salinity

The sensitivity of the overturning to the restoring sea surface temperature is negative in high latitudes , meaning that a cooling of the restoring temperature would enhance the overturning. Experiments with a different cost function, the heat transported by the meridional circulation in mid-latitudes, confirmed that the pattern of sensitivity is robust to the precise definition of the cost function, and systematically exhibit the same high latitude pattern (not shown).

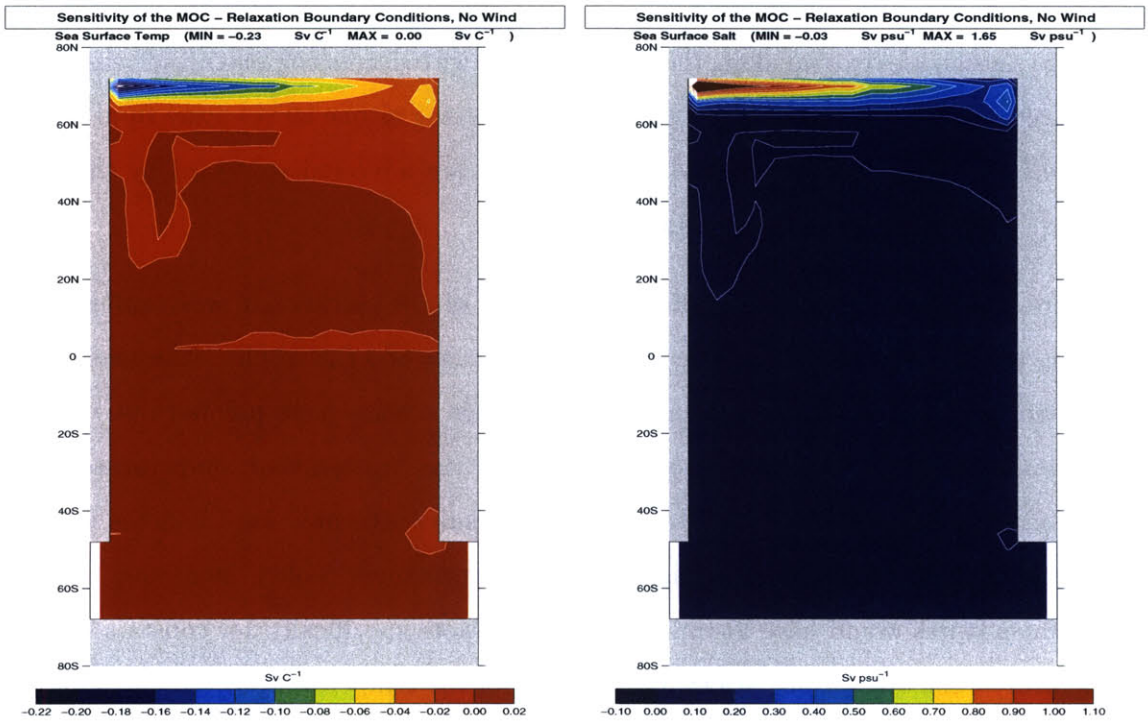

Figure 3-7: Sensitivity of the maximum value of the streamfunction ψ_{MAX} to the relaxation sea surface temperature: $\frac{\partial \psi_{MAX}}{\partial T_{obs}}$ in $Sv\,^{\circ}C^{-1}$ (left) and to the relaxation sea surface salinity $\frac{\partial \psi_{MAX}}{\partial S_{obs}}$ in Sv (right); Relaxation boundary conditions, no wind.

The sensitivity to the relaxation temperatures in Fig.3-7 as well as to the relaxation salinities have a clear maximum over the densest spot in the model, the northwest corner. This coincides with the site of the neutrally buoyant column. The sign is such that a decrease in the relaxation sea surface temperature, or an increase in the relaxation sea surface salinity increases the meridional overturning. The sensitivity pattern is therefore limited to regions where it can have a direct impact on the buoyancy of the basin's waters on very short

time scales. The relaxation time scale effectively erases the effect of a tempearture anomaly after a year at most; perturbations in the restoring sea surface temperature imposed away from the regions of convection and downwelling will be effectively erased before they can be advected towards those regions. The role of the northwest corner can be understood through its control of the temperature of the abyssal waters, $-0.5\,^{\circ}C$ in this basin. More specifically, by controlling the temperature of the deep western boundary current, the convecting corner can have an impact on the zonal temperature gradient below the thermocline and on the strength of the meridional overturning. The effect of salinity is smaller, but also works through its effect on the density of the deep water.

Large sensitivities extend along the northern wall, with decreasing magnitude eastwards, this reflects the decreasing impact of the buoyancy forcing as one moves away from the site of convection. Perturbations applied in that region are advected westward by the bolus transport of the GM parameterization.

There is a reversal in the sign of the sensitivity of the meridional overturning to the restoring temperature and salinity between high latitudes and the tropics. The sensitivities in the tropics are, howver, very small. A number or studies have pointed out that the overturning's strength scales as a positive power of the North-South temperature gradient(Zhang, 1998; Huang, 1999; Scott, 2000). The results presented here indicate that the overturning would only increase if high latitude temperatures cooled, increasing low latitude temperatures would have virtually no impact. More specifically, for constant tropical temperatures, the overturning scales as a function of the temperature in the northern part of the basin. This statement is, however, limited to perturbations in restoring temperature much smaller than those used by the authors cited above.

A small patch of large sensitivity can be seen along the eastern boundary at its southernmost point, this coincides with the site where shallow convection is allowing the formation of the southern hemisphere overturning cell. In this case, the part of the column, which is neutrally buoyant, coincides with the site of downwelling. For small perturbations in the buoyancy forcing, increasing this southern hemisphere cell would also enhance the northern overturning, a somewhat surprising finding, which disagrees with previously published results (Marotzke and Klinger, 2000). There is no southern hemisphere overturning in the experiments that include wind; this issue was, therefore, not pursued in detail.

3.3.6 Summary of Findings

As anticipated, diapycnal mixing plays a dominant role in the tropical regions while isopycnal mixing and thickness diffusion play a greater role in high latitudes, both are important along the large isopycnal slopes of the western boundary current. The important role played by the tropics seems to confirm the thermodynamic principles outlined by Sandström (1908), Jeffreys (1925) and Munk and Wunsch (1998): upward advection of heat is balanced by downward diffusion. The strength of the meridional overturning is then determined by the power available to return the fluid to the surface across the ocean's stratification. Note that this "diffusion" is only a crude parameterization for small scale mixing thought to be related to the breaking of internal gravity waves and internal tides (Gregg, 1987; Polzin et al., 1997).

As observed by Scott (2000) in a model forced by buoyancy alone, enhancing the downward mixing of heat along either boundary in mid-latitudes will sustain a more intense overturning than enhancing it in the middle of the basin. The eastern boundary sustains the overturning through downwelling in the thermocline and diffusive warming of the boundary below it. The role of the western boundary seems closely related to the strength and heat transport of the western boundary current, which here extends to the northern boundary. Because sensitivities are large over a broad area in the tropics, the effect of a perturbation is greatest in that region. Perturbing each boundary region individually has approximately the same impact on the overturning, one that is smaller than the effect of a perturbation in the tropics. A 10% increase in the magnitude of the vertical mixing over the entire basin yields a $\Delta\psi \sim 0.34\,Sv$ increase in the magnitude of the overturning.

The sensitivity to the buoyancy forcing is geographically limited to the region that sets the temperature of the abyssal waters along the western boundary, again in direct relation with the thermal wind balance.

3.4 The Role of Wind Forcing

This set of simulations seeks to analyze the impact of a zonally averaged wind forcing, which is derived from observations (Jiang et al., 1999), on the circulation and on the sensitivity patterns. The boundary conditions imposed on the surface temperatures and salinities are the same as in the pure buoyancy forcing simulations.

3.4.1 Circulation

There are a number of notable differences in the circulation pattern when wind is included, notably the presence of gyres and the separation of the western boundary current from the coast at $50° N$. There is a strong eastward current in the circumpolar channel and 2 to $3 Sv$ of deep water upwells in the open channel (see Fig.2-4). The thermocline structure is now the product of a wind driven ventilated thermocline as well as a diffusive internal thermocline (Samelson and Vallis, 1997). The northern hemisphere overturning intensity increases slightly when compared to the no wind case ($+1 Sv$). This model is less sensitive to wind forcing than that of Tsujino and Suginohara (1999), who observed a significant increase in the strength of the overturning when wind forcing was included. The structure of the overturning cell is quite similar to the no wind case, convection takes place in the northwest corner and downwelling in the northeast. There is no overturning cell in the southern hemisphere.

3.4.2 Diapycnal Mixing

The two most notable differences, which can be observed when wind is added to the forcing parameters, are in the eastern equatorial region and along the western boundary. The patterns are otherwise quite similar, notably the dynamics along the eastern boundary.

Equatorial Dynamics

The co-location of the local sensitivity maximum to both diapycnal mixing (Fig. 3-10) and zonal wind stress (Fig. 3-14) in the eastern equatorial region can be explained by the role played by the easterlies in lifting the thermocline on the eastern side of the basin and deepening it on the western side (Pond and Pickard, 1983). The divergence of the Ekman transport at the equator and its associated upwelling further reduce the depth of the thermocline in that region and increase the efficiency of the downward diffusion of heat. Both effects can be observed in the East-West section of T_{zz} at $2° N$, the left hand side in Fig. 3-8, which is for reference plotted against the equivalent profile obtained without wind (right-hand side). (Note that under relaxation boundary conditions temperature plays a dominant role over salinity in determining the vertical buoyancy gradients in the tropics). The $\kappa_d \cdot T_{zz}$ term in the equatorial heat budget (Fig.3-9) is close to being an order of

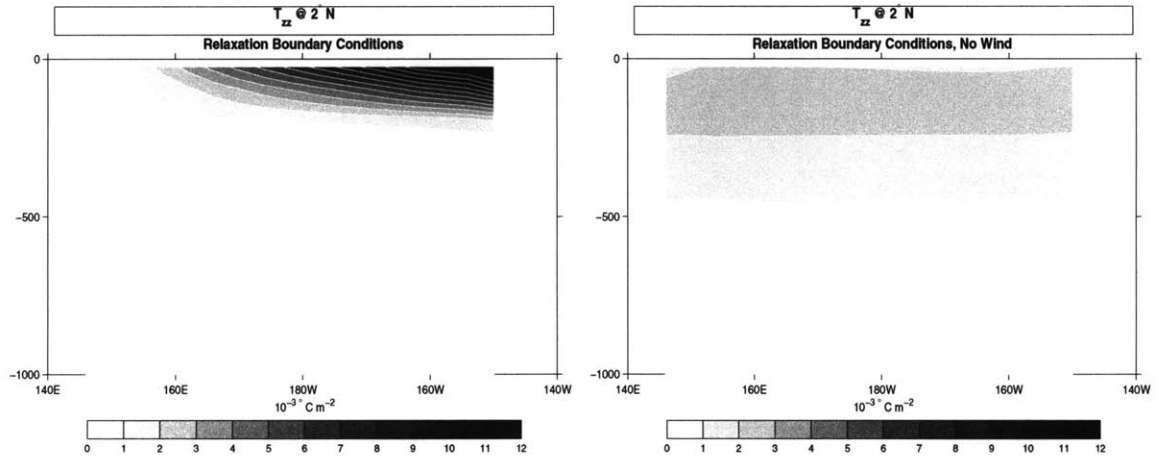

Figure 3-8: Vertical section along $2° N$ latitude of the second derivative of the vertical temperature gradient T_{zz}, in $°Cm^{-2}$. Left: Relaxation boundary conditions with wind forcing. Right: Relaxation boundary conditions with no wind forcing.

magnitude larger than it was in the no-wind simulation (Fig.3-3). The sensitivity maximum in the eastern equatorial region increases from $3.6 \cdot 10^2 \frac{Sv}{m^2 s^{-1}}$ under pure buoyancy forcing and relaxation boundary conditions to $5.2 \cdot 10^2 \frac{Sv}{m^2 s^{-1}}$ when wind is present.

The vertical profile of the sensitivity pattern, shown on the right in Fig. 3-9 for the point of maximum sensitivity at $2° N$, indicates that the maximum value is confined to the near surface, confirming that the sensitivity is related to the shallow Ekman suction process. Contrary to the no wind case, the overturning is less sensitive to mixing in the regions of Ekman pumping (North of $15° N$ and South of $5° S$).

While wind plays a role in determining the large sensitivity to mixing near the surface, it also determines much of the thermocline's stratification. The two thermocline structure outlined by Samelson and Vallis (1997) and Vallis (2000) is clearly visible in profiles of the vertical temperature gradient. The region sandwiched between the upper ventilated thermocline and the lower internal thermocline at a depth of approximately $500\,m$ exhibits very large curvatures in the temperature profile and corresponds to the location of the secondary maximum in sensitivity to diapycnal mixing.

An analysis of the vertical heat budget (Fig.3-9) highlights many of these features. The vertical advective-diffusive balance holds approximately below the ventilated thermocline. The influence of the advective terms in the uppermost $200 - 300\,m$ of the thermocline is much greater than without wind forcing. It is, however, also in this near-surface layer that

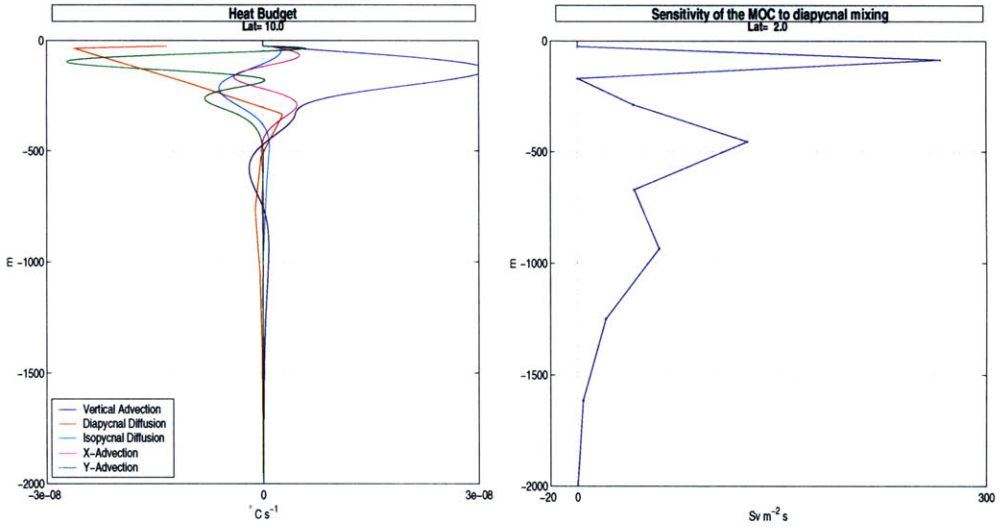

Figure 3-9: Left: Vertical profile of the heat budget at $10°\ N$ in the the middle of the basin, all curves are in $°C\, m^{-1}\, s$. The blue line represents vertical heat advection:wT_z; the red line represents diapycnal heat diffusion: $\sim \kappa_d T_{zz}$;the light blue line represents isopycnal heat diffusion: $\sim \kappa_i(T_{xx} + Tyy)$ the pink and green lines represents respectively heat advection in the x- and y- directions: uT_x, vT_y. Right: Vertical profile at $2°\ N$ along the eastern boundary of the sensitivity to the diapycnal mixing $\left(\frac{\partial \psi_{MAX}}{\partial \kappa_d}\right)$, in $Sv\, m^{-2}\, s$; Relaxation boundary conditions with wind forcing.

the heat diffusion term is the largest.

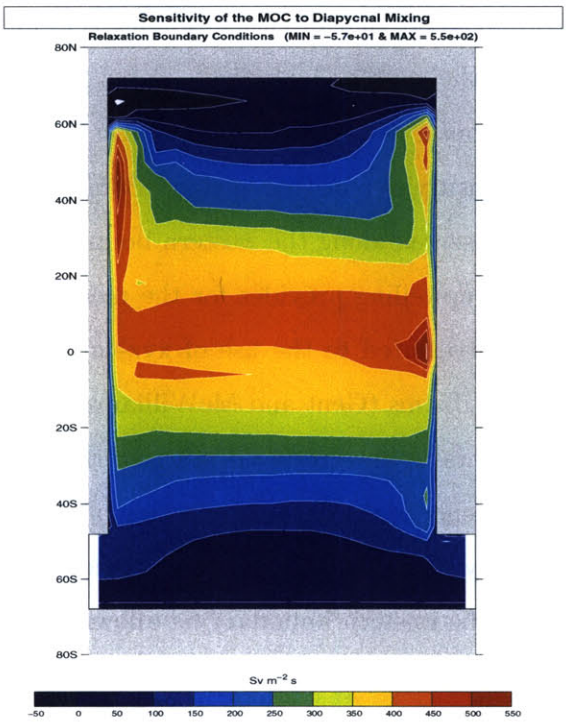

Figure 3-10: Sensitivity of the maximum value of the streamfunction ψ_{MAX} to the diapycnal mixing: $\frac{\partial \psi_{MAX}}{\partial \kappa_d}$ in $Sv\, m^{-2}\, s$; Relaxation boundary conditions, wind. This figure represents the response of a perturbation applied throughout each water column.

While the sensitivity is concentrated along the equator and close to the surface when wind is included, the overall effect of a perturbation in diapycnal mixing in the tropics on the overturning remains quantitatively similar to what was estimated in the no wind scenario.

Western Boundary Dynamics

While the sensitivity to mixing along the eastern boundary is similar in both the wind and no-wind simulations, the sensitivity at the western boundary is greatly enhanced and dominates when wind forcing is added to the model. This factor was absent in the model used by Scott and Marotzke (2001) when they analyzed the sensitivity of the overturning strength to the location of diapycnal mixing. The effect of a uniform perturbation $\Delta\kappa_d = 3{\cdot}10^{-6}\, m^2 s^{-1}$ imposed in that region increases from $0.015\, Sv$ in the no-wind case to $0.024\, Sv$ when wind is included.

A large fraction of the 11 Sv of bottom water formed in the northern part of the basin upwells in the northern hemisphere, only about 5 Sv cross the equator (Fig. 2-3). The circulation at the western wall shows that intense upwelling is taking place between 20° and 40°N, thereby strengthening the western boundary current through vertical mass convergence as well as through horizontal re-circulations (Colin De Verdière, 1988). It is therefore not a surprise to see large sensitivities in that region. Böning et al. (1995) discussed the "excessive" upwelling often observed along the western boundary in ocean models, and the effective shortcut, which this upwelling provides for the meridional overturning. Much of this spurious upwelling was attributed to the use of xyz- mixing schemes, and the introduction of the Gent and McWilliams (Gent and McWilliams, 1990), which is used in all of the present simulations, appears to have resolved much of this issue. More recently, Huck et al. (1999) analyzed the influence of the parameterization of lateral boundary layers on the thermohaline circulation. They concluded that more sophisticated frictional closures further reduced the upwelling along the western boundary by allowing horizontal recirculations of geostrophic currents impinging along the coasts.

At 200 m, the depth of the clear maximum, the sensitivities are three times larger than in the no wind case. Sensitivities drop off north of 50° N, in direct relation with the western boundary current, which separates from the coast at that latitude. The depth dependency of the pattern is interesting in that high sensitivities are systematically observed in the currents, which feed into the western boundary current. This takes place at 10° N at 200 m, at 20° N and along the equator at 335 m and at $20-30°$ N and 20° S at a depth of 525 m.

The mechanism responsible for those high sensitivities along the western boundary is the local maximum in $|T_{zz}|$ observed between 40° and 60° N, and the associated increased effectiveness of the diapycnal mixing process. The high upwelling velocities have the effect of compressing the isotherms and sharpening gradients in that region. The T_{zz} section, shown with the sensitivity field along the western boundary in Fig.3-11, has a clear maximum in the uppermost $200-300\,m$ of the western boundary current. While heat can effectively be mixed downwards in that region, it is nowhere implied that the western boundary current is in vertical advective diffusive *balance*, meridional and vertical advection are in fact the dominant terms in the heat budget.

A perturbation in diapycnal mixing induces a local diffusive warming at the location of

the perturbation (if $T_{zz} > 0$) and cooling above it. The response to this localized disturbance can be treated similarly to the response to a positive potential vorticity anomaly. The perturbation will be anticyclonic at the level of the perturbation and cyclonic above and below it. The associated perturbation to the temperature field will be a cooling above and below the perturbation and vertical flow towards the anomaly. The vertical depth of penetration of this perturbation is given by the Rossby height $\sim \frac{Lf}{N}$. Given the small stratification of the deep ocean, the perturbation reaches the bottom of the basin. The equilibrated response to much of this anomalous upwelling preferably takes place along the eastern, and to some extent, the northern boundary. The induced flow perturbation is, therefore, primarily zonal, but projects somewhat onto the meridional plane where it contributes to enhancing the overturning.

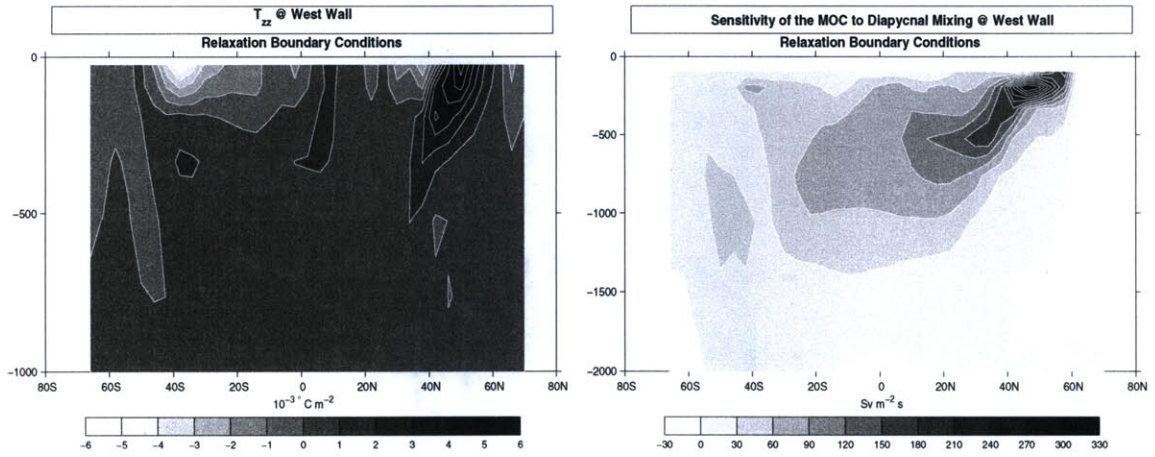

Figure 3-11: Left: Curvature of the vertical temperature ($T_z z$ in $°C\,m^{-2}$) along the basin's western boundary. Right: Sensitivity of the streamfunction maximum to diapycnal mixing $\frac{\partial \psi_{MAX}}{\partial \kappa_d}$ in $Sv\,m^{-2}\,s$ along the western boundary.

3.4.3 Isopycnal Mixing and Thickness Diffusion

Besides the stronger sensitivity in the region of the western boundary current near $40°\ N$ the pattern of sensitivity to isopycnal mixing and thickness diffusion is similar to what was observed in the absence of wind forcing (Fig.3-12).

The western boundary current is unsurprisingly the region where isopycnal slopes are the largest. The isopycnal thickness gradients are larger when wind forcing is included,

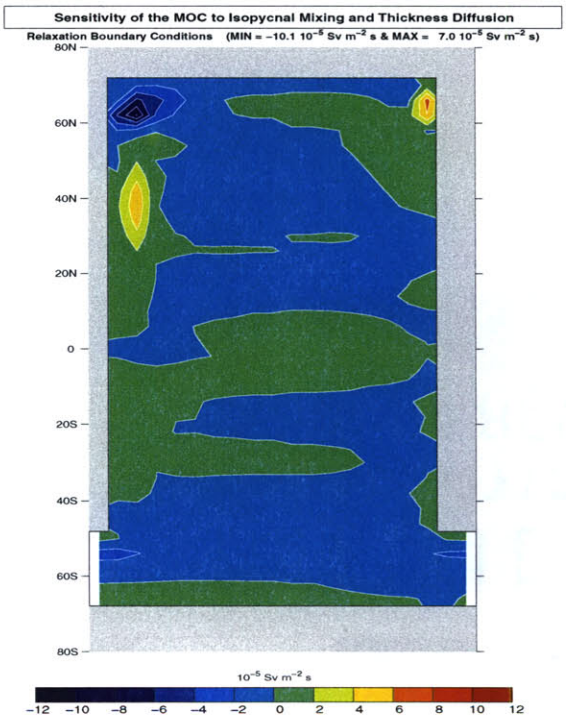

Figure 3-12: Sensitivity of the maximum value of the streamfunction ψ_{MAX} to the isopycnal mixing: $\frac{\partial \psi_{MAX}}{\partial \kappa_i}$ in $Sv\, m^{-2}\, s$; Relaxation boundary conditions, wind. This figure represents the response of a perturbation applied throughout each water column.

primarily because the western boundary current is stronger in the latter simulation, but also because the separation of the western boundary current from the coast induces large temperature gradients in the meridional direction, as well as in the zonal direction. This explains to a large degree the increased sensitivity to thickness diffusion around $40 - 50° N$ when wind is included, and why the strong sensitivities do not extend north of $50° N$ (Fig.3-13, left). The reversal of direction in temperature gradients in the cold deep western boundary current explains the sign reversal of the sensitivity field. The meridional velocity field along the western boundary is shown for reference on the right of Fig.3-13, it's zero contour corresponds to the change in sign in the sensitivity plot. The mechanism used to relate a change in thickness diffusion to a change in overturning is otherwise similar to what was described in the absence of wind.

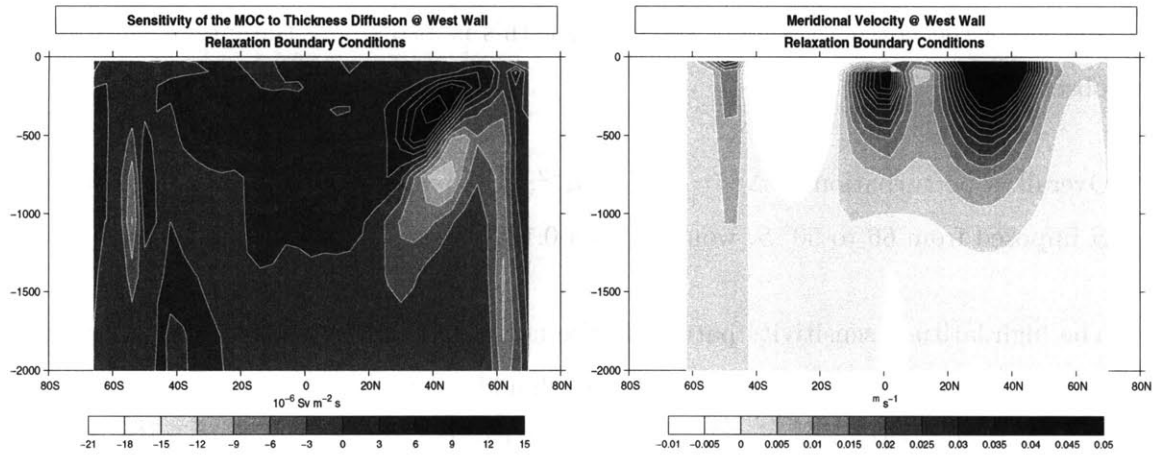

Figure 3-13: Left: Sensitivity of the streamfunction maximum to isopycnal mixing and thickness diffusion $\frac{\partial \psi_{MAX}}{\partial \kappa_i}$ in $Sv\, m^{-2}\, s$ along the western boundary. Right: Meridional velocity along the western boundary in $m\, s^{-1}$.

The negative sensitivities observed in the circumpolar channel are a logical consequence of the role played by the eddy transport in flattening isopycnals. In that region, the meridional streamfunction is sensitive to upwelling, hence the negative values in sensitivity observed between 300 and $1500\, m$ in the Deacon cell .

3.4.4 Wind Stress

With the exception of the eastern equatorial region and Ekman upwelling, the sensitivity pattern to wind stress is concentrated in high latitudes (Fig.3-14), in both hemispheres.

The role played by the southern latitudes is easiest to understand: it is clear from the behavior of the meridional streamfunction in Fig.2-3 (that figure displays the overturning obtained under mixed boundary conditions, but the result is not fundamentally different under relaxation boundary conditions) that a significant fraction of the deep water upwells in the latitudes of the channel. The Deacon cell is the product of wind stress divergence in that region. The wind stress peaks around $50°\ S$ (Fig.3-20), upwelling therefore takes place polewards and downwelling equatorwards of that latitude, this cell closes below the level of the sill, here set at a depth of $2500\,m$ (Toggweiler and Samuels, 1995). Although much of the Deacon cell is canceled by the eddy induced bolus velocity of the Gent-McWilliams scheme, the remaining circulation is sufficient to upwell between a third and a quarter of the deep water formed in the northern hemisphere, notably because it can draw up the water still lying below $2500\,m$. Peak upward velocities take place below $1500\,m$, both along the sill and along the northern edge of the channel, this is also where the largest sensitivities are observed.

Overall, a perturbation of $\Delta\tau_x = 0.01\,N\,m^{-2}$, approximately 10% of the wind stress at $55°\ S$ imposed from 66 to $50°\ S$, would yield a $0.12\,Sv$ increase in the overturning.

The high latitude sensitivity pattern in the northern hemisphere is strongly dependent on the local definition of the cost function and should not be considered as a robust feature of the sensitivity of the overturning. The high latitude pattern is, for example, different if the cost function is the heat transported by the meridional overturning circulation (not shown). The band of negative sensitivities along $60°\ N$ is related to the direct response of the flow to a westerly wind perturbation: a near surface northerly Ekman transport and balancing return deep geostrophic flow. This induced cell opposes the overturning directly and explains the negative values of the sensitivity. A positive zonal wind perturbation along the northern boundary would force upwelling along the boundary by driving water away from it. By cooling the boundary, wind perturbations could affect the buoyancy of the water in the Northwest corner.

This high latitude sensitivity pattern contasts with the results of Tsujino and Suginohara (1999). These authors attributed the enhancement of the overturning's strength observed when wind forcing was included to enhanced heating in the region of Ekman upwelling.

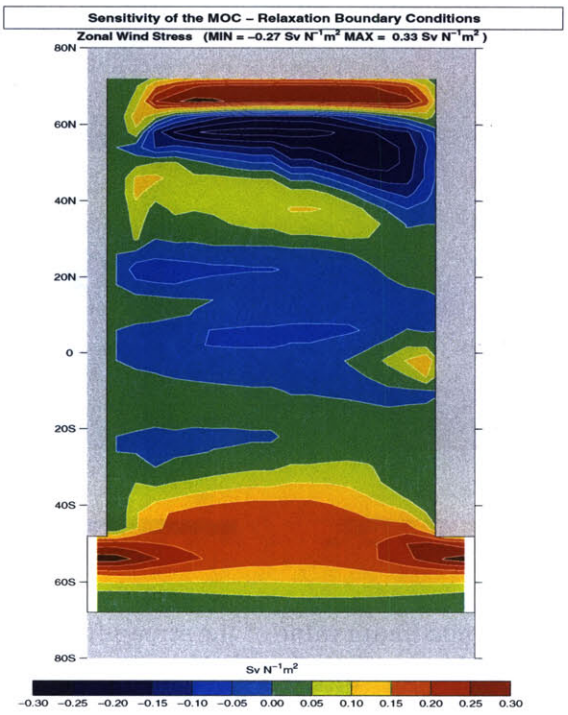

Figure 3-14: Sensitivity of the maximum value of the streamfunction ψ_{MAX} to the zonal wind stress: $\frac{\partial \psi_{MAX}}{\partial \tau_x}$ in $Sv\, N^{-1} m^2$; Relaxation boundary conditions, wind.

3.4.5 Relaxation Temperature and Salinity

The similarity between the patterns of sensitivity to the temperature and salinity relaxation terms in the wind and no-wind simulations indicates that the role played by the wind forcing has relatively little impact on the efficiency of the direct buoyancy forcing.

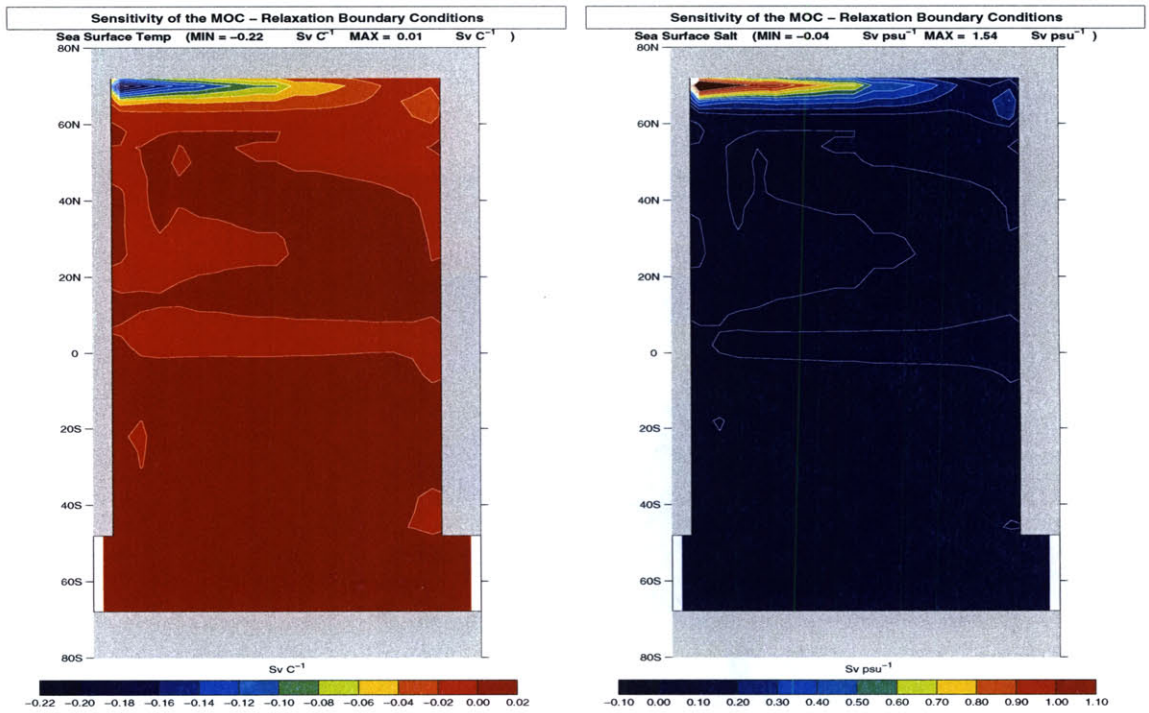

Figure 3-15: Sensitivity of the maximum value of the streamfunction ψ_{MAX} to the relaxation sea surface temperature and salinity: $\frac{\partial \psi_{MAX}}{\partial T_{obs}}$; $\frac{\partial \psi_{MAX}}{\partial S_{obs}}$ in $Sv\,°C^{-1}$; Sv; Relaxation boundary conditions, wind.

3.4.6 Summary of Findings

Three major changes are observed when wind forcing is added. The first is the increased sensitivity to diapycnal mixing in the eastern equatorial region, in direct relation with the role of the easterlies in setting thermocline depths in that region and equatorial Ekman upwelling. The second change is the heightened sensitivity to the wind itself in the open channel region, this effect is related to the presence of the Deacon cell and the upwelling associated with it. The third finding is the increase in sensitivity to mixing in the western boundary current region because of larger stratification.

3.5 The Role of Heat and Freshwater Forcing

This section seeks to illustrate and explain the differences in the sensitivity maps, which are obtained by imposing the same effective surface forcing, but formulating that forcing in a variety of ways. The circulation was initially spun up under mixed boundary conditions. The equivalent relaxation and flux boundary conditions, summarized in Table 3.1, were diagnosed after the initial equilibrium was reached (5000 yr). All simulations were performed with the same wind stress forcing.

Restoring BC	Mixed BC	Flux BC
$\lambda^{-1}\left(T - SST_{diag}\right)$	$\frac{\overline{Q_{obs}}}{\rho \cdot c_p \cdot \Delta z} + \lambda^{-1}\left(T - \overline{SST_{obs}}\right)$	$\frac{Q_{diag}}{\rho \cdot c_p \cdot \Delta z}$
$\lambda^{-1}\left(S - SSS_{diag}\right)$	$\left(\overline{E - P_{obs}}\right)\frac{S_{ref}}{\Delta z}$	$\left(\overline{E - P_{obs}}\right)\frac{S_{ref}}{\Delta z}$

Table 3.1: Formulation of the surface buoyancy forcing terms for mixed, restoring and flux boundary conditions. The bar refers to a zonal averaging over the Atlantic basin, $_{obs}$ refers to a field derived from observations (Levitus and T.P.Boyer, 1994a,b; Jiang et al., 1999), $_{ref}$ refers to a reference salinity (35) and $_{diag}$ refers to a field, which has been diagnosed from the spinup under mixed boundary conditions.

Under "mixed" boundary conditions, the net water flux at the ocean-atmosphere interface is prescribed. The heat flux boundary condition contains both the observed heat flux as well as a term relaxing temperatures towards climatology. The three simulations were designed to have the same effective flux of heat and freshwater at the ocean's surface, these fluxes are simply formulated in three different ways.

The heat flux field field under flux boundary conditions (Q_{diag}) was diagnosed from the effective exchange of heat taking place between the atmosphere and the ocean at the end of the spinup of the model under mixed boundary conditions, it is therefore different from the zonally averaged field used under mixed boundary conditions (Q_{obs}). Because the effective heat flux forcing at the ocean's surface remains constant, the flow differs very little from what is observed under mixed boundary conditions.

The fields used under restoring boundary conditions differ from those used in the previous sections. The sea surface temperature and salinity fields towards which the flow is relaxed are not derived from observations but diagnosed from the end of the spinup under mixed boundary conditions.

The ocean goes from having quasi-fixed surface temperatures and salinities under restor-

ing boundary conditions, to allowing first the salinity (mixed boundary conditions) then the temperature (flux boundary conditions) to evolve forced by precipitation and heat flux fields. The only quantities held fixed under flux boundary conditions are the amount of heat and freshwater entering the basin.

The mixed boundary conditions are thought to be the most realistic of the three formulations. The sea surface salinity has no influence on the atmospheric hydrological cycle, the boundary condition should therefore be formulated as a flux. The difference between the ocean and the atmosphere's temperatures does, however, influence the heat exchange at the ocean's surface. This is represented by the restoring term in the mixed boundary conditions. By providing the two extreme formulations, the idea was to determine which sensitivity patterns depended on the nature of the surface forcing, and which were independent of it. Note that restoring boundary conditions are often used in ocean only model studies.

Depending on the boundary conditions, the sensitivity to the restoring sea surface temperature, heat flux or a combination of the two will be examined. The sensitivity to the salinity forcing will be either the restoring sea surface salinity or the net precipitation field.

3.5.1 Circulation

The circulation pattern, which was shown in Fig. 2-3, is virtually identical under the three boundary formulations. Convective overturning of the water column takes place at the model's coldest point, the northwest corner. The actual downwelling and mass transport take place near the northeast corner and along the eastern boundary. The overturning peaks at $11.5\,Sv$ and the amount of heat transported northward by the circulation is $0.7\,PW$.

3.5.2 Diapycnal Mixing

The most striking difference between the sensitivity to diapycnal mixing observed under relaxation, and mixed or flux boundary conditions, is the increase in sensitivity in the equatorial region: $\frac{\partial \psi_{MAX}}{\partial \kappa_d} = 400 - 500\,Sv\,m^{-2}\,s$ under relaxation boundary conditions, $\frac{\partial \psi_{MAX}}{\partial \kappa_d} = 1200 - 1500\,Sv\,m^{-2}\,s$ under mixed or flux boundary conditions. The three cases are plotted on the same scale in Fig.3-16.

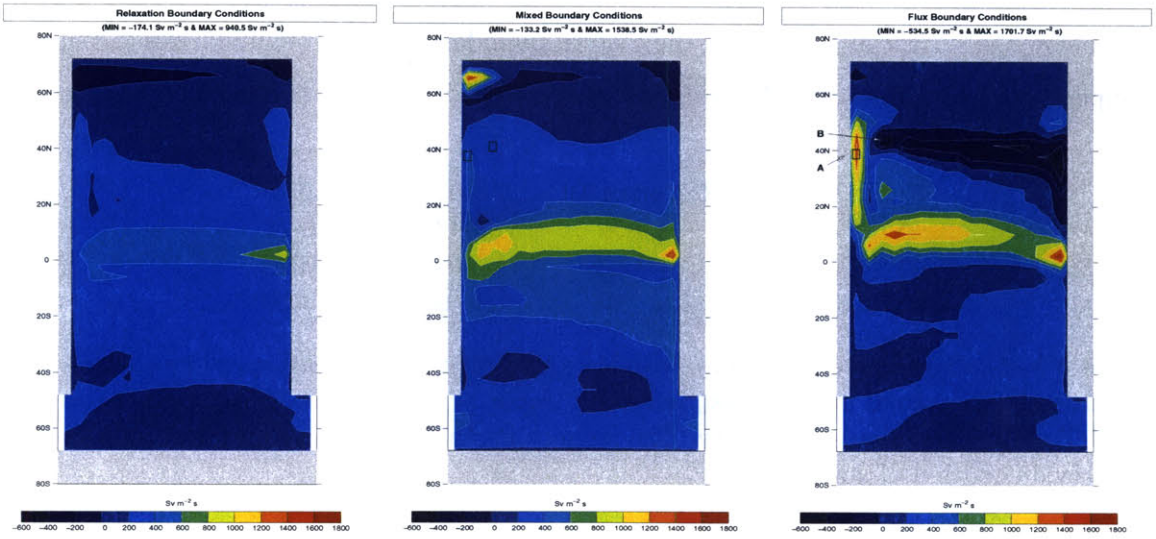

Figure 3-16: Sensitivity of the streamfunction maximum to diapycnal mixing $\left(\frac{\partial \psi_{MAX}}{\partial \kappa_d}\right)$ in $Sv\, m^{-2}\, s$. Left: Restoring boundary conditions. Middle: Mixed boundary conditions. Right: Flux boundary conditions. The three plots are on the same scale.

Tropical Dynamics

Near surface tropical sensitivities are, in all three cases, concentrated in the $0 - 10^{\circ}\, N$ latitude band where Ekman suction is taking place. This confirms the hypothesis outlined by Samelson and Vallis (1997) that the MOC is effectively insulated from buoyancy forcing by the ventilated thermocline in the region of the Ekman pumping.

The local maximum remains located at the eastern boundary because of wind induced coastal upwelling. It is however, twice as large under flux or mixed boundary conditions as in the restoring case. The entire equatorial region is generally much more sensitive when the surface density is not fixed. This is related to the effect that a perturbation in the diapycnal mixing can have on the vertical density profile and its gradients. Considering an extreme scenario in which the surface density is held fixed, increasing the diapycnal mixing could only reduce the vertical density gradients, thereby reducing the efficiency of the vertical advective-diffusive process. Under constant flux boundary conditions, the surface density is no longer fixed. An increase in the downward diffusion of heat can reduce the sea surface temperature, thereby at least maintaining vertical buoyancy gradients and the efficiency of the diffusion process. Restoring boundary conditions are obviously closer to the first scenario, while mixed boundary conditions present an intermediate case. Table 3.2 illustrates

this point. The diapycnal mixing coefficient is increased by 10% ($\Delta\kappa_d = 3 \cdot 10^{-6}\, m^2\, s^{-1}$) just below the surface at 2° N along the eastern boundary;Table 3.2 summarizes the surface temperature and salinity which result.

	Restoring BC	Mixed BC	Flux BC
ΔT ($°C$)	-0.069	-0.066	-0.22
ΔS	0.0064	0.039	0.023
$\Delta\rho$ ($kg\, m^{-3}$)	$1.8 \cdot 10^{-5}$	4.2 · 10−5	$6.1 \cdot 10^{-5}$

Table 3.2: Sea surface temperature, salinity and density perturbations induced by a perturbation in diapycnal mixing ($\Delta\kappa_d = 3 \cdot 10^{-6}\, m^2\, s^{-1}$) applied one level below the surface at 2° N along the eastern boundary. The density perturbation was estimated by using the linearized equation of state.

The surface buoyancy perturbation is smallest under restoring boundary conditions. It is interesting to note that salinity contributes approximately two-thirds of the overall buoyancy perturbation under mixed boundary conditions, but less than a third under flux boundary conditions. This is a direct consequence of the restoring term imposed on the surface temperature under mixed boundary conditions.

The similarity between the sensitivity maps under mixed and flux boundary conditions implies that the larger salinity perturbations compensate for much of the reduced changes in temperature.

It is in all cases the ability of the eastern boundary to carry Kelvin waves northward where they can transfer their energy into enhancing downwelling (McDermott, 1996), which allows the meridional overturning to show a global response to a perturbation initially localized along the equator.

Western Boundary Dynamics

The source of sensitivity to κ_d in the western boundary current is in all cases predominantly at $200\, m$, only partly at lower levels. The maximum sensitivity at 40° N and $200\, m$ is $240\, Sv\, m^{-2}\, s$ under restoring boundary conditions, $360\, Sv\, m^{-2}\, s$ under mixed boundary conditions and $1300\, Sv\, m^{-1}\, s$ under flux boundary conditions. These differences point to the heat flux and the constraint imposed on the sea-surface temperature as playing a key role in determining this pattern.

A Green's function perturbation analysis shows that a localized increase in the vertical

diffusion coefficient results in an increase in the downward diffusion of heat, with localized cooling above the perturbation. The dominant response in the perturbation heat budget comes through changes in the horizontal temperature field (the $v \cdot T'_y$ and $u \cdot T'_x$ terms) and more importantly for the overturning, through a perturbation in the vertical velocity ($w' \cdot T_z$). Most of the equilibrated response to a change in mixing is local, but part of it makes its way to the eastern boundary and produces a global impact on the overturning. The perturbation is communicated to the eastern boundary primarily through boundary and equatorial Kelvin waves. These waves convert their energy into a perturbation of the vertical flow in the northeast corner. Under flux boundary conditions, advection of perturbations in the rapid near-surface circulation can also generate a global response. Fig.3-17 shows the surface temperature response, under mixed (left) and flux (right) boundary conditions, to a near surface perturbation in κ_d. The perturbation is located at 38° N at the western wall. The perturbation is advected by the western boundary current and further northward into the polar basin. This process is, however, inhibited under mixed boundary conditions when compared to flux boundary conditions.

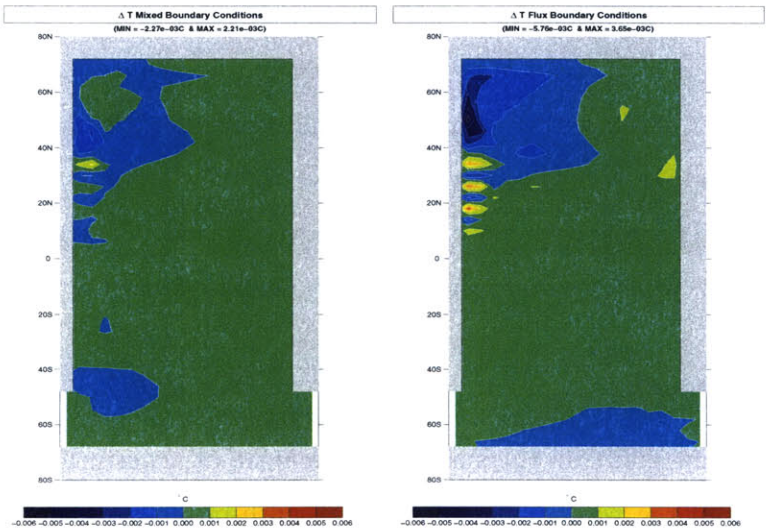

Figure 3-17: Equilibrated response (ΔT in $°C$) to a perturbation in diapycnal mixing imposed at 38° N at the western boundary at a depth of $95\,m$: $\Delta\kappa_d = 3 \cdot 10^{-6} m^2\, s^{-1}$. Left: Mixed boundary conditions. Right: Flux boundary conditions.

The key measure, which determines the magnitude of the response of the meridional streamfunction appears to be the magnitude of the temperature perturbation in the north-

west corner, above the convection site. The northeast corner, where downwelling takes place, is also important. The surface cooling in the western boundary current in Fig.3-17 quickly locks onto the site of convection. This allows the cooling to extend through the water column and forces enhanced clockwise recirculation along the northern boundary, with downwelling in the northeast corner. Although surface salinity perturbations are also observed, the effect of temperature perturbations is clearly dominant (Table 3.3). This explains why the sensitivities in the western boundary current are so much larger under flux boundary conditions.

	Mixed BC	Flux BC
ΔT $(°C)$	-0.0023	-0.0065
ΔS	0.00070	0.00031
$\Delta\rho$ (kgm^{-3})	$9.7 \cdot 10^{-7}$	$15.3 \cdot 10^{-7}$

Table 3.3: Sea surface temperature, salinity and density perturbations induced by a perturbation in diapycnal mixing ($\Delta\kappa_d = 3 \cdot 10^{-6}\, m^2\, s^{-1}$) applied one level below the surface at $38°\, N$ along the western boundary. The density perturbation was estimated by using the linearized equation of state.

The importance of the western boundary current as a determinant of the overturning's strength is directly related to its role as the dominant vehicle of Equator to Pole heat and mass transport. The sensitivity can be attributed to the effectiveness of the vertical diffusion process, and the variety of mechanisms, which allow a global response to a locally induced upwelling. This role does not cease at the western boundary itself, but extends to all of the tributaries, which feed into the western boundary current at various depths.

Mid-Latitude Dynamics

Figure 3-18 shows the effect on the surface temperature of a perturbation in κ_d imposed at $41°\, N$, $8°$ East of the western boundary at a depth of $500\, m$, under both mixed and flux boundary conditions. Under mixed boundary conditions the overturning's intensity is observed to decrease, it increases under flux boundary conditions. This was predicted in both cases by the adjoint model. In the first case, the cooling induced above the level at which the diffusion coefficient is increased is largely damped before the perturbation reaches the surface. Under flux boundary conditions, this perturbation extends to the surface and is advected to the northeast corner, where it reduces downwelling. The northwest corner

is in fact warmed under flux boundary conditions, while it experiences a slight cooling under mixed boundary conditions. This difference alone explains why the sensitivity of the meridional overturning to mid-latitude mixing is in one case negative and positive in the other.

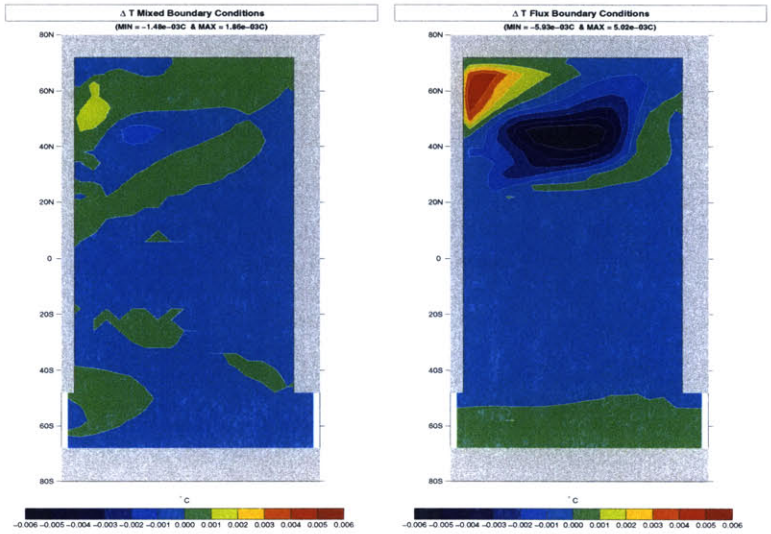

Figure 3-18: Equilibrated response (ΔT in $°C$) to a perturbation in diapycnal mixing imposed at 38° N, 8° east of the western boundary at a depth of $500\,m$: $\Delta\kappa_d = 3{\cdot}10^{-6} m^2\, s^{-1}$

Quantitative Comparison

This section has shown how important a careful formulation of the surface boundary conditions in climate modeling really is: the sensitivity of the meridional overturning to mixing changes in most locations by a factor of two or three, and sometimes changes sign when surface boundary conditions switch from restoring to flux forms. These changes can be attributed to two factors: restoring terms damp near-surface temperature and salinity perturbations *and* prevent them from being advected in the basin by the circulation.

Table 3.4 provides a quantitative estimate of the effect of a small perturbation, $\Delta\kappa_d = 3 \cdot 10^{-6}\, m^2\, s^{-1}$, applied over some of the key regions. The effect of a 10% global increase in diapycnal mixing would be to enhance the overturning maximum by $0.4 - 0.6\, Sv$. The overturning is most sensitive under mixed boundary conditions, primarily because there is a large area of negative sensitivity present under flux boundary conditions in mid-latitudes,

which is absent under mixed boundary conditions. As noted previously, the western boundary current region generates a greater response under flux boundary conditions than in the other cases. Approximately a third of the global response is generated in the $[2° N; 15° N]$ latitude band, and close to half in the $[15° S; 15° N]$ tropical region.

	Restoring BC	Mixed BC	Flux BC
Equator: $[2° N; 15° N]$	0.12	0.20	0.18
Tropics: $[15° S; 15° N]$	0.19	0.30	0.22
Western Boundary Region: $[2° N; 50° N]$	0.023	0.033	0.055
Total	0.42	0.60	0.42

Table 3.4: Estimated effect (in Sv) on the maximum value of the meridional streamfunction ψ_{MAX} of a $\Delta\kappa_d = 3 \cdot 10^{-6}\, m^2\, s^{-1}$ perturbation in the diapycnal mixing applied throughout a specific region.

3.5.3 Wind Stress

While the sensitivity to the wind forcing is concentrated in high latitudes under relaxation boundary conditions (Fig.3-14), the tropics dominate under mixed or flux boundary conditions (Fig.3-19).

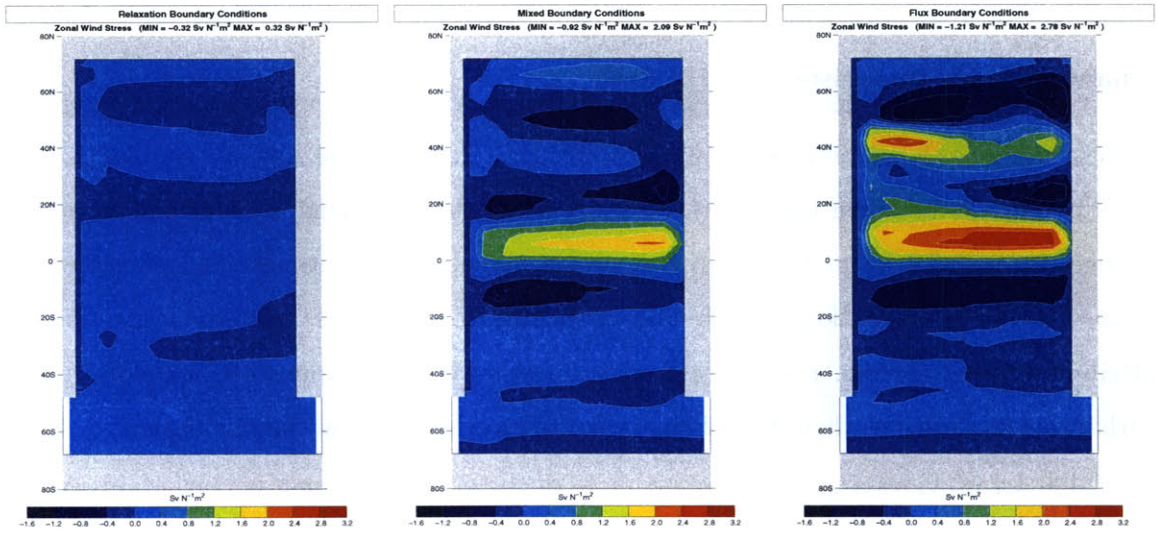

Figure 3-19: Sensitivity of the streamfunction maximum to the zonal wind stress $\left(\frac{\partial \psi_{MAX}}{\partial \tau_x}\right)$ in $Sv\, N^{-1}\, m^2$. Left: Restoring boundary conditions. Middle: Mixed boundary conditions. Right: Flux boundary conditions. The three plots are on the same scale.

Given the role played by Ekman pumping already highlighted within the context of the equatorial sensitivity to diapycnal mixing, it is not surprising to see that the latitudes at which the sensitivity bands switch from being positive to negative correspond to the zero crossings of the wind stress curl, shown for reference on the right in Fig. 3-20.

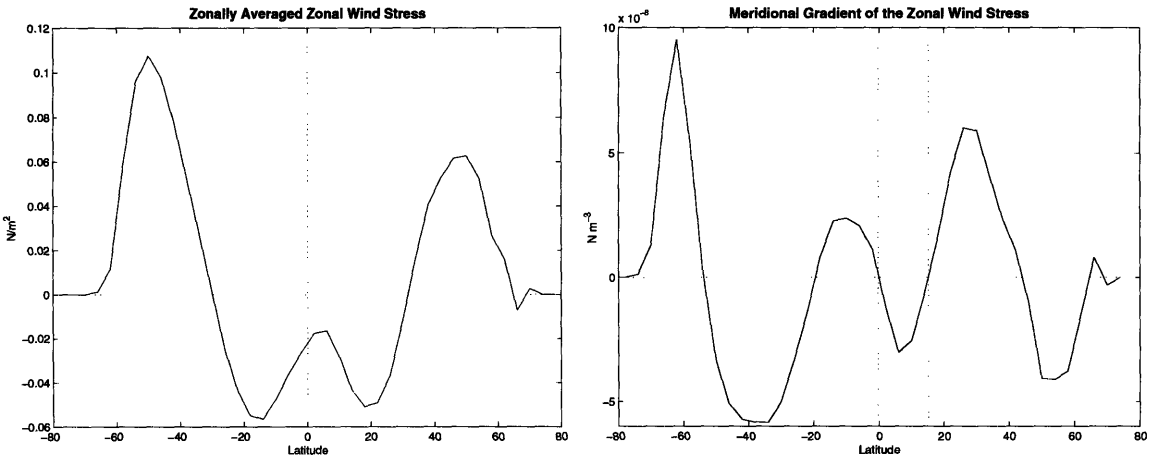

Figure 3-20: Left: Observed zonal mean wind stress (τ_x), in $N\,m^{-2}$. Right: Meridional gradient of the zonal wind stress ($\frac{\partial \tau_x}{\partial y}$), in $N\,m^{-3}$.

The polarity of the pattern is such that increasing the upwelling increases the overturning while enhancing the downwelling has the opposite effect. This effect will naturally decay towards the pole as the influence of shallow upwelling or downwelling on the structure of the thermocline decreases. This mechanism is similar to the one invoked by Tsujino and Suginohara (1999). It is, however, surprising that these authors obtained a strong sensitivity in the region of Ekman downwelling in a model forced with restoring boundary conditions. The tropical sensitivity pattern is here clearly enabled by the switch away from relaxation boundary conditions, notably because significant surface salinity perturbations are possible under mixed boundary conditions.

The role played by wind stress in the tropics is similar under mixed and flux boundary conditions. The most important new feature is the importance of the $40 - 50°\,N$ latitude band in the latter case. In the eastern part of the basin, the sensitivity is due to the direct control, which the wind exerts over the west to east flow intensity. This feature will be discussed in relation to the role played by the buoyancy forcing in that region. In the western half of the basin, the sensitivity to the wind forcing is related to its control of the

northern extent of the western boundary current, and consequently of the effectiveness with which heat and moisture can be advected northwards.

Quantitative Comparison

The effect of a *westerly* wind perturbation $\Delta\tau_x = 0.005\,N\,m^{-2}$ (approximately 10% of the value of the wind stress in low- and mid-latitudes), applied uniformly over various latitude bands is summarized in Table 3.5. It makes little sense to apply a uniform global perturbation since that would violate the conservation of angular momentum around the planet. The impact of uncertainty in the Earth's angular momentum on the ocean's circulation could, however, be explored in the future with the adjoint method.

While the circumpolar channel plays a very important role under restoring boundary conditions, the sensitivity is smaller under the other forcing scenarios. Chapter 5 will address these differences in detail. It is the equatorial region which dominates under mixed and flux boundary conditions, with an effect one order of magnitude greater than under restoring boundary conditions. Sensitivities are logically largest under flux boundary conditions since that is when increased Ekman upwelling can best be balanced by changes in stratification.

	Restoring BC	Mixed BC	Flux BC
Antarctic Circumpolar Channel: $[66°\,S; 50°\,S]$	0.061	0.021	0.015
Equator: $[2°\,N; 15°\,N]$	0.035	0.37	0.55
Tropics, Northern Hemisphere: $[18°\,N; 30°\,N]$	-0.014	-0.094	-0.055*
Tropics, Southern Hemisphere: $[10°\,S; 2°\,S]$	0.015	-0.075	-0.11

Table 3.5: Estimated effect (in Sv) on the maximum value of the meridional streamfunction ψ_{MAX} of a $\Delta\tau_x = 0.005\,N\,m^{-2}$ perturbation in the zonal wind stress applied throughout a specific region. *: the perturbation was applied only over the eastern half of the basin.

3.5.4 Precipitation and Heat Flux

The pattern of sensitivity to the observed heat flux or the restoring temperature under mixed boundary conditions (upper left-hand panel in Fig.3-21) does not differ in any significant way from the pattern of sensitivity to the restoring sea surface temperature calculated under relaxation boundary conditions. This indicates that the restoring time scale is in either case

sufficiently short to prevent any perturbation distant from the site of convection from being effective.

Under mixed boundary conditions interesting features are observed in the sensitivity to the net water flux field (Fig.3-21, lower left-hand panel), because the effects of increased rainfall or evaporation can now be advected by the surface circulation. The sign of the sensitivity is everywhere such that an increase in precipitation, and concurrent decrease in salinity, would decrease the strength of the overturning. With the exception of the northwest corner, increases in the moisture flux in the tropics, and more precisely within the area enclosed by the subtropical gyre, has a greater impact on the meridional overturning than increases in other latitudes. The time dependent development of the pattern, which is similar to what was shown in detail in Fig.2-12, and the dominance of the northwest corner hints to an important role for the advection of salinity perturbations towards the site of convection. Because that corner sets the buoyancy of the bottom water, or at the very least that of the deep western boundary current, it determines in part the zonal density gradient below the thermocline. These results support the notion that the thermohaline circulation is thermally driven (Rahmstorf, 1996). The circulation is inhibited by a net input of freshwater. The sign of the sensitivity to the freshwater flux would be reversed if the circulation was driven by both thermal and haline forcings.

It is surprising to observe no reversal in the sign of the sensitivity between high latitudes and the tropics. The experiments of Huang (1999) and Scott (2000) were performed under restoring boundary conditions. Their common conclusion that increasing the South to North temperature gradient increases the overturning, is therefore not necessarily applicable under mixed or flux boundary conditions. The analysis of Zhang et al. (1999), which reproduces the hysteresis behavior of the meridional overturning under increasing freshwater forcing observed by Rahmstorf (1995), used mixed boundary conditions. Their results show a decrease in the overturning strength for increasing freshwater forcing, which in their model corresponds to increased precipitation in high latitudes *and* increased evaporation in the tropics, the two effects are not isolated from one another. The adjoint result indicates that only the former effect weakens the overturning, the latter intensifies it. Table 3.6 also shows that, under mixed boundary conditions, the dominant mechanism should be the increase in evaporation in the tropics. The apparent disagreement with the results of Zhang et al. (1999) and Rahmstorf (1995) could have multiple sources besides model differences.

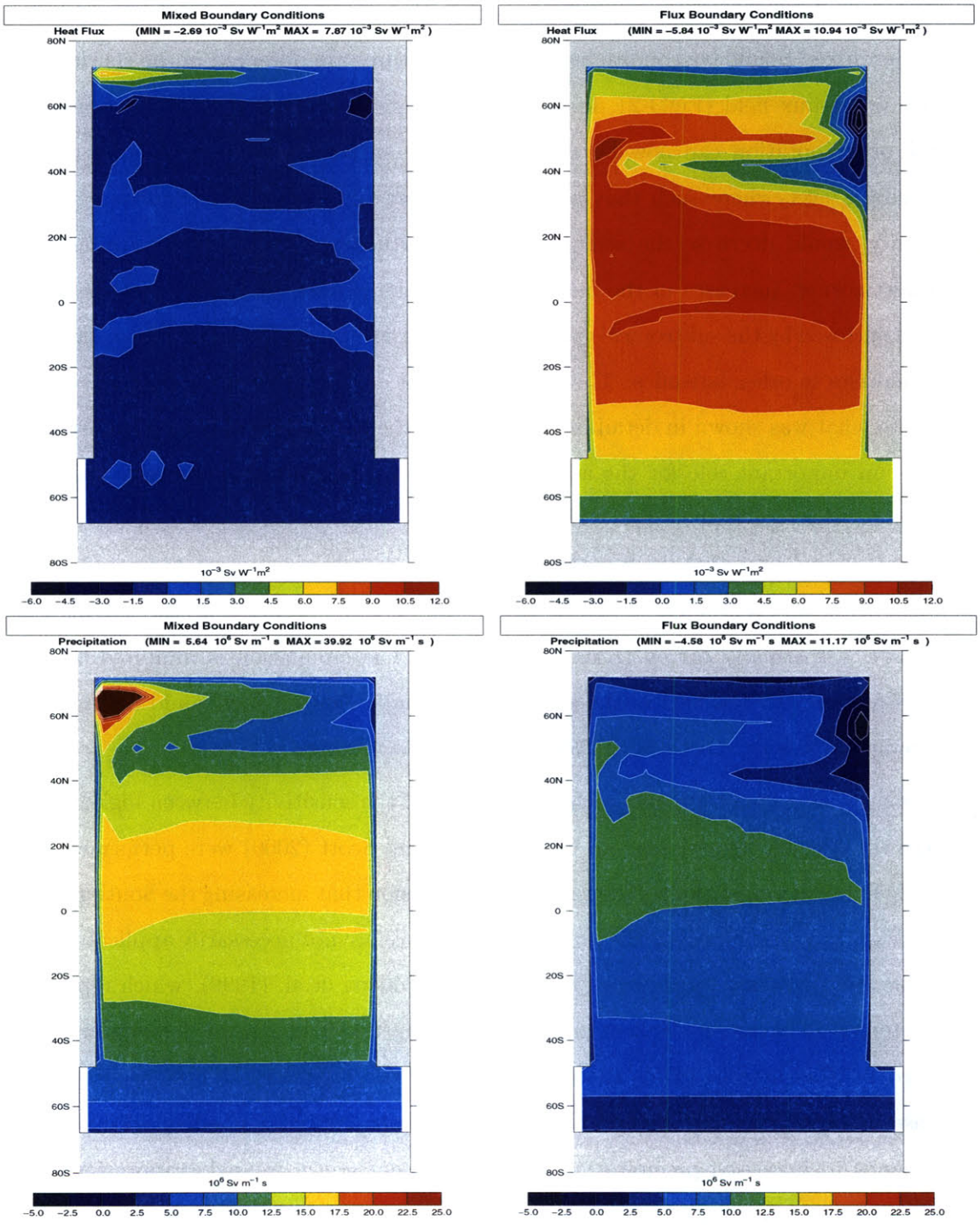

Figure 3-21: Sensitivity of the streamfunction maximum to the heat flux $\left(\frac{\partial \psi_{MAX}}{\partial Q}\right)$ in $Sv\,W^{-1}\,m^2$ (top) and to the freshwater flux $\left(\frac{\partial \psi_{MAX}}{\partial E-P}\right)$ in $Sv\,m^{-1}\,s$ (bottom) . Left: Mixed boundary conditions. Right: Flux boundary conditions.

Although this was not shown in detail, the boundary condition imposed on temperature, notably the restoring time scale, has a strong impact on the sensitivities to the freshwater flux. The rate of increase in freshwater forcing in Zhang et al. (1999) and Rahmstorf (1995) is sufficiently slow for the model to be deemed in a permanent state of quasi-equilibrium. It is, however, possible that the behavior of the overturning is more indicative of a response to a transient sensitivity pattern (e.g. a 100 year pattern of the type shown in Fig.2-12), which is concentrated in high latitudes. It takes 200-300 years for the steady-state pattern show in Fig.3-21 to emerge and for the tropical sensitivities to become dominant. Note that the adjoint result agrees with Wiebe and Weaver (1999), who noted that the *equilibrated* response to a climate change type of perturbation was in fact a net increase in the overturning's strength. The weakening of the circulation is a transient phenomenon, which does not last beyond the point when the forcing ceases to increase. The results obtained with the adjoint model are furthermore a linearization around a steady-state, as such they can only be expected to be valid over a very small portion of the hysteresis curve shown in either Zhang et al. (1999) or Rahmstorf (1995).

Under flux boundary conditions, on the right in Fig.3-21, the role played by the buoyancy forcing, both heat and moisture, is no longer limited to the polar region. Two separate mechanisms determine these sensitivity patterns: the direct interaction of the heat and moisture fluxes with downwelling at the eastern boundary, and the advection of heat and moisture in the basin and their influence on the density of abyssal waters set in the northwest corner. The elongated band of sensitivity at 40° N is aligned with the northern edge of the subtropical gyre and the strong East to West current in that region. A positive perturbation in the heat flux in that band will be advected towards the boundary, where it downwells quasi-adiabatically. The sign is such that a warming or enhanced precipitation along the eastern boundary will result in an increase of the overturning. This increase in buoyancy of the boundary intensifies zonal density gradients and the vertical shear in the flow. This hypothesis is confirmed by the sensitivity to the meridional wind stress, which although set to a nominal value of zero everywhere, indicates that a southerly wind perturbation along the east coast and its associated Ekman coastal downwelling would enhance the circulation.

With the exception of the eastern boundary, the sign of the sensitivity is everywhere such that an increase loss of heat by the ocean or a buoyancy loss through evaporation would enhance the overturning. The sensitivity to precipitation is no greater than under

mixed boundary conditions. The sensitivity to perturbations in the heat flux has, however, increased dramatically, a logical consequence of the change in the formulation of the boundary conditions.

The mixing energy required to upwell the abyssal waters is proportional to the density difference between surface and sub-thermocline layers ($\iint \kappa_d \cdot g \cdot (\rho_{bottom} - \rho_{surface}) \cdot dx \cdot dy$, (Huang, 1999)). Reducing the vertical density gradient reduces the required mixing energy, or, alternatively, for a constant mixing energy allows the upwelling of more deep water. Density gradients are greatest in the tropics, reducing the surface density in that region could be an effective mechanism for enhancing the overturning. This is not, however, taking place under mixed or flux boundary conditions because advection towards high latitudes is both a more rapid and more efficient way of impacting the overturning than local vertical diffusion.

The region of greatest sensitivity is bounded by the direct recirculation within the subtropical gyre that feeds into the western boundary current, the current region itself and its outflow into the high latitude region. Since the western boundary current controls the exchange of water between the tropical and subtropical regions, and hence the heat exchange between South and North, it is not surprising to see this result. It appears that by controlling the amount of heat transported by the western boundary current, heating or rainfall in the subtropical gyre, in the western boundary current or at its outflow controls the density of the abyssal waters, which return southward as deep currents. Since much of this return flow takes place in the deep western boundary current, cooling it or increasing its salinity also increases the East to West density contrast, which balances the meridional overturning.

Quantitative Comparison

Tables 3.6 and 3.7 summarize the effect of heat and freshwater flux perturbations, or their equivalent sea surface temperature and salinity perturbations, when added in individual portions of the basin. The basis for the comparison was chosen as an arbitrary $\Delta Q = 4\,W\,m^{-2}$ going from the ocean into the atmosphere. The equivalent sea surface temperature perturbation under relaxation boundary conditions is $\Delta SST = -0.1\,^{\circ}C$. In order to maintain the same overall impact, the perturbations used under mixed boundary conditions were $\Delta Q = 2\,W\,m^{-2}$ and $\Delta SST = -0.05\,^{\circ}C$. Note that there is nothing to force the contri-

butions of the heat flux and relaxation terms to be equally partitioned. The freshwater, respectively salinity perturbation, which would give a similar change in buoyancy is an increase of $\Delta P = 5.8\,mm\,yr^{-1}$ in evaporation, or an increase in the restoring salinity of $\Delta SSS = 0.027$. The relation between temperature and salinity perturbations is derived from the linearized equation of state, which is not accurate in high latitudes for cold temperatures.

	Restoring BC	Mixed BC	Flux BC
Polar Region: [68° N; 72° N]	0.21	0.28	0.22
Eastern Boundary: [38° S; 62° S]	-0.014	-0.012	-0.08
Western Boundary Current: [18° N; 50° N]	-0.0002	-0.0012	0.72
Tropics [2° N; 20° N]	-0.0018	-0.003	3.87

Table 3.6: Estimated effect (in Sv) on the maximum value of the meridional streamfunction ψ_{MAX}. Flux BC: $\Delta Q = 4\,W\,m^{-2}$ perturbation in the net heat flux. Restoring BC: $\Delta SST = -0.1\,°C$ perturbation in the relaxation sea surface temperature. Mixed BC: combined effect of $\Delta Q = 2\,W\,m^{-2}$ and $\Delta SST = -0.05\,°C$ perturbations.

	Restoring BC	Mixed BC	Flux BC
Polar and Northwest Region: [58° N; 72° N]	0.33	0.075	0.012
Eastern Boundary: [38° S; 62° S]	-0.022	0.003	-0.0002
Western Boundary Current: [18° N; 50° N]	0.0021	0.046	0.033
Tropics [2° N; 20° N]	0.0035	0.29	0.19

Table 3.7: Estimated effect (in Sv) on the maximum value of the meridional streamfunction ψ_{MAX}. Mixed and Flux BC: $\Delta P = 5.8\,mm\,yr^{-1}$ perturbation in the net precipitation field. Restoring BC: $\Delta SSS = 0.027$ perturbation in the sea surface salinity.

The most noticeable feature is the shift from sensitivities that are concentrated in high latitudes under restoring boundary conditions to high values in the tropics under flux boundary conditions. Under mixed boundary conditions, the overturning is most sensitive to temperature perturbations in high latitudes and salinity perturbations in low latitudes. It is also interesting to note that both polar *and* tropical regions are substantially more sensitive to the freshwater forcing under mixed than flux boundary conditions, this compensates in part the fact that surface temperatures are tied to observations by the restoring term.

The meridional overturning circulation is more sensitive to the implicit freshwater forcing than to equivalent heat flux perturbations under restoring boundary conditions. The results

obtained under mixed boundary conditions show an overturning, which is equally sensitive to high latitude changes in the net amount of heat entering that region as to perturbations in the amount of rainfall and evaporation in the tropics. The situation under flux boundary conditions is entirely dominated by perturbations in the net heat flux in low latitudes and in the western boundary current.

3.5.5 Isopycnal Mixing and Thickness Diffusion

The sensitivity to isopycnal mixing and thickness diffusion for the three forcing configurations is shown in Fig.3-22. There is a lot of detail in high latitudes in the northern hemisphere, which is cost function specific and not consistent between the three figures. The high sensitivities do, however, highlight the importance of the bolus transport in that region.

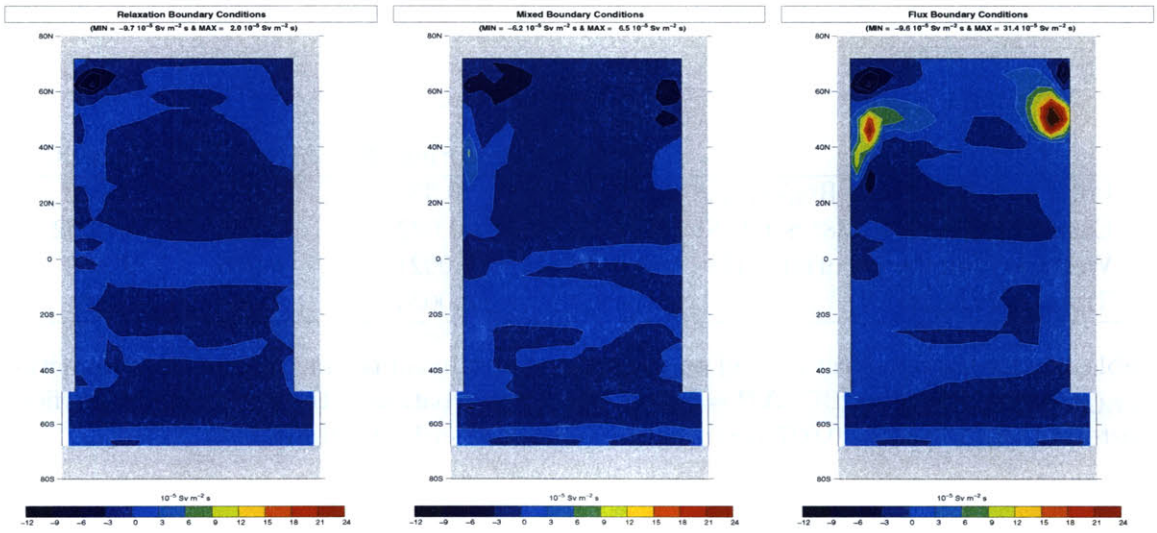

Figure 3-22: Sensitivity of the streamfunction maximum to isopycnal mixing and thickness diffusion $\left(\frac{\partial \psi_{MAX}}{\partial \kappa_i ; \kappa_{td}}\right)$ in $Sv\, m^{-2}\, s$. Left: Restoring boundary conditions. Middle: Mixed boundary conditions. Right: Flux boundary conditions. The three plots are on the same scale.

Western Boundary Current

The sensitivity to the thickness diffusion in the western boundary current is, at 7 to $8 \cdot 10^{-5} \frac{Sv}{m^2 s^{-1}}$, similar under relaxation or mixed boundary conditions, the value jumps to

$2 \cdot 10^{-4} \frac{Sv}{m^2 s^{-1}}$ under flux boundary conditions. This patch of high sensitivity corresponds to the latitude band over which isopycnals are distorted northward and upward by the current and where isopycnal thickness gradients are largest. The greater perturbations in stratification, which are allowed under flux boundary conditions, are the source of much of the increase in sensitivity. The importance of the western boundary region is in fact masked by the opposing sensitivity patterns in the western and deep western boundary currents.

Under flux boundary conditions, the two regions of large sensitivity to isopycnal mixing and thickness diffusion correspond to the regions of enhanced sensitivity to the buoyancy forcing: the outflow from the western boundary current at $55° N$ and the eastern boundary between 40 and $60° N$. A meridional section along the eastern boundary between 40 and $60° N$ indicates that the region of high sensitivity coincide with the boundary between down- and upwelling, where isopycnals slope steeply downwards, sensitivities are positive just below this boundary. The projection of the isopycnal mixing component onto the vertical allows it to contribute to the downward mixing of heat and warming of that boundary in a role similar to the one played by diapycnal mixing.

Quantitative Comparison

Table 3.8 summarizes the effect of an increase in isopycnal mixing and thickness diffusion, $\Delta\kappa_i = 100\ m^2\, s^{-1}$, in various regions on the overturning. The sensitivity patterns tend to be specific to each forcing configuration, which limits the possibility of comparing any effects quantitatively.

	Restoring BC	Mixed BC	Flux BC
Antarctic Circumpolar Channel: $[58° S; 54° S]$	-0.10	-0.12	-0.06
Antarctic Circumpolar Current: $[54° S; 50° S]$	0.34	0.12	0.11
Western Boundary Region: $[34° N; 50° N]$	0.07	0.16	0.96
Polar Region: $[62° N; 70° N]$	-0.4	-1.2	-0.06
Total	-2.6	-0.6	3.9

Table 3.8: Estimated effect (in Sv) on the maximum value of the meridional streamfunction ψ_{MAX} of a $\Delta\kappa_i = 10 \cdot 10^{-6}\, m^2\, s^{-1}$ perturbation in the isopycnal mixing applied throughout a specific region.

The bolus transport plays the greatest role in the Antarctic Circumpolar Channel under restoring boundary conditions, it is under flux boundary conditions that the western

boundary dominates. The overall effect of the western boundary current alone is approximately twice what is shown above for the entire water column. A rapid calculation shows that a 10% perturbation in $\kappa_{i,td}$ along the western boundary under mixed or flux boundary conditions has an impact on the overturning that is approximately three times greater than a similar perturbation in the diapycnal mixing ($\Delta\psi_{\kappa_d} = \frac{\partial\psi}{\partial\kappa_d}\Delta\kappa_d = 5 \cdot 10^2 \cdot 3 \cdot 10^{-7} = 1.5 \cdot 10^{-4}\ Sv$; $\Delta\psi_{\kappa_i} = \frac{\partial\psi}{\partial\kappa_{td}}\Delta\kappa_{td} = 5 \cdot 10^{-5} \cdot 10 = 5 \cdot 10^{-4}\ Sv$).

Under both mixed and restoring boundary conditions, the polar regions contribute a large fraction of the total sensitivity to the isopycnal mixing.

3.6 Summary and Discussion

Our study shows that, in a climatological ocean model, air-sea boundary conditions are a crucial determinant of the wind-stress sensitivity.

The important role played by the tropics in setting the overturning's strength seems to confirm the thermodynamic principles outlined by Sandström (1908), Jeffreys (1925) and Munk and Wunsch (1998): upward advection of heat is balanced by downard diffusion. The strength of the meridional overturning is then determined by the power available to return the fluid to the surface across the ocean's stratification. Note that this "diffusion" is only a crude parameterization for small scale mixing thought to be related to the breaking of internal gravity waves and internal tides (Gregg, 1987; Polzin et al., 1997).

As observed by Scott (2000) in a model forced by buoyancy alone, enhancing the downward mixing of heat along either boundary in mid-latitudes will sustain a more intense overturning than enhancing it in the middle of the basin. The eastern boundary sustains the overturning through downwelling in the thermocline and diffusive warming of the boundary below it. The large vertical temperature contrast between the western and deep western boundary currents along the western boundary induce efficient mixing in that region.

The sensitivity to the buoyancy forcing is geographically limited to the region that sets the temperature of the abyssal waters along the western boundary, in direct relation with the thermal wind balance.

Surface wind stress has two effects on the ocean's stratification, which concentrate the sensitivity in the eastern equatorial region. Ekman suction increases the stratification along the equator while Ekman pumping decreases it in the rest of the tropics. The equatorial

easterlies lift the thermocline on the eastern side of the basin, further increasing the stratification and the efficiency of the vertical mixing process in that region.

The most striking difference between the sensitivity maps obtained under relaxation boundary conditions and those obtained under mixed or flux boundary conditions is the generally greater sensitivities in the latter cases. This is not surprising, relaxation terms are constraints imposed onto the circulation, which make it much less sensitive to perturbations than a system with more freedom. It is the ability of the flow to advect buoyancy perturbations towards high latitudes under flux boundary conditions, which allows high sensitivities to heat and freshwater fluxes to extend throughout the basin. Both high and low latitudes play an important role under mixed boundary conditions, the case thought to be the most realistic.

There is no single region or parameter, which clearly stands out as being dominant. It does, however, appear that the tropics, and in particular the north equatorial band, become increasingly important as the constraints on the surface forcing are relaxed. Under flux boundary conditions, a 10% increase in wind stress in the $2 - 15^{\circ} N$ band would increase the overturning by $\sim 0.5\, Sv$, an increase of similar magnitude in the diapycnal mixing would increase it by $0.2\, Sv$. Perturbations in the buoyancy forcing terms have an even greater impact. The tropics are important even without any wind stress forcing, but the specific importance of the eastern equatorial region is undoubtedly tied to the combination of easterlies and Ekman upwelling in increasing the stratification.

The polar region plays a crucial role in sustaining the meridional overturning. It is argued that this role is tied to a control of the buoyancy of the abyssal waters, notably of the deep western boundary current by convection in the northwest corner.

The analysis in this simplified framework has highlighted the importance of the zonal overturning cell in balancing the meridional circulation (Scott, 2000). By adiabatically warming the eastern boundary above the thermocline and cooling the western boundary throughout the depth of the basin, this cell creates the zonal temperature gradient required to sustain the vertical shear of the flow synonymous with meridional overturning. The warming of the eastern boundary is compounded by diffusive warming below the thermocline. Convection sets the temperature of the deep western boundary current, which is the source of much of the upwelling water along the western boundary.

Chapter 4

Description of the Realistic Geography Models

Chapter 3 examined the response of an idealized ocean basin to various types of surface boundary conditions. This chapter will focus on the role of exchanges between basins in a coarse resolution realistic geography model. These exchanges are associated with oceanic transport mechanisms, advection and diffusion, in the ocean model forced by mixed surface boundary conditions. The coupled ocean - energy and moisture balance model provides the ocean's surface with interactive surface fluxes, and enables a number of important feedback mechanisms between the ocean and the atmosphere. It also allows for the rapid exchange of information between basins and across latitudes.

4.1 Ocean Model

The ocean model is the MIT OGCM, it is described in detail in Marshall et al. (1997a,b). This model is designed to study ocean processes ranging from the non-hydrostatic scale of convection to the hydrostatic global scale. The configuration of the model has a realistic geography and bathymetry on a constant $4^\circ \times 4^\circ$ resolution grid, it has 15 layers in the vertical with thicknesses ranging from $50\,m$ near the surface to $690\,m$. at the bottom. Time stepping is asynchronous, $\Delta t = 40\,min$ for the momentum equations and $\Delta t = 1\ day$ for the tracer advection (Bryan, 1984). Since there is no seasonal cycle in this model setup, the asynchronous scheme should have no consequences on the steady-state flow field. The following sections will show that this model reproduces reasonably well the known large-

scale features of the ocean circulation. The Redi tensor allows for the diffusion of tracers along three-dimensional isopycnal surfaces instead of horizontally (Redi, 1982). The Gent Mc-Williams scheme parameterizes the advective effect of the geostrophic eddies with a "bolus velocity", which is added to the Eulerian-mean velocity (Gent and McWilliams, 1990; Danabasoglu and McWilliams, 1995). A table summarizing the values used for key model parameters is provided in Appendix A.

4.2 Energy and Moisture Balance Atmosphere

To investigate the impact of atmospheric feedbacks, an energy and moisture balance model is coupled to the ocean model. The model is drawn from the work of Wang et al. (1999a,b) and Nakamura et al. (1994) with some minor modifications. This energy and moisture balance atmosphere is a highly parameterized zonally averaged transport model. The concept underlying this model is that the amount of heat and freshwater transported from the tropics towards higher latitudes by the atmosphere is a function of the meridional temperature gradient at the ocean's surface. This parameterization represents only the role played by atmospheric eddies in transporting heat, it neglects the role of the Hadley cell in low latitudes. The latitudinal profiles of atmospheric heat and freshwater transport are specified from observations and held fixed throughout the integration. However, the amplitude of each profile is determined by the eddy transport parameterization and recalculated at every time step. The fluxes of heat and moisture at the ocean-atmosphere interface are calculated by assuming that the atmosphere has vanishing heat and moisture retention capacities, an assumption which is true on an annual mean time scale. The wind stress is not interactive and is derived from the European Center for Medium Range Weather Forecasting (ECMWF) reanalysis data from 1980 to 1987 (Trenberth et al., 1989).

4.2.1 Heat Flux

The flux of heat per unit area at the ocean - atmosphere boundary is determined from the sum of the net radiative forcing and the divergence of the atmospheric heat transport:

$$Q_{mod} = \gamma \left(S(1-\alpha) - I + \frac{\partial H_d}{\partial y} \right) \tag{4.1}$$

where $\frac{\partial \cdot}{\partial y} = \frac{1}{r\cos(\phi)} \frac{\partial(\cdot \cos(\phi))}{\partial \phi}$, ϕ is the latitude.

The factor γ accounts for the fact that the annual net flux of heat must vanish over land, γ is therefore calculated as the ratio of the total number of grid points in a latitude band to the number of ocean points. Since a net annual mean heat flux into or out of an ice sheet is possible, Greenland and Antarctica are counted as ocean points. The net radiative forcing at the top of the atmosphere is the sum of its longwave and shortwave components. The incoming shortwave radiation, S, and the planetary albedo, α, are parameterized as Legendre polynomials fit to observations, and forced to be symmetric about the equator (Wang, 1997). This model does not allow for any albedo feedback, S and α are held fixed throughout the integrations.

The net longwave flux, I, is parameterized as a function of the temperature of the atmosphere at the surface:

$$I = F_0 + F_1 T_s(\phi) \tag{4.2}$$

The coefficients F_0 and F_1 were determined from NASA's Earth Radiation Budget Experiment (ERBE) longwave radiation data and the Levitus sea surface temperature: $F_0 = 195\,Wm^{-2}$, $F_1 = 2.78\,Wm^{-2}C^{-1}$ (Wang et al., 1999a). The meridional atmospheric temperature profile, T_s, is determined from the sea surface temperatures by fitting a second order Legendre polynomial to the area-weighted average temperature over the $0° - 35°N/S$ and $35° - 80°N/S$ latitude bands. This parameterization relies on the assumption that the zonal mean atmospheric surface temperatures remain close to the zonal mean sea-surface temperatures, which is generally true.

$$T_s = T_0 + T_2 \mathcal{P}_2 \tag{4.3}$$

The expansion coefficients T_0 and T_2 are determined separately in the Northern and Southern hemispheres, $\mathcal{P}_2$ is the second Legendre polynomial.

The atmospheric heat transport is the sum of sensible and latent heat fluxes. The heat transport parameterization focuses entirely on mid-latitude eddies, it neglects changes in the mean-meridional circulation in low latitudes.

$$H_d(35°N/S) = 2\pi r \cos(\phi) \int_0^\infty \left(\rho_a C_p \overline{v'T'} + \rho_a L_v \overline{v'q'}\right) dz \tag{4.4}$$

where z represents the depth of the atmosphere, ρ_a is the atmospheric density, L_v the latent heat of condensation, C_p the specific heat of dry air, q is the specific humidity, v is the meridional velocity and T the potential temperature. The overbar represents a zonal and time mean, while primes are the deviations from the time average. Both the eddy sensible and latent heat transport parameterizations are based on baroclinic instability theory (Held, 1978; Stone and Miller, 1980) and take the form of a power law of the temperature gradient at $35°N/S$. The latitudinal pattern of atmospheric heat transport is specified from observations (Trenberth and Solomon, 1994; Schmitt et al., 1989; Reeh, 1994; Perry et al., 1996), its intensity is determined by the sum of eddy sensible and latent heat transport at $35°N/S$:

$$H_d(35°N/S) = 2\pi r\cos(\phi)\left(L_v C_F e^{\frac{-5420}{T}} + C_S\right)\left(\frac{\partial T}{\partial y}\right)^n \tag{4.5}$$

C_F and C_S are the eddy latent and sensible transport coefficients. $n = 2.5$ is the value appropriate for $35°N/S$.

4.2.2 Freshwater Flux

The flux of freshwater per unit area into or out of the ocean is given by the divergence of the atmospheric transport of water vapor (f_w). The observed runoff (R) of freshwater from land is added to complete the atmospheric water budget:

$$\text{Evaporation} - \text{Precipitation} - \text{Runoff} = \frac{\partial \mathrm{f_w}}{\partial \mathrm{y}} - \mathrm{R} \tag{4.6}$$

The atmospheric moisture transport parameterization relies on the same empirical and theoretical concepts as the one for the heat transport (Stone and Yao, 1990):

$$f_w(35°N/S) = 2\pi r\cos(\phi)\int_0^\infty \rho_a \overline{v'q'}\, dz \tag{4.7}$$

$$f_w(35°N/S) = 2\pi r\cos(\phi) C_F e^{\frac{-5420}{T}}\left(\frac{\partial T}{\partial y}\right)^n \tag{4.8}$$

While the intensity of the atmospheric freshwater transport is determined by equation 4.8, the latitudinal distribution is specified from observations (Jiang et al., 1999). In order to maintain a stable meridional overturning circulation in the Atlantic in the coupled runs,

separate profiles are used for the Atlantic and Pacific basins. A common profile is used over the Southern Ocean.

The runoff R is derived from observations (Perry et al., 1996; Jiang et al., 1999). In order to maintain a balanced hydrological cycle and avoid a net gain or loss of mass in the oceans, the runoff is scaled at each time step by the ratio δ between *Precipitation - Evaporation* and *Runoff* in the coupled model simulations.

4.3 Model Spinup and Coupling

The ocean model is spun up from rest in an uncoupled mode by imposing a Haney type boundary condition on the temperature tendency equation and a virtual salt flux on the equation determining the evolution of the salinity field (Haney, 1971). The model requires approximately 3000 years for the deep ocean to equilibrate with the forcing. The ocean's surface is relaxed toward an apparent atmospheric temperature $T^\star$ on a $\lambda_s^{-1} = 60$ day time scale. $T^\star$ can be interpreted as the temperature that the air would have in the absence of any transport of heat by the ocean. It is approximated by $T^\star = T_{obs} - \frac{Q_{obs}}{\lambda_s}$, where T_{obs} is the Levitus sea surface temperature field. The boundary conditions can be summarized as follows:

$$F_w = (E - P - R)_{obs} \tag{4.9}$$

$$Q = \lambda_s(T - T^\star) = Q_{obs} + \lambda_s(T - T_{obs}) \tag{4.10}$$

Q_{obs} and $(E - P - R)_{obs}$ are the fields derived by Trenberth and Solomon (1994); Schmitt et al. (1989); Reeh (1994); Perry et al. (1996), they are shown for reference in figure 4-1.

The freshwater forcing field derived from observations has large uncertainties. The choice was made not to "correct" the flux by imposing a term relaxing salinities towards observations. This decision was made both because of the unphysical nature of that type of boundary condition: the moisture flux is in no way affected by the salinity, and because of the desire to keep the boundary conditions for the "ocean only" simulations as close as possible to those of the coupled energy and moisture balance atmosphere - ocean model.

The energy and moisture balance model model is coupled by changing the surface bound-

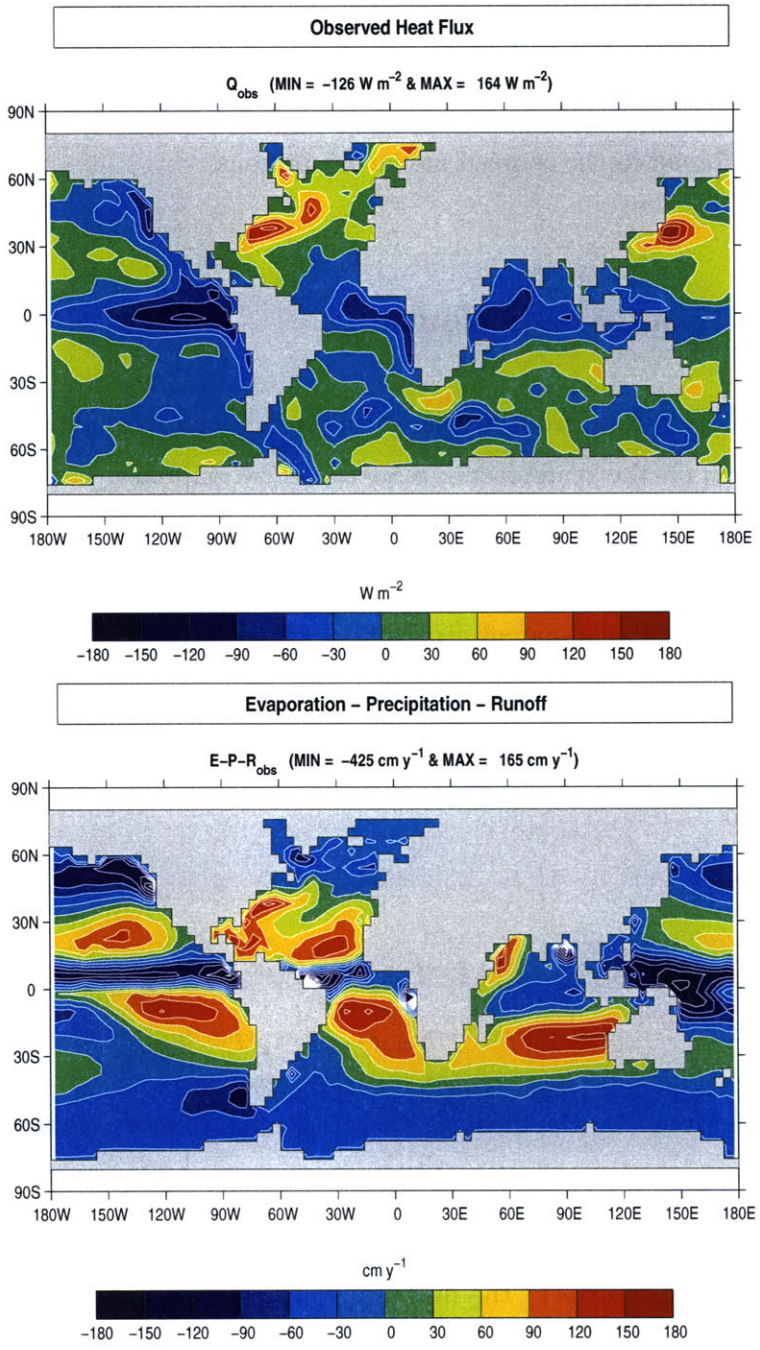

Figure 4-1: Top: Ocean - atmosphere heat flux Q_{obs} in $W\,m^{-2}$. Bottom: Precipitation + Runoff - Evaporation in $cm\,y^{-1}$.

ary conditions to the following form:

$$F_w = (E - P)_{mod} - \delta \cdot R_{obs} \quad \bullet \tag{4.11}$$

$$\delta = \frac{\int_0^{360^\circ} \int_{-80^\circ}^{80^\circ} (P - E)\, d\phi\, d\lambda}{\int_0^{360^\circ} \int_{-80^\circ}^{80^\circ} R\, d\phi\, d\lambda}$$

$$Q = Q_{mod} + \lambda_m (T - T_{zon}) \tag{4.12}$$

The subscript $_{mod}$ indicates that the flux is calculated by the energy and moisture balance model described in equations 4.1 and 4.6. The relaxation of the sea surface temperature towards its zonal mean, T_{zon}, on a $\lambda_m^{-1} = 60$ day time scale is added to reproduce the effect of the atmospheric circulation, which is predominantly zonal, in homogenizing the temperature at the ocean's surface (Kamenkovich et al., 2000a). The observed runoff is from Reeh (1994); Perry et al. (1996).

4.4 Equilibrated State

The ocean model is spun up from rest for 3000 years. The coupled form of the model is then integrated for a further 3000 years to allow for a complete equilibration.

4.4.1 Temperature

The sea surface temperature at the end of the spinup period (not shown) is similar to the Levitus climatology, Fig. 4-2 . This can be expected from the presence of a relaxation term in the surface heat flux parameterization at that stage. The temperature extrema are, however, more than a degree larger than observed.

The temperature after coupling and equilibration, shown in Fig.4-3, has a much more zonal structure. This was a foreseeable result in view of the zonal nature of the energy balance model and of the relaxation of the sea surface temperatures to the zonal mean. The effect of the Gulf Stream and North Atlantic currents on the temperature distribution are, however, still clearly visible: isotherms are deflected northward in the Western Atlantic along the east coast of the United States and in the eastern North Atlantic near Scandinavia. The choice of the relaxation time scale to the zonal mean temperature has relatively little impact on the distribution of the isotherms, provided the time scale is between two months

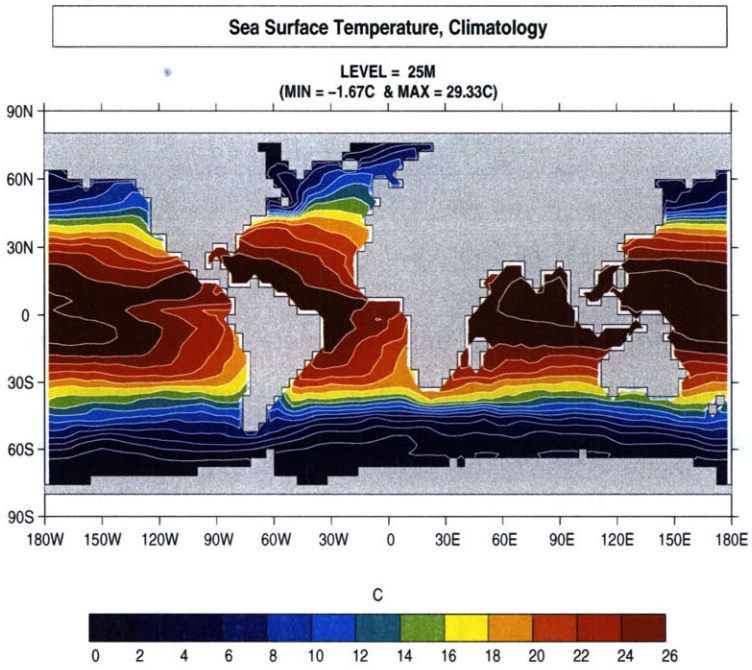

Figure 4-2: Sea surface temperature climatology, in $°C$ (Levitus and T.P.Boyer, 1994b)

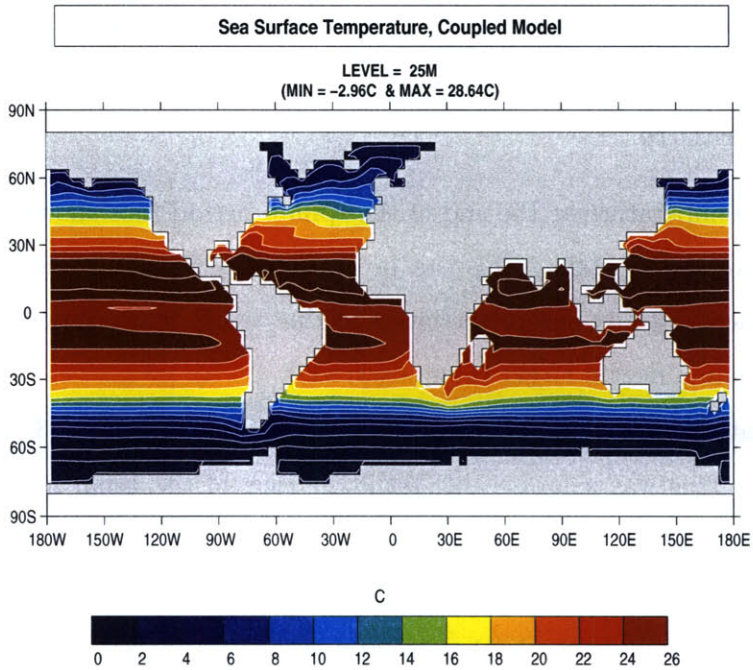

Figure 4-3: Sea surface temperature in the coupled model after 3000 years of coupled integration, in $°C$

and a year. The temperature maximum in the subtropics is close to observations, while the minimum is too low by a little over a degree.

The global average sea surface temperature differs by less than $0.3°C$ between the ocean-only and the coupled cases, both are also very close to the observations: $\overline{SST_{obs}} = 18.6°C$

4.4.2 Salinity

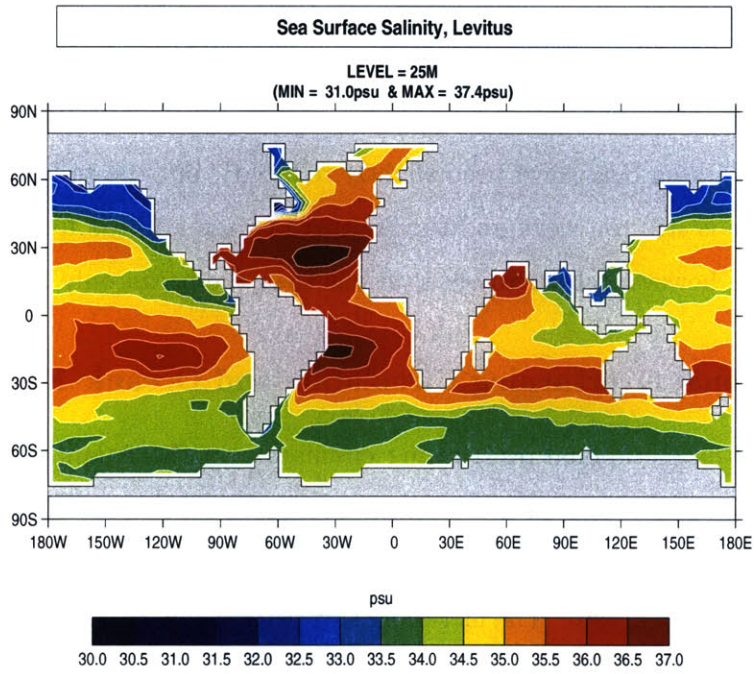

Figure 4-4: Sea surface salinity climatology (Levitus and T.P.Boyer, 1994a)

There exist regionally strong contrasts between the Levitus climatology, Fig. 4-4, and the salinities obtained at the end of the spinup run, Fig. 4-5: there is no relaxation term and the surface salinities depend entirely on the freshwater flux. The sea surface salinities diagnosed at the end of the spinup run are generally in good agreement with observations in the Atlantic basin. The Pacific Basin is, however, fresher than observed, in particular close to South-East Asia and Australia and in the Northeast Pacific. The Southern Ocean suffers from the same discrepancy. The global average sea surface salinity is 1.7 lower than observed, which is compensated by greater salinities at depth. Deviations in salinity are a common problem in ocean GCM's forced with freshwater or virtual salt fluxes (Jiang et al., 1999), partly because those fluxes are poorly known (Schmitt et al., 1989) but also because

of the dependence of the ocean dyamics on the subgrid scale parameterizations.

Amending the boundary condition on the salinity tendency equation by adding a term relaxing the salinities to observations in the manner of Large et al. (1997) would correct this drift, even for relaxation time scales as long as two years (Jiang et al., 1999). The unphysical nature of the salinity relaxation terms would severely compromise the ocean feedbacks, which the adjoint analysis is seeking to explore. Preventing the freshening of the regions surrounding Antarctica would, however, have allowed the formation of more Antarctic Bottom Water.

The coupled model maintains most of the features observed at the end of the spinup run, albeit in a slightly more zonal form. The salinity gradient in the Northeast Pacific and in the South China Seas have been slightly reduced[1], but the salinity gradient in the Northern Atlantic is still too weak and the Southern Ocean still too fresh. The overall sea surface salinity is, however, closer to observations than the ocean only case by 1.

4.4.3 Meridional Overturning Circulation and Oceanic Heat Transport

The intensity of the meridional overturning circulation in the Atlantic is best compared to the estimates of 17 Sv derived at $24°N$ by Roemmich and Wunsch (1985); Ganachaud and Wunsch (2000) and of 27 Sv at $55°N$ estimated with inverse modeling methods by Macdonald and Wunsch (1996). The meridional overturning circulation peaks at 29 Sv close to $55°N$ at the end of the spinup run, it is 17 Sv $24°N$, Fig 4-7. The peak intensity decreases by 3 Sv after coupling in the energy and moisture balance model while the transport at $24°N$ increases by 2 Sv, Fig 4-8. These changes are relatively minor and indicate that the coupled model establishes a steady state, which is similar to the stable state obtained at the end of the ocean's spinup. The absence of drift in the coupled model can be attributed to the model's construction and to the coupling procedure. The energy balance model re-calculates the magnitude of the atmospheric transports at every time step. The latitudinal distribution of the fluxes of heat and freshwater were, however, derived from the observations used as surface forcing fields in the ocean only model. There are, therefore, no dramatic changes in the forcing after the energy balance model is coupled to the ocean.

The heat transported by the ocean can be partitioned between the heat advected by the

[1]the salinity minimum of 17 is due to the discharge of the Amazon which is geographically much more concentrated than in the E-P-R field used to spin up the ocean model

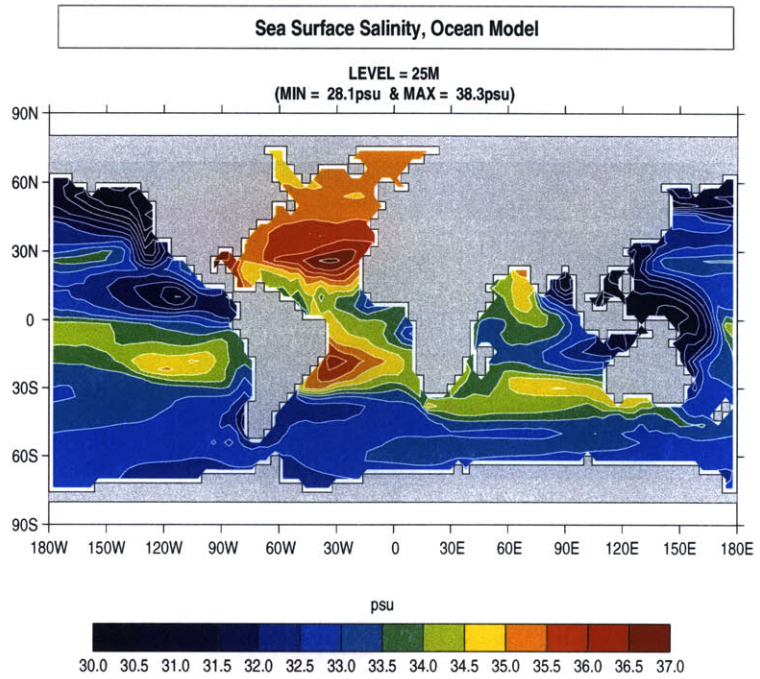

Figure 4-5: Sea surface salinity in the uncoupled ocean model (no atmosphere) after 3000 years of integration. The surface boundary conditions are 4.9 and 4.10

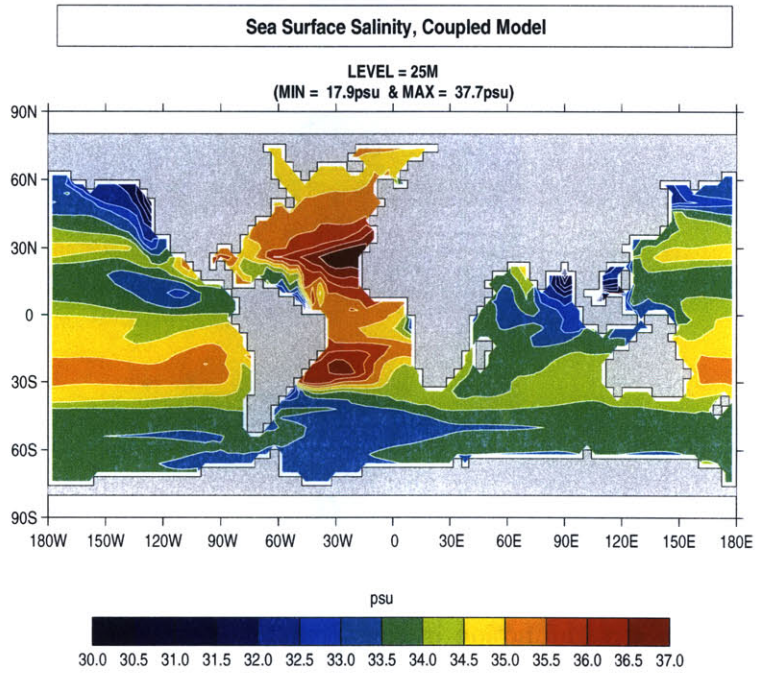

Figure 4-6: Sea surface salinity in the coupled model after 3000 years of coupled integration

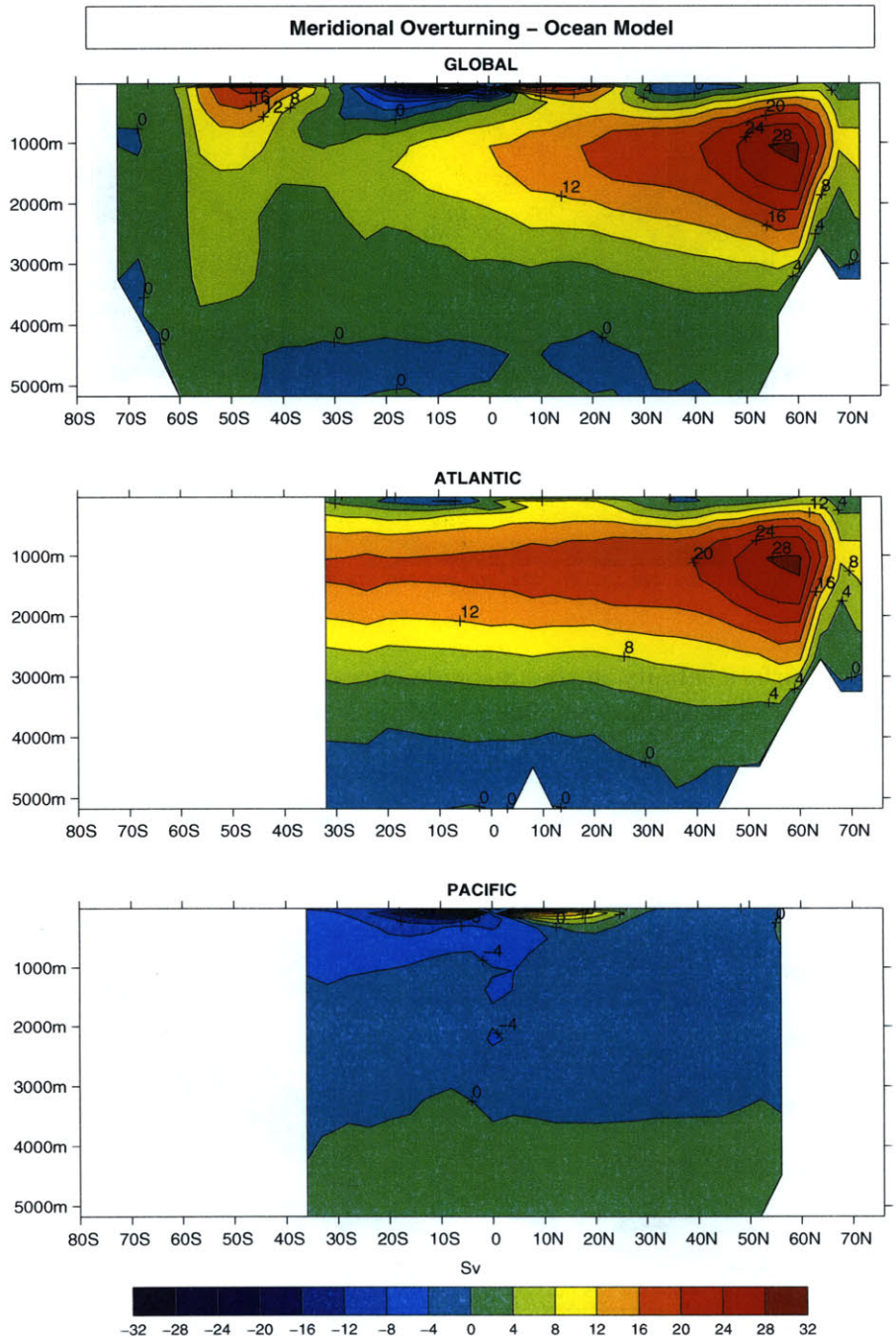

Figure 4-7: Meridional streamfunction in the ocean (no atmosphere) model, in Sv. Top: global streamfunction integrated across the basins. Middle: streamfunction in the Atlantic basin. Bottom: streamfunction in the Pacific.

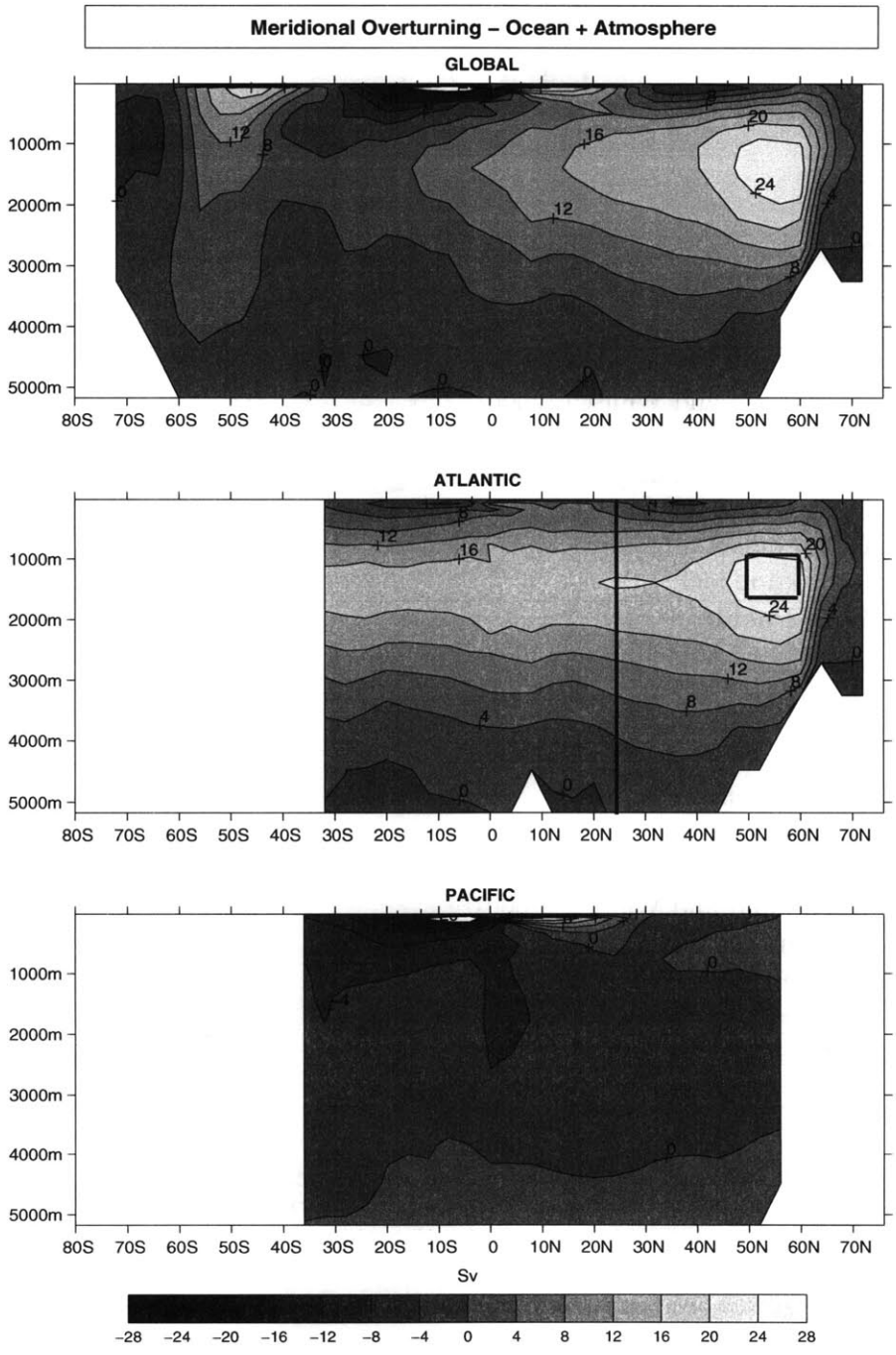

Figure 4-8: Meridional streamfunction in the coupled model, in Sv. Top: global streamfunction integrated across the basins. Middle:streamfunction in the Atlantic basin. Bottom: streamfunction in the Pacific. The boxed in area and section represent the diagnostics used in chapter 5.

	$40°N$	$24°N$	$30°S$
Atlantic			
Ganachaud and Wunsch (2000)	0.6	1.3	0.3
Hall and Bryden (1982)		1.2	
Trenberth and Solomon (1994)	0.5	1.1	0.2
Jiang et al. (1999)	1.0	1.2	0.6
Ocean model	0.8	1.0	0.4
Coupled model	0.8	0.9	0.2
Indo-Pacific			
Ganachaud and Wunsch (2000)	0.0	0.5	-1.2
Bryden et al. (1991)		0.7	
Trenberth and Solomon (1994)	0.2	1.1	-1.8
Jiang et al. (1999)	0.0	0.8	-1.2
Ocean model	0.1	0.3	-1.0
Coupled model	0.0	0.4	-1.1
Total			
Ganachaud and Wunsch (2000)	0.6	1.8	-0.9
Hall and Bryden (1982),Bryden et al. (1991)		2.0	
Trenberth and Solomon (1994)	0.7	2.2	-1.6
Jiang et al. (1999)	1.0	1.9	-0.6
Ocean model	0.9	1.3	-0.6
Coupled model	0.8	1.3	-0.9

Table 4.1: Estimates of the total heat transport by the ocean across 40° N, 24° N and 30° S in the Atlantic and Indo-Pacific basins and globally, in PW.

zonal mean circulation ($\rho_0 c_p \int_0^L \int_{-H}^0 \bar{v}\bar{T}\, dz\, dx$), essentially the meridional overturning circulation, and the heat transported by deviations from the zonal mean,($\rho_0 c_p \int_0^L \int_{-H}^0 v'\bar{T}'\, dz\, dx$), essentially the heat advected by the gyre. This partitioning is very similar in both model setups: at $24°N$, the meridional overturning advects 1.1 PW northward in the Atlantic and the gyre contributes 0.1 PW of southward heat transport. The total heat transport in the Atlantic is within the uncertainty of the estimates derived by Macdonald and Wunsch (1996); Ganachaud and Wunsch (2000) with inverse modeling methods, Trenberth and Solomon (1994); Jiang et al. (1999) from analysis of meteorological data or Hall and Bryden (1982) and Bryden et al. (1991) from hydrographic section data. The good agreement with observations suggests that the parameterization of the transport of heat by eddies is adequate and that unresolved motions, such as boundary jets, make no significant contribution to the total heat transport. The dependency of the heat transport on the model resolution is, however, a topic, which requires further study.

The zonal relaxation time scale in the coupled model has relatively little impact on the amount of heat transported by the ocean in the Atlantic: The heat transported by the meridional circulation decreases by 0.2 PW when the zonal relaxation time scale increases from two to six months, this if offset by a similar increase in the southward gyre transport. This indicates that the two month relaxation time scale does not prevent the Western Boundary Current, and the Gulf Stream in particular, from developing the structure that it would attain in the absence of such a constraint.

Both models underestimate the heat transported by the Pacific and Indian Oceans, this explains why the overall oceanic heat transport at $24°$ N is smaller than most observations.

The atmospheric component of the coupled model transports 3.5 PW of heat in the northern hemisphere and close to 4 PW in the southern hemisphere, both directed towards the poles. This is slightly more than observations suggest (Peixoto and Oort, 1992).

4.5 Summary

The characteristics of the ocean and coupled models are similar, notably the intensity of the meridional volume transport and the ocean' heat transport. The upper ocean temperature structure is slightly more zonal in the coupled model. Both models exhibit similar deviations from the observed sea surface salinity field.

Chapter 5 will examine the response of these models, when they are subject to perturbations in the parameters and boundary conditions thought to control the intensity of the meridional overturning circulation. The overall intensity of the overturning is sufficiently close to observations, and certainly within the range of uncertainty of $\pm 6\, Sv$ given by Macdonald and Wunsch (1996), for the model results to be considered adequate starting points for further calculations.

Chapter 5

What Drives the Meridional Overturning Circulation?

5.1 Introduction

This chapter examines the sensitivity of the meridional overturning circulation in realistic geography models to parameters, for example diapycnal mixing, and surface boundary conditions. The objective is to use the results obtained with the adjoint model to review several theories, which have been elaborated to explain the intensity of the meridional overturning circulation and its associated heat transport.

5.1.1 Rate Limiting Mechanisms

The mechanisms illustrated schematically in Fig.5-1 are thought to play a role in setting the overturning strength.

- Heat and freshwater fluxes exert a direct control over the buoyancy of the surface water in the Northern Atlantic, hence on convection and downwelling in the Labrador, Norwegian and Greenland Seas (Broecker et al., 1985). These fluxes can also influence the overturning through atmospheric and oceanic feedback effects (Nakamura et al., 1994; Marotzke and Stone, 1995).

- By transporting heat through the thermocline, diapycnal mixing can balance the upwelling of abyssal waters (Munk and Wunsch, 1998). Wind and tides are thought

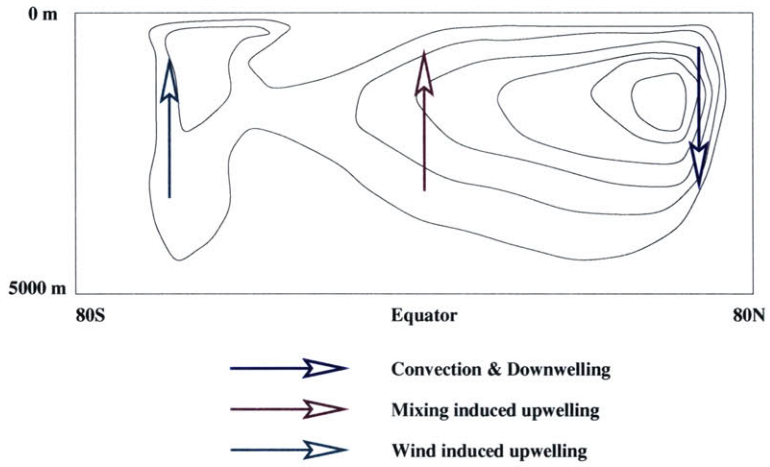

Figure 5-1: Illustration of three mechanisms thought to drive the meridional overturning circulation. The thin lines represent the meridional streamfunction.

to supply the energy for the mixing process through internal wave fields. In this model, the mixing intensity is prescribed as an effective diffusion coefficient. The effect of changes in the wind stress on mixing rates is therefore not taken into account.

- Wind stress has been proposed (Toggweiler and Samuels, 1995; Gnanadesikan, 1999) as possibly determining the steady-state intensity of the overturning circulation through its dynamical control of upwelling in the Southern Oceans.

Each section of this chapter will address one of these three hypotheses by analyzing the results of the ocean model forced with mixed boundary conditions and of a coupled ocean - EMBM system. A brief section discusses the conflicting results obtained with the different versions of the model in the western boundary current region. The end of the chapter will seek to compare quantitatively each of these mechanisms and their role in determining our knowledge of the meridional overturning circulation.

5.1.2 Application of the Adjoint

The adjoint model provides the sensitivity of a diagnostic, here the strenght of the meridional overturning circulation, to all model parameters and boundary conditions in a single integration. It is therefore theoretically ideally suited to determine the relative importance of parameters and boundary conditions in controlling the intensity of the overturning circulation, provided certain conditions are met.

The first restriction is purely computational. It is not practical, at this point, to integrate the adjoint model, even in a coarse resolution, for more than a few hundred years. The sensitivity fields seem to have equilibrated by year $200 - 300$ (see chapter 2 for a detailed description of the equilibration process). This does not perfectly guarantee that the ocean's slowest processes, such as slow upwelling in the Pacific, would not have an impact on the meridional overturning on longer time scales (Danabasoglu et al., 1996). The integrations presented in this chapter have been carried out for 400 years, and the assumption is made that the dominant signals have become visible by that point.

The second restriction relates to uncertainties in the surface boundary conditions, such as wind stress, and in the model parameters, such as diapycnal mixing. A quantitative comparison of the effect of perturbations in the parameters on the overturning's intensity requires the multiplication of the sensitivities obtained with the adjoint model with a perturbation in the field or parameter (e.g. $\Delta\psi_{MAX} = \frac{\partial\psi_{MAX}}{\partial\tau_x}\Delta\tau_x$). While the uncertainty and the natural variability in fields such as wind stress is quantifiable, other fields are much less precisely known, for example the globally averaged value of the diapycnal mixing is unknown to a factor of three or more (Gregg, 1987). Furthermore, there exists convincing evidence that mixing may vary significantly with geographic location (Polzin et al., 1997).

This leads to the third caveat. While the underlying model trajectory may be nonlinear, the adjoint method does require the perturbation growth to be linear. This, theoretically, restricts the validity of the analysis to small perturbations in the underlying fields. The validity of the linearity assumption may also be location dependent, a 10% perturbation in the heat flux that leads to a linear model response in the tropics can change the convection pattern in the Labrador Sea, with strongly nonlinear consequences. The meridional overturning circulation is known to be unstable, when subject to large increases in the freshwater forcing in high latitudes (Rahmstorf, 1995). The steady-state of the ocean model is, however, not near a bifurcation point; it does not collapse when small perturbations are added to the forcing fields. Because the adjoint represents a linearization around the model's steady-state, it does not "know" about the model's bifurcation points.

5.1.3 Cost Functions

Two different diagnostics of the circulation are used to verify the robustness of the solutions. The first is the average value of the meridional streamfunction in the neighborhood of its

maximum (ψ_{MAX}), between $\phi = 52$ and $60°\,N$ at depths between 1055 and $1395\,m$ in the Atlantic basin. These diagnostics are calculated by summing properties over the discrete grid of the numerical model, they are represented here as integrals for convenience:

$$\psi(\phi, z) = r \cdot \cos(\phi) \cdot \int_{\lambda_1}^{\lambda_2} \int_{z}^{z_B} v \, dz' \, d\lambda' \tag{5.1}$$

$$\psi_{MAX} = \overline{\psi}(52 - 60°\,N, 80 - 0°\,W, 1055 - 1395\,m) \tag{5.2}$$

The second diagnostic is the amount of heat transported by the zonally averaged circulation at $24°\,N$ in the Atlantic. This term represents over 90% of the total heat transport in the Atlantic.

$$HT(24°N, 80 - 0°\,W) = r \cdot \cos(24°N) \cdot \int_{\lambda_1}^{\lambda_2} \int_{z_B}^{0} \overline{v}\overline{T} \, dz' \, d\lambda' \tag{5.3}$$

Both diagnostics were highlighted in Fig.4-8.

These two diagnostics should allow the separation between the sensitivity patterns, which are independent of the precise choice of the cost function and truly related to the intensity of the overturning, from those that can be related to the local definition of the diagnostic. The robust patterns can be expected, a priori, to have the same sign since both the heat transport at $24°\,N$ and the maximum value of the streamfunction are positive.

5.1.4 Sensitivity to Time Dependent Forcing

In its uncoupled configuration, the ocean model is forced by a flux of freshwater that is fixed in time. The adjoint solution is therefore equivalent to the difference between the effect on ψ_{MAX} of an infinitesimal perturbation in the water flux applied at a single point and maintained throughout the integration and an unperturbed run, divided by the magnitude of the perturbation. In the coupled model, the freshwater flux is recalculated by the energy and moisture balance model at every time step. The adjoint sensitivity is therefore an initial value sensitivity, it corresponds to a perturbation applied for one day only. In order to reconstruct the sensitivity to a permanent perturbation and compare the result obtained in the coupled model to the uncoupled one, sensitivities need to be integrated over time.

$$\frac{\partial \psi_{MAX}}{\partial F_w} = \int_o^T \left.\frac{\partial \psi_{MAX}}{\partial F_w}\right|_t dt \sim \sum_{t=0}^{t=T} \left.\frac{\partial \psi_{MAX}}{\partial F_w}\right|_t \Delta t \tag{5.4}$$

To obtain an accurate pattern, initial value sensitivities were calculated on a monthly basis for the first year, yearly for the next nine and every 25 years for remaining 390 years. These intervals are sufficient to capture the evolution of the sensitivity. Using day-to-day instead of monthly sensitivity maps for the first year did not change the results significantly (not shown).

The same procedure is used to calculate the sensitivity to the heat flux forcing in the coupled model. The heat flux sensitivity in the stand alone ocean model requires a similar procedure because of the time dependent sensitivity to the surface temperature:

$$\frac{\partial \psi_{MAX}}{\partial Q} = \frac{\partial \psi_{MAX}}{\partial Q_{obs}} \frac{\partial Q_{obs}}{\partial Q} + \frac{\partial \psi_{MAX}}{\partial T_0} \frac{\partial T_0}{\partial Q} + \frac{\partial \psi_{MAX}}{\partial T_{obs}} \frac{\partial T_{obs}}{\partial Q} = \frac{\partial \psi_{MAX}}{\partial Q_{obs}} + \lambda_s \left(\sum_{t=0}^{t=T} \frac{\partial \psi_{MAX}}{\partial T_0} \Big|_t \Delta t - \frac{\partial \psi_{MAX}}{\partial T_{obs}} \right) \tag{5.5}$$

As in equation 5.4, the sensitivity to the surface temperature needs to be integrated over time. In practice, the sensitivity to the surface temperature $\left(\frac{\partial \psi_{MAX}}{\partial T_0}\right)$ drops off quite rapidly. The climatological sensitivity is therefore primarily determined by the boundary value sensitivities to the observed heat flux and restoring temperature.

5.2 The Role of Buoyancy Forcing on Convection and Downwelling

Deep oceanic convection in the North Atlantic is driven by localized intense cooling events in the Norwegian, Labrador and Greenland Seas. The near-surface buoyancy loss destabilizes the water column, which overturns and becomes vertically homogeneous on fairly rapid time scales (Jones and Marshall, 1993; Marshall and Schott, 1999). The hypothesis originally suggested by Stommel (1961) and later Broecker et al. (1985), and adopted by many authors (Broecker et al., 1990; Zaucker et al., 1994; Manabe and Stouffer, 1995; Weaver, 1995; Rahmstorf, 1995) is that convection drives the meridional overturning circulation by forcing a southward flow at depth through mass convergence in the downwelling branch. This argument often implicitly assumes that convection and downwelling are somehow synonymous, and that increasing convective activity would automatically enhance the mass transport in the downwelling branch of the meridional circulation. Convection and downwelling may not be as intimately tied as often assumed, the rate at which convection

neutralizes the stratification can be varied by several orders of magnitude without affecting the actual volume transport associated with the overturning streamfunction (Marotzke and Scott, 1999). Highly idealized simulations show that convective mixing and downwelling are not necessarily co-located. The deepest convection in rectangular basins tends to take place in the northwest corner where the surface water is densest, downwelling usually takes place in the northeast corner where the zonal flow impinges on the boundary (Marotzke and Scott, 1999). In these studies, it is the zonal density and pressure differential set up by the convection and downwelling patterns, which drives the southward flow of the abyssal waters.

The ocean's abyss is filled with $2.5 - 3°C$ water in both the ocean and coupled models. This is the temperature of the convecting water, which is forced primarily in the Labrador and Greenland Seas in the ocean model and in the Labrador Sea in the coupled model. Water downwells along the Norwegian coastline, at temperatures of $4 - 6°C$.

5.2.1 Model Results

Heat Flux

The sensitivity pattern to the heat flux forcing is similar in both uncoupled, Fig.5-2 (top), and coupled cases, Fig.5-4: both peak in the northern part of the Atlantic basin where convection is taking place. The maximum is in the Greenland Sea in the uncoupled version of the model and in the Labrador Sea in the coupled version. This is related to slightly different convection patterns in the two configurations of the model. The large positive values in the Labrador and Greenland Seas can be attributed to the direct effect of a perturbation in the heat flux on the buoyancy of the surface and abyssal waters. The sign of the sensitivity is such that an increase in the loss of heat by the ocean to the atmosphere ($\Delta Q > 0$) leads to an increase in the magnitude of the streamfunction ($\Delta\psi_{MAX} > 0$).

The pattern of sensitivity to the heat flux is quite robust to the definition of the diagnostic, high sensitivities are observed in the Labrador and Greenland Seas regardless of the definition of the cost function (see Fig.5-2 and 5-3). The band of negative sensitivities, which can be observed at $24° N$ in the eastern Atlantic in the map of sensitivity of the heat transport to the temperature forcing (Fig.5-3), can be attributed to the direction of the currents in that region. The basin mean meridional flow is northward through the

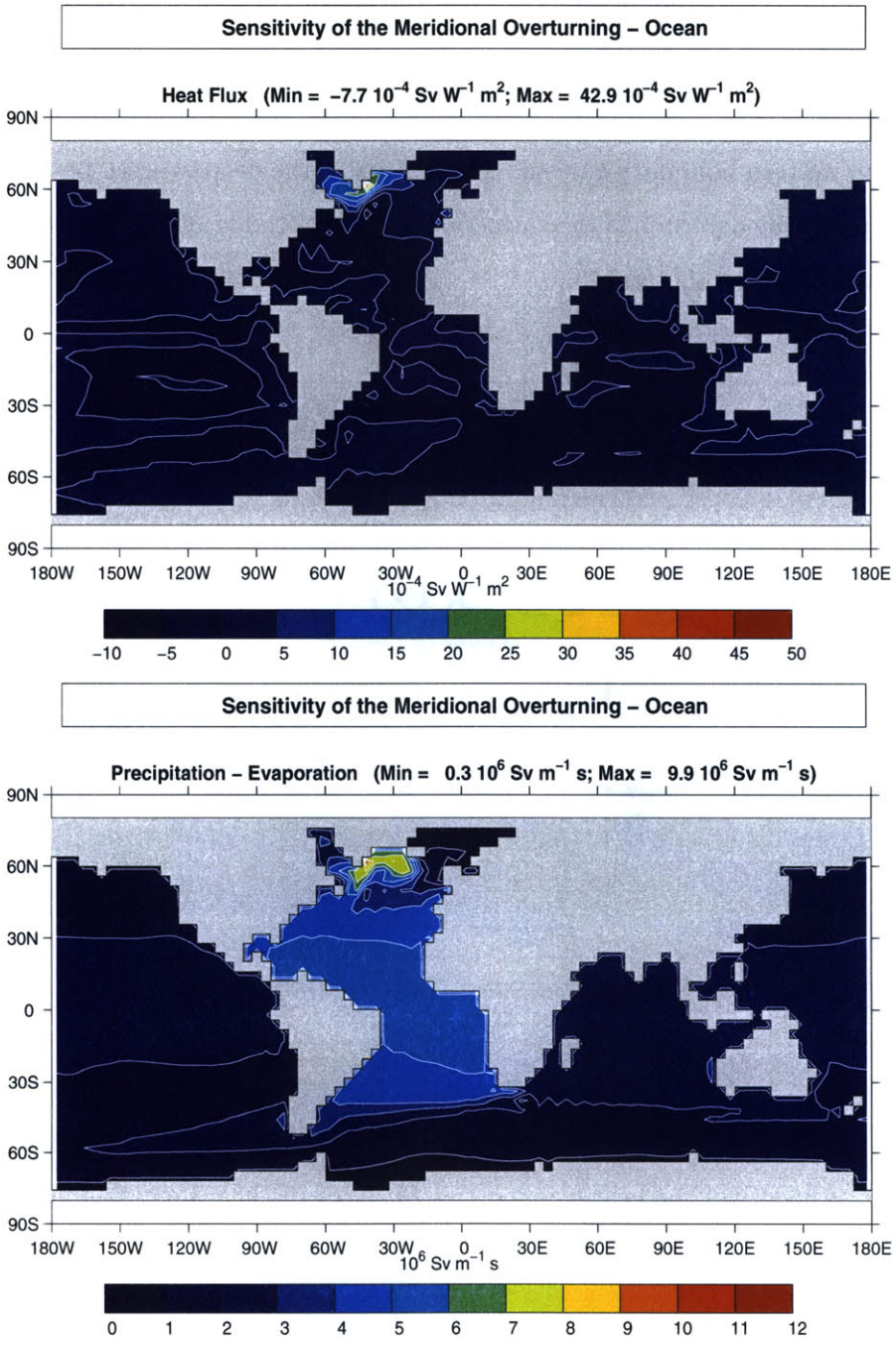

Figure 5-2: Sensitivity of the maximum value of the streamfunction ψ_{MAX} to the heat flux: $\frac{\partial \psi_{MAX}}{\partial Q}$ in $Sv\,W^{-1}\,m^2$ and to the freshwater flux: $\frac{\partial \psi_{MAX}}{\partial F_w}$ in $Sv\,m^{-1}\,s$ in the ocean model. The model's boundary conditions are $F_w = (E - P - R)_{obs}$ and $Q = Q_{obs} + \lambda_s(T - T_{obs})$.

thermocline at 24° N. Heating the ocean's surface ($\Delta Q < 0$) south of that latitude will therefore enhance the overall heat transport. The negative sensitivity values are explained by the fact that the heat flux is positive when the ocean loses heat to the atmosphere and negative when the ocean gains heat.

The flow patterns at depth (not shown) shows currents connecting the convection site with the deep western boundary current. The density of the deep western boundary current is therefore primarily determined by convection in the Labrador and Greenland Seas, hence the large sensitivities at those sites.

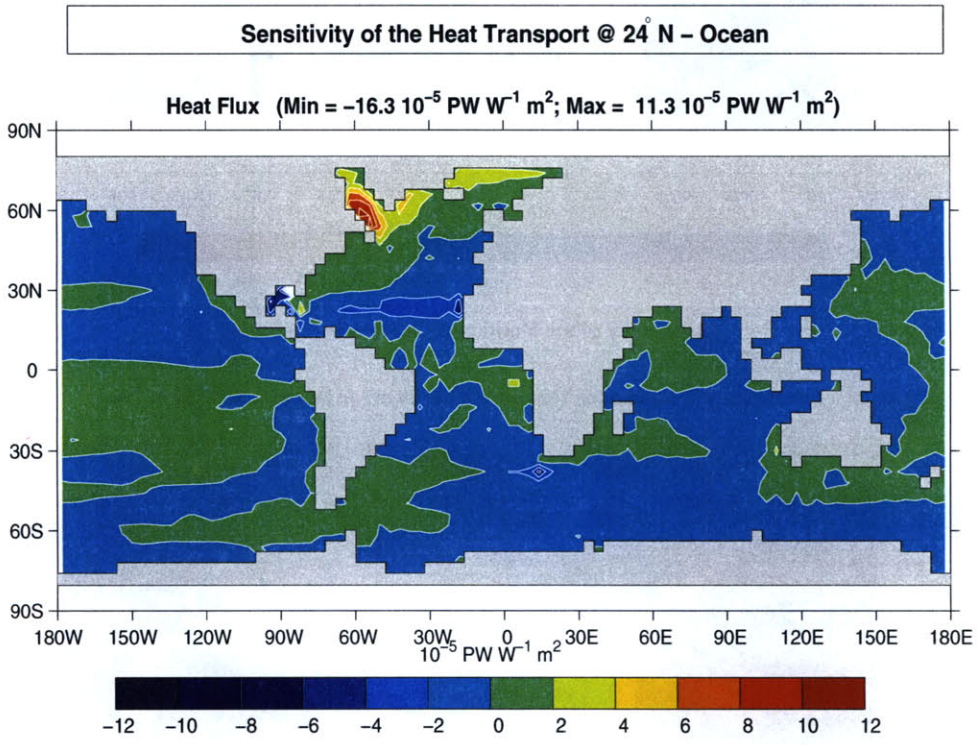

Figure 5-3: Sensitivity of the heat transport at 24° N to the heat flux: $\frac{\partial HT}{\partial Q}$ in $PW\,W^{-1}\,m^2$ in the ocean model. The model's boundary conditions are $F_w = (E - P - R)_{obs}$ and $Q = Q_{obs} + \lambda_s(T - T_{obs})$.

Advective ocean temperature feedbacks do not play a role in the uncoupled model. An increase in the heat gain in the sub-tropics or mid-latitudes will, in theory, increase the northward heat transport, thereby raising high latitude temperatures and consequently weakening the overturning. As noted by Nakamura et al. (1994), this feedback is weak if the relaxation time scale imposed on the sea surface temperature is short, which is the

case in these simulations. A simple scale analysis suggests that information is lost with an e-folding time scale equivalent to the relaxation time scale. Even the most rapid currents in the model ($\mathcal{O}(0.1\,ms^{-1})$) will not be able to transport information over more than $500\,km$ without seeing most of it dissipate. This explains why the region where large sensitivities are observed is confined to the neighborhood of the convection site, where perturbations can rapidly influence the cost function and the density of the abyssal waters.

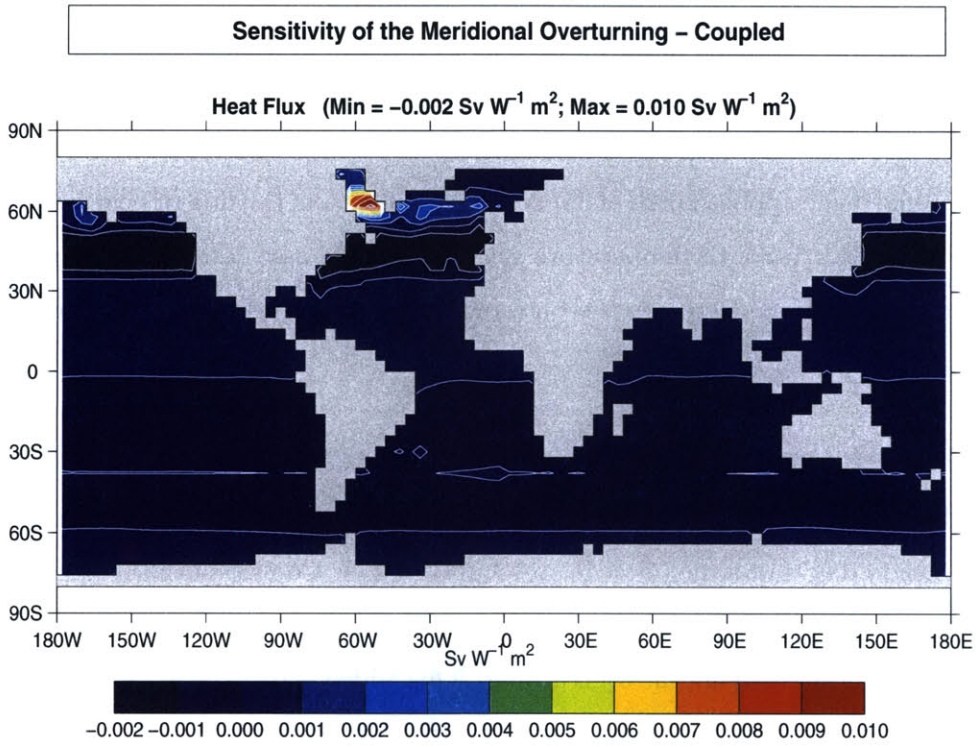

Figure 5-4: Sensitivity of the maximum value of the streamfunction ψ_{MAX} to the heat flux: $\frac{\partial \psi_{MAX}}{\partial Q}$ in $Sv\,W^{-1}\,m^2$ in the coupled ocean, energy and moisture balance model. The model's boundary conditions are $F_w = (E-P)_{mod} - R_{obs}$ and $Q = Q_{mod} + \lambda_m(T - T_{zon})$.

The atmosphere communicates information across and between basins much more rapidly than the ocean. In the energy balance model used for this study, information about a change in the sea-surface temperature at any location is in fact communicated to the rest of the world instantaneously through changes in atmospheric heat and water transport. The role played by atmospheric transport is evident from the zonally banded structure of the sensitivity pattern in Fig.5-4. This zonally homogeneous sensitivity is clearly superimposed onto the ocean-only sensitivity map shown in Fig.5-2. Sensitivities in the northern hemisphere

are slightly positive in the $0 - 35°$ N latitude band, they are slightly negative between 35 and $55°$ N and in the extreme northern part of the Atlantic basin.

Adding heat into the ocean in low latitudes ($\Delta Q < 0$) increases the equator to pole temperature contrast, and by extension the South to North heat and moisture transport (see equations 4.5 and 4.8 for the exact mathematical representation). This has two effects, the first is to increase high latitude temperatures, the second is to decrease the salinity in that region. Both contribute to increasing the water's buoyancy near the sites of convection. The sensitivity field obtained in the ocean-only case (Fig.5-2) indicates that this will inhibit the overturning.

The reverse logic applies north of $35°$ N, where increasing the flux of heat into the ocean will reduce the North-South temperature gradient and its associated energy and moisture transport. This in turn decreases the buoyancy at the convection site, thereby increasing the overturning.

The band of positive sensitivities that extends from $55°$ to $70°$ N across the Atlantic and Pacific basins is due to the term, which restores sea surface temperatures to their zonal mean on a sixty day time scale ($Q = Q_{mod} + \lambda_m(T - T_{zon})$. Cooling of the ocean anywhere in that latitude band decreases this zonal mean temperature, thereby increasing the heat loss by the ocean and intensifying the overturning. This added feature contributes to enhancing the maximum sensitivities in the northern Atlantic in the coupled model.

Because of the zonal nature of the atmospheric model, a perturbation imposed in the subtropical Pacific has the same impact on atmospheric transport and buoyancy in the northern Atlantic as a perturbation in the subtropical Atlantic. The instantaneous and absolute nature of this transport is clearly one of the less realistic features of the model, its only real objective is to represent the role played by the atmosphere in homogenizing temperatures, in both the zonal and meridional directions. The model was elaborated with integrations over time scales of decades or more or mind. It reproduces the rapidity of transport by the atmosphere, when compared to the ocean, on climatological time scales. Modeling studies have shown that rapid atmospheric teleconnections can link changes in one basin to the others over short time scales (Mikolajewicz et al., 1997).

Freshwater Flux

The sensitivity of the overturning to the net freshwater forcing in the uncoupled and coupled models are shown in Fig.5-2 (bottom panel) and Fig.5-5, respectively. Both patterns have a clear maximum in the polar region which is co-located with the maximum sensitivity to the heat flux forcing. The peak is approximately twice as large in the coupled model and located in the Labrador Sea instead of the Greenland Sea.

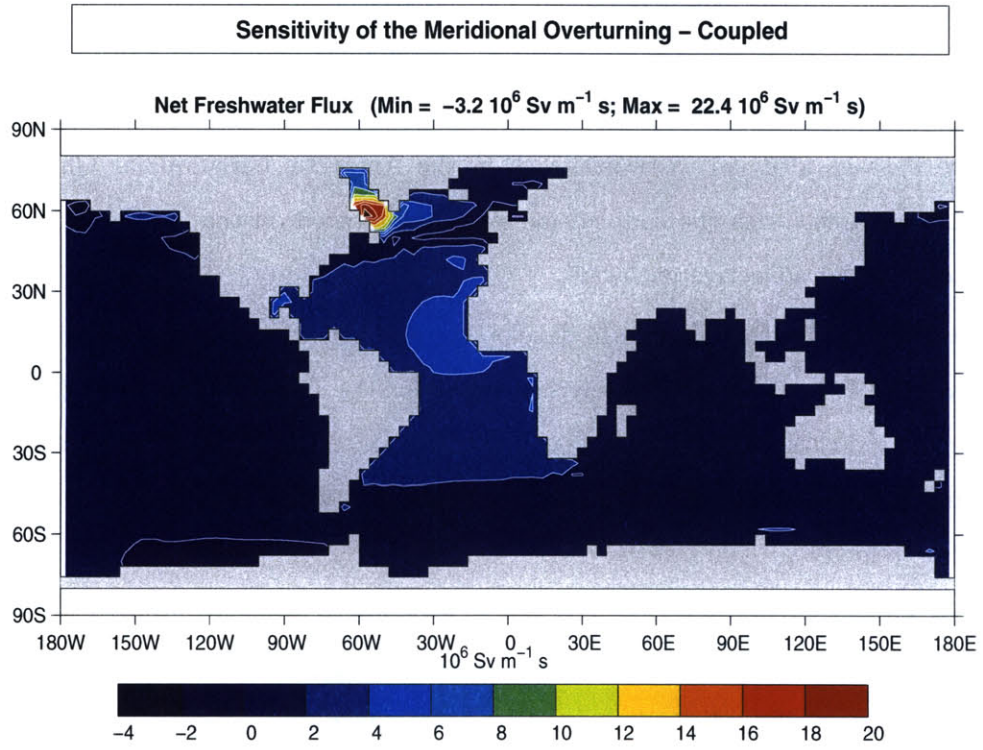

Figure 5-5: Sensitivity of the maximum value of the streamfunction ψ_{MAX} to the freshwater flux: $\frac{\partial \psi_{MAX}}{\partial F_w}$ in $Sv\, m^{-1}\, s$ in the coupled ocean, energy and moisture balance model. The model's boundary conditions are $F_w = (E-P)_{mod} - R_{obs}$ and $Q = Q_{mod} + \lambda_m(T - T_{zon})$.

While the efficiency of heat advection was limited by the formulation of the boundary condition in the ocean model, the flux boundary condition on the surface salinity does not impose any constraint on the oceanic salt advection feedback. This explains the sensitivities to freshwater forcing in the equatorial and tropical regions when compared to the sensitivity pattern to the heat flux forcing, which was concentrated in high latitudes. The salt advection feedback is positive: the overturning contributes to the transport of freshwater anomalies toward the pole, where it can weaken the overturning, thereby reducing

the advective mechanism (Marotzke and Stone, 1995). The sign of the sensitivity is indeed everywhere such that a positive salinity perturbation ($\Delta F_w > 0$, i.e. more evaporation or less precipitation) increases the overturning.

The role played by advection is evident from the sensitivity map shown in Fig.5-2 (bottom): moderate sensitivity values are seen extending westward from the Drake passage into the Antarctic Circumpolar Channel and eastward from the Cape of Good Hope into the Indian Ocean. These sensitivities extend beyond the Indonesian throughflow to the tropical Pacific. The Indian Ocean sensitivities are particularly interesting, they extend only as far south as the latitude of the Agulhas current, which feeds water into the Atlantic basin. This indicates that the waters located south of $40° S$ can only enter the Atlantic basin via the Drake Passage after an eastward track in the Antarctic Circumpolar Channel. The sensitivities obtained with the coupled model, when plotted on the same scale as Fig.5-2, exhibit very similar advective pathways.

The time taken for this pattern to develop supports the notion that advection plays an important role. It takes approximately fifty years for the signal to appear at the southern tip of Africa, and close to one hundred years for it to extend to the Indonesian throughflow. These time scales translate into a speed of $7 - 8\ mm\, s^{-1}$, which is close to the average near surface flow velocity.

The pattern calculated with the coupled model (Fig.5-5)differs only in a few locations from the ocean-only case. This indicates that oceanic advective effects are the primary source of the sensitivity, a logical consequence of the fact that salinity perturbations have no direct impact on the atmospheric heat and moisture transport. The band of negative sensitivities in the Northern Atlantic extends westward from one of the sites, where much of the downward mass transport originates. This is a pattern reminiscent of the one shown in Fig.3-21 (bottom right panel) under flux boundary conditions in an idealized framework. Figure 3-21 showed a clear path between surface warming, advection along the northern edge of the subtropical gyre, downwelling at the eastern boundary and the strength of the meridional overturning circulation. The same connection between a warming of the eastern boundary and a stronger vertical shear in the meridional flow can be made in the realistic geography model. It is not clear why there is an area of negative sensitivities in the northern Pacific, but salinity perturbations must somehow induce a temperature response that affects the atmospheric transport. These sensitivities cannot be related directly to the meridional

streamfunction, since the cost function is calculated in the Atlantic basin only.

5.2.2 Discussion

Three hypotheses can be considered to link temperature and salinity perturbations to the overturning. The first relates changes in buoyancy to the "efficiency" of convection, and by extension downwelling and the overturning (Rahmstorf, 1994). This concept does, however, require some clarification. The role of convection is to set the density of the deep western boundary current and of much of the western boundary. The water downwells, in this model, primarily between the UK and Iceland and along the Norwegian coast. This determines the density along the eastern boundary. The downwelling water spreads westward at depths between 1000 and 2000 m, this is shown in Fig.5-6 in the coupled model. A more precise definition for the "efficiency" of convection is really the control, which it exerts on the zonal density contrast below the thermocline (Marotzke, 1997). The advection of buoyancy perturbations, by the Gulf Stream in the subtropical gyre and by the eddy induced transport of tracers at higher latitudes, towards the sites of convection and downwelling, is a key determinant of the sensitivity patterns. Atmospheric feedbacks play an added role in the coupled model in determining the global sensitivity pattern to heat flux perturbations. These results support the notion that the meridional overturning circulation is thermally driven (Rahmstorf, 1996). The circulation is inhibited by a net input of freshwater. The sign of the sensitivity to the freshwater flux would be reversed if the circulation was driven by both thermal and haline forcings.

The second hypothesis focuses on the influence of temperature and salinity perturbations on the density of the abyssal water, and by extension on the amount of energy, which must be supplied to upwell these waters. One would, however, expect that increases in density would increase the requisite energy, or, for constant mixing energy, decrease the overturning. This is not observed. The third hypothesis links surface freshening or increases in temperature, notably in the tropics, to a decrease in the buoyancy differential between surface and sub-thermocline waters. By extension, this would allow more upwelling for a given energy input (Huang, 1999). The positive sensitivities to heat loss and evaporation contradict this hypothesis. Hypotheses two and three, and whether the meridional overturning circulation is "pushed down" or "pulled up", (Marotzke and Scott, 1999) will be revisited in the section devoted to mixing.

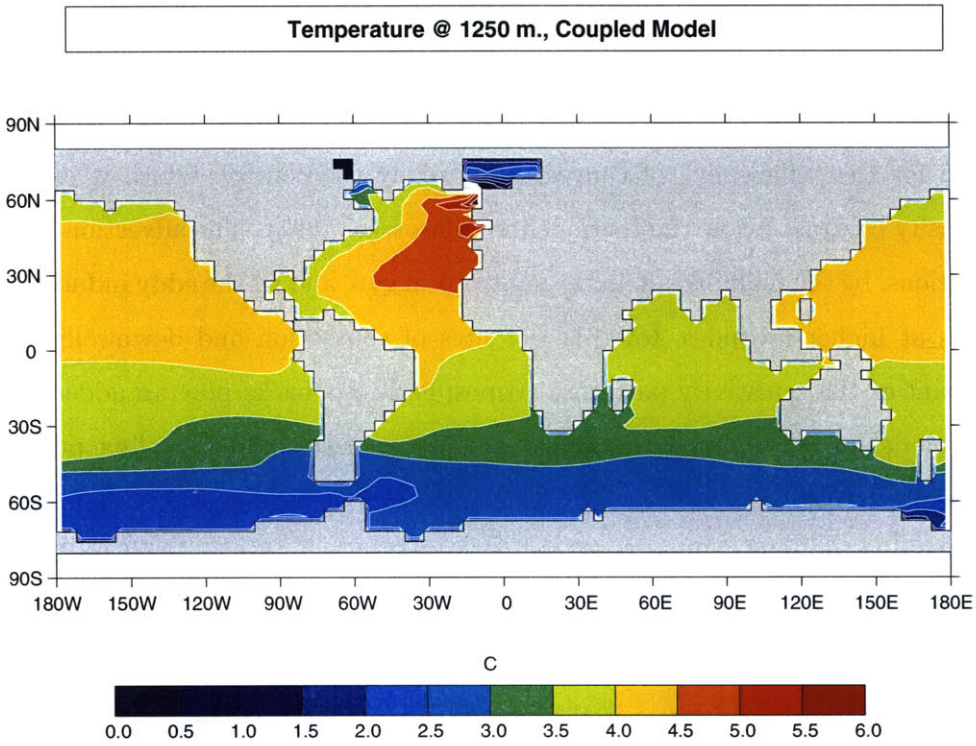

Figure 5-6: Temperature at $1250\,m$ in the coupled model

5.3 Mixing and Tropical Upwelling

The ocean is heated at a higher geopotential than it is cooled. This simple thermodynamic argument known as Sandström's theorem should confine the meridional overturning to a thin surface layer, leaving the abyss motionless (Sandström, 1908). A deep circulation can only exist if the geopotential of the heating is lowered (Jeffreys, 1925). This can be achieved by mixing heat downwards, through turbulent breaking of internal gravity waves (Gregg, 1987; Polzin et al., 1997), a process parameterized by diapycnal diffusion in coarse resolution models ($\frac{\partial}{\partial z'}\kappa_d\frac{\partial T}{\partial z'}$ where z' is the direction perpendicular to the isopycnal surface). Tides and wind stress are thought to provide the source of energy required to generate the ocean's internal gravity wave spectrum (Munk and Wunsch, 1998). The parameterization of mixing in terms of a constant diffusion coefficient neglects the influence of wind and tides on the mixing rate. The sensitivity of the overturning to wind stress therefore also fails to include its influence on mixing. While the deep ocean may be close to a vertical advective-diffusive balance, with upwelling of abyssal water being compensated with downward diffusion of heat, the upper ocean certainly is not (see e.g. Samelson and Vallis (1997)). Ekman upwelling in the regions of wind stress divergence can, for example, influence the vertical velocity field and the structure of the thermocline (Vallis, 2000), while the horizontal advection terms often dominate the heat budget.

The adjoint analysis has the potential to highlight the geographical locations and depth in the water column where the meridional overturning circulation exhibits the greatest sensitivity to diapycnal mixing. A number of studies, notably Ledwell and Hickey (1995); Ledwell and Bratkovich (1995), point to large spatial inhomogeneities, with mixing being concentrated along boundaries and mid-oceanic ridges. Diapycnal mixing is, however, a spatially uniform parameter in the model used for this analysis. It is, therefore, possible that the present adjoint model is generating large sensitivities to mixing in regions where the background mixing should in fact be very small.

5.3.1 Model Results

The pattern of sensitivity to a column by column perturbation in the value of diapycnal mixing is shown in Fig.5-7 for the ocean model. The top panel represents the sensitivity when the cost function is the streamfunction maximum, the bottom panel shows it when the

diagnostic is the heat transport at $24° N$. Fig.5-8 is the sensitivity of ψ_{MAX} to diapycnal mixing in the coupled model.

The sensitivity pattern is very robust, both to a change in cost function and to coupling to the atmosphere. The equatorial and tropical regions dominate in all cases, in particular the $10° S - 15° N$ latitude band. The pattern robustness does not, however, extend into the western boundary current. The conflicting signals about the importance of this region in determining the overturning will be dealt with in a later section. The importance of the equatorial region can be traced to large sensitivities in the near surface layers, between 100 and $200\,m$. The connection to the wind stress divergence and Ekman up- and downwelling patterns is therefore a logical one. The effect of Ekman upwelling is to compress isopycnals in the equatorial region, thereby increasing the efficiency of the downward diffusion of heat. This process is particularly effective in the eastern part of the basin, where the easterly wind stress further lifts the thermocline, while it deepens it in the western part of the basin. Sensitivities are weaker outside of the band of Ekman upwelling because of the decrease in stratification associated with the downward motion.

There are two key differences between the coupled and uncoupled models. The streamfunction maximum is more sensitive to changes in the equatorial diffusivity when atmospheric feedbacks are included, and the sensitivities extend into the Pacific and Indian Oceans. The role played by the atmosphere is straightforward. Increasing diffusivities in a positively stratified environment will draw heat downward from the surface, thereby cooling it. This, in turn, reduces the meridional temperature contrast and its associated heat and moisture transport. The net result is to reduce the buoyancy of the water in the North Atlantic. The sensitivity analysis of the overturning to buoyancy forcing indicates that this will increase the intensity of the overturning circulation. This process is reversed North of $35° N$, thus explaining why the sensitivity bands are negative in mid-latitudes. The sensitivity pattern to wind stress (Fig.5-9) is in many respects similar to the sensitivity to mixing, and can be explained by the effect of wind stress perturbations in inducing local upwelling and cooling of the surface.

5.3.2 Discussion

The adjoint model confirms the sensitivity studies of Scott and Marotzke (2001), which indicated that the overturning was most sensitive to changes in mixing in the tropics. The

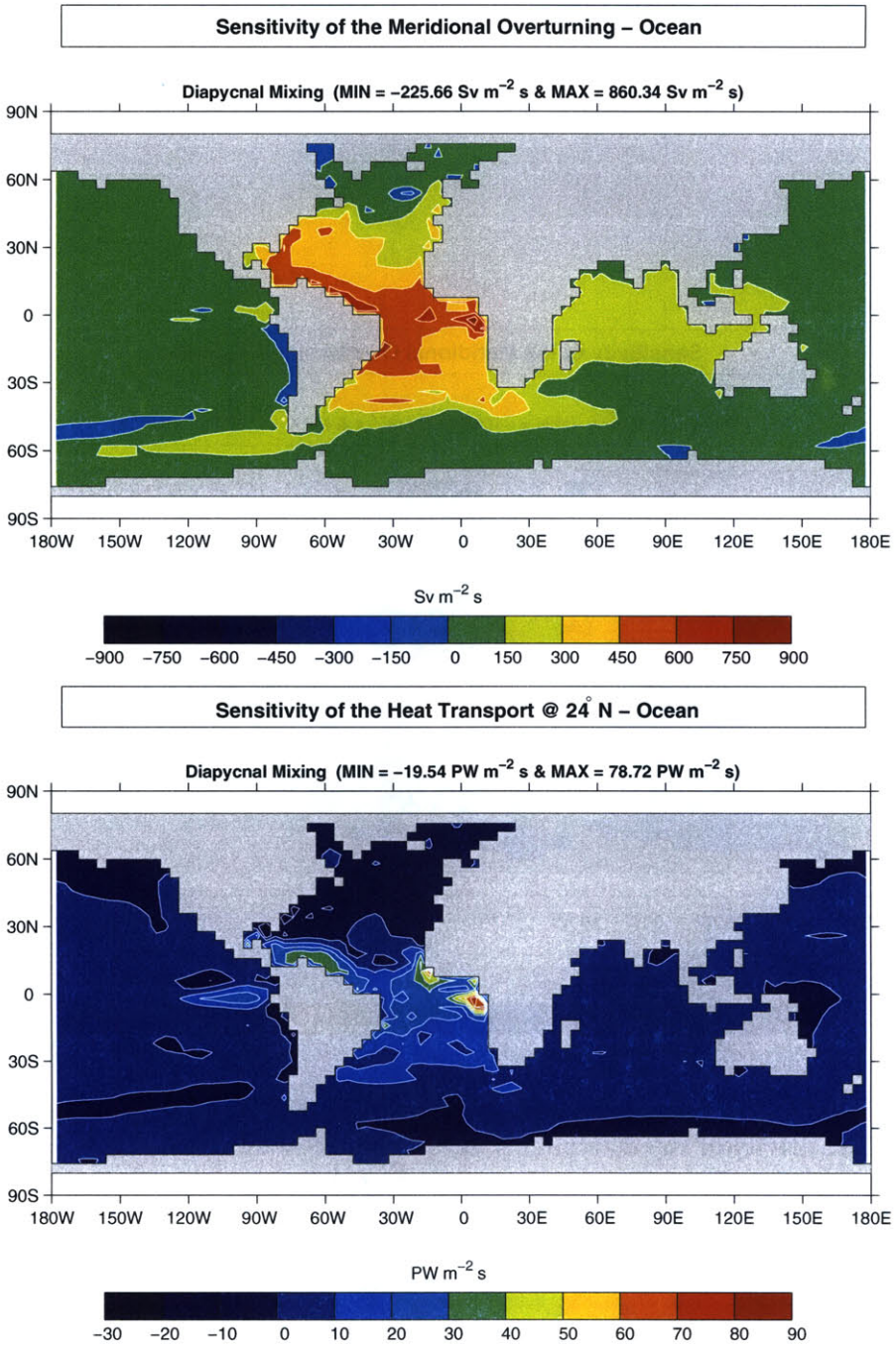

Figure 5-7: Sensitivity of the maximum value of the streamfunction ψ_{MAX} to a column by column perturbation in the diapycnal mixing in the ocean model. Top: $\frac{\partial \psi_{MAX}}{\partial \kappa_d}$ in $Sv\, m^{-2}\, s$. Bottom: $\frac{\partial HT_{24^\circ N}}{\partial \kappa_d}$ in $PW\, m^{-2}\, s$. The model's boundary conditions are $F_w = (E - P - R)_{obs}$ and $Q = Q_{obs} + \lambda_s(T - T_{obs})$.

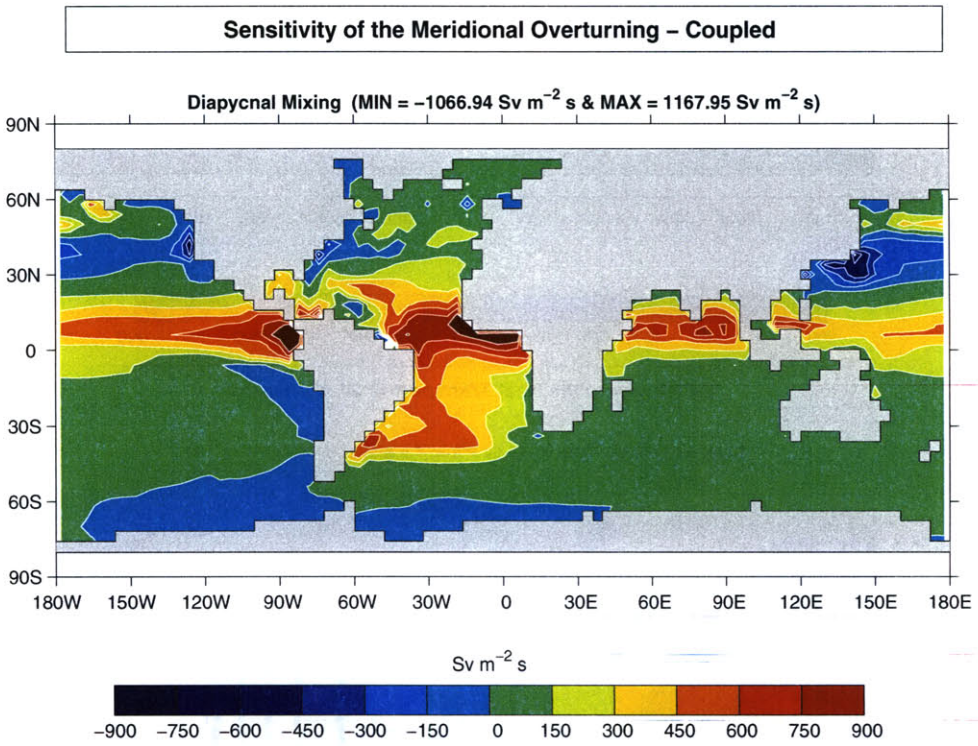

Figure 5-8: Sensitivity of the maximum value of the streamfunction ψ_{MAX} to a column by column perturbation in the diapycnal mixing: $\frac{\partial \psi_{MAX}}{\partial \kappa_d}$ in $Sv\, m^{-2}\, s$ in the coupled model. The model's boundary conditions are $F_w = (E-P)_{mod} - R_{obs}$ and $Q = Q_{mod} + \lambda_m(T - T_{zon})$.

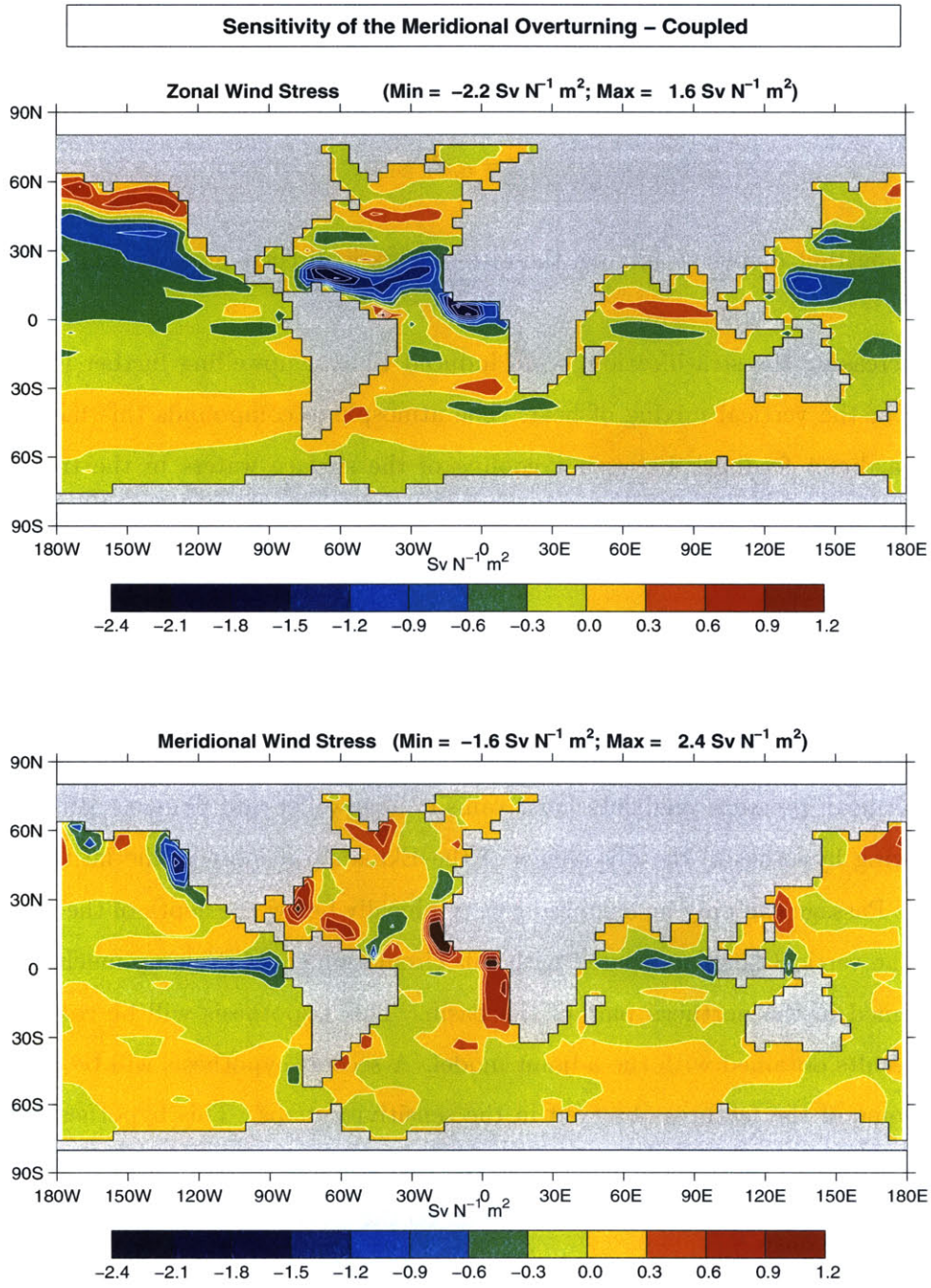

Figure 5-9: Sensitivity of the maximum value of the streamfunction ψ_{MAX} to the wind stress, both zonal and meridional: $\frac{\partial \psi_{MAX}}{\partial \tau_{x,y}}$ in $Sv\, N^{-1}\, m^2$ in the coupled ocean, energy balance model. The model's boundary conditions are $F_w = (E-P)_{mod} - R_{obs}$ and $Q = Q_{mod} + \lambda_m(T - T_{zon})$.

source of mechanical energy available for mixing is wind and tides (Munk and Wunsch, 1998). Part of this energy is converted into potential energy through a vertical buoyancy flux through breaking internal gravity waves and complicated coastal processes. The rate of work done against gravity (ϵ) in a stably stratified fluid is:

$$\epsilon = \kappa_d N^2$$

For a constant diapycnal mixing, the rate of work is directly proportional to the stratification N.

By increasing the stratification, wind induced Ekman upwelling further increases the efficiency of the vertical mixing of heat. The atmosphere compounds this mechanism by allowing a direct feedback between a cooling of the surface waters in the tropics and a decrease in the buoyancy of the water in the northern part of the Atlantic where convection and downwelling take place.

5.4 Wind Stress in the Southern Oceans

In a latitude band with no continental barriers, notably in the Antarctic Circumpolar Channel, zonal mean pressure gradients must vanish. Toggweiler and Samuels (1995) outlined the following hypothesis: the divergence of the Ekman transport in the latitude band of the Drake Passage can only be balanced geostrophically below the depth of the topographic ridges. The vertical flows associated with this circulation could draw up much of the deep water formed in the northern part of the basin. This hypothesis will be re-examined in light of results obtained with the adjoint model. A second hypothesis will be presented to explain some of the features observed in the sensitivity maps. This hypothesis will focus on the general role played by "gateways", the regions that control the flow of water into and out of the Atlantic basin, and in particular on the "warm water route" via the Agulhas current suggested by Gordon (1986).

5.4.1 Model Results

Three areas show unexpected high sensitivities to wind stress (Fig.5-10) and mixing (Fig.5-16): the region which includes the Agulhas current and the Agulhas retroflection south of the Cape of Good Hope, the Indonesian throughflow, and the Chilean coastline. These three

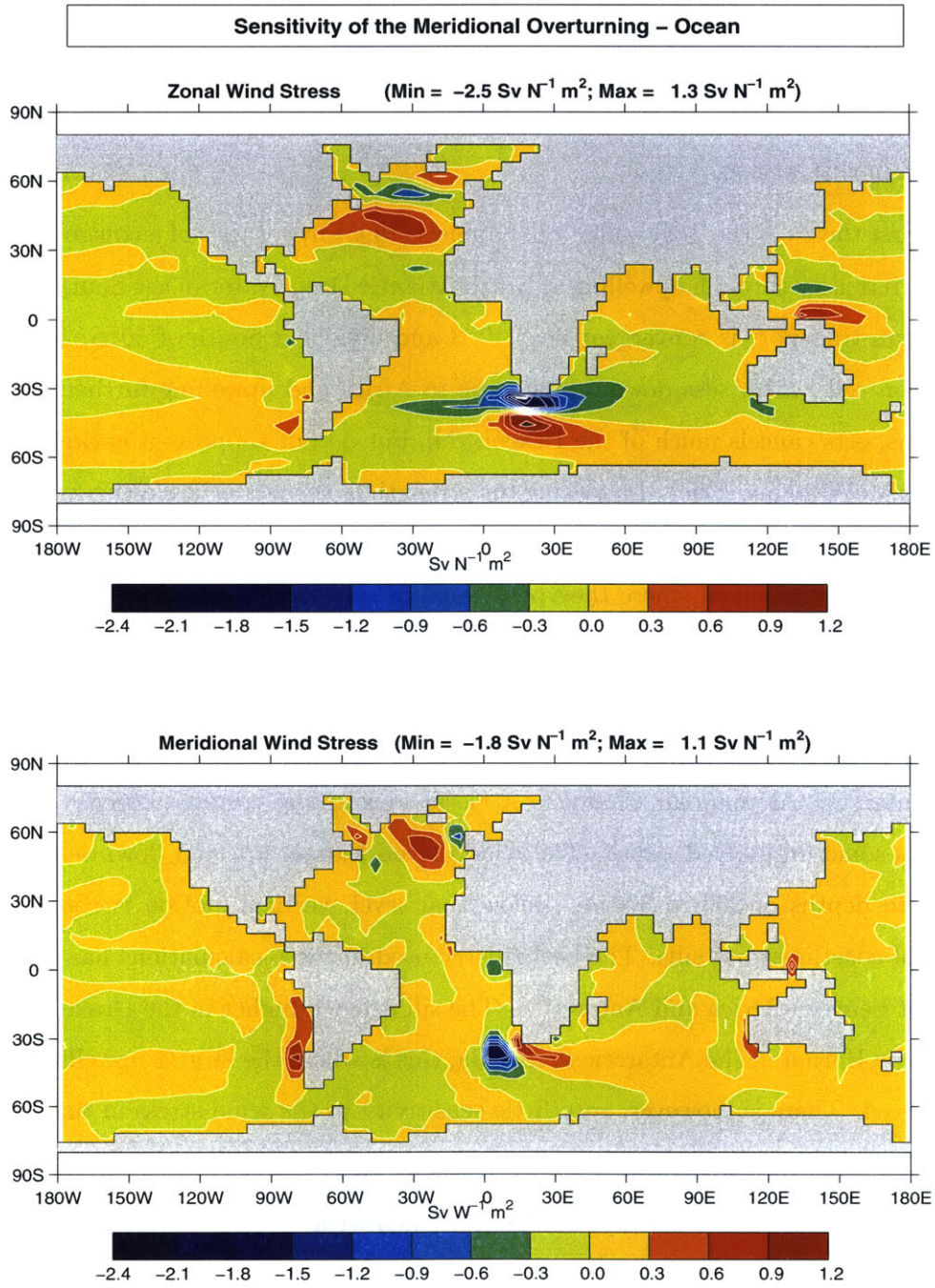

Figure 5-10: Sensitivity of the maximum value of the streamfunction ψ_{MAX} to the wind stress, both zonal and meridional: $\frac{\partial \psi_{MAX}}{\partial \tau_{x,y}}$ in $Sv\, N^{-1}\, m^2$ in the ocean model. The model's boundary conditions are $F_w = (E - P - R)_{obs}$ and $Q = Q_{obs} + \lambda_s(T - T_{obs})$.

regions share in common the control of the water exchanged between basins. The Agulhas current and the Drake Passage allow water to flow into the Atlantic from the Indian and Pacific basins, the Indonesian archipelago allows the exchange of water between the Pacific and the Indian oceans.

The consistency between the two hypotheses outlined above and these features will be examined in this section.

The first theory is the Toggweiler and Samuels (1995) hypothesis of a control of the overturning's intensity through upwelling of North Atlantic Deep Water in the Southern Oceans. The Ekman transport is convergent near $40°S$ and divergent South of $50°S$. This induces the Deacon cell, which sees downwelling close to Africa and upwelling further South. The eddy transports cancels much of the Deacon cell, but do not suppress it entirely (Danabasoglu and McWilliams, 1995). Increasing the strength of the westerlies in the Agulhas Basin ($\circ 40°$ S) reduces the convergence of the Ekman transport, thereby weakening the Deacon cell. Increasing the winds where they peak, near $50°S$, tends to intensify the Deacon cell. One could, therefore, anticipate positive sensitivities around $50°S$ and negative sensitivities further North and South where intensifying the westerlies would weaken the cell. This is approximately what is observed south of Africa in Fig.5-10, but not throughout the rest of the Antarctic Circumpolar Channel. A closer look at the vertical velocity pattern also highlights some unresolved issues. The wind driven Ekman up- and downwelling extends at most to depths of 200 to $300\,m$. Below that level, vertical motion is confined to the vicinity of coastlines and sills. The bathymetry used in these calculations has only a small sill height between Africa and Antarctica. The sill is much higher in the Drake Passage between Cape Horn and the Antarctic Peninsula, this is where the largest upwelling velocities are observed. There is, however, very little sensitivity to the wind stress in that region.

Following the simple analytical model of Gnanadesikan (1999), the volume of upwelling water in the Southern Oceans (T_S) can be described with:

$$T_S = \left(\frac{\tau}{\rho f} - \frac{\kappa_{td} D}{L_y^s} \right) L_x \tag{5.6}$$

where τ is the zonal wind stress over the ACC, L_x the circumference of the Earth in the Drake Passage, L_y^s the North-South extent of the Drake Passage, D the depth of the pycnocline and κ_{td} the thickness diffusion. This equation shows that while the zonal wind

stress acts to enhance the volume transport $\left(\frac{\partial T_S}{\partial \tau} > 0\right)$, the eddy induced velocity acts to reduce it $\left(\frac{\partial T_S}{\partial \kappa_{td}} < 0\right)$. This simple model is partially verified by the adjoint analysis. Increasing the wind stress can indeed increase the overturning, but only if the increase is applied over a small portion of the channel south of Africa. The sensitivity to the eddy induced transport is negative in a significant fraction of the Southern Oceans (Fig.5-11), but the maximum is again clearly in the region of the Agulhas Plateau.

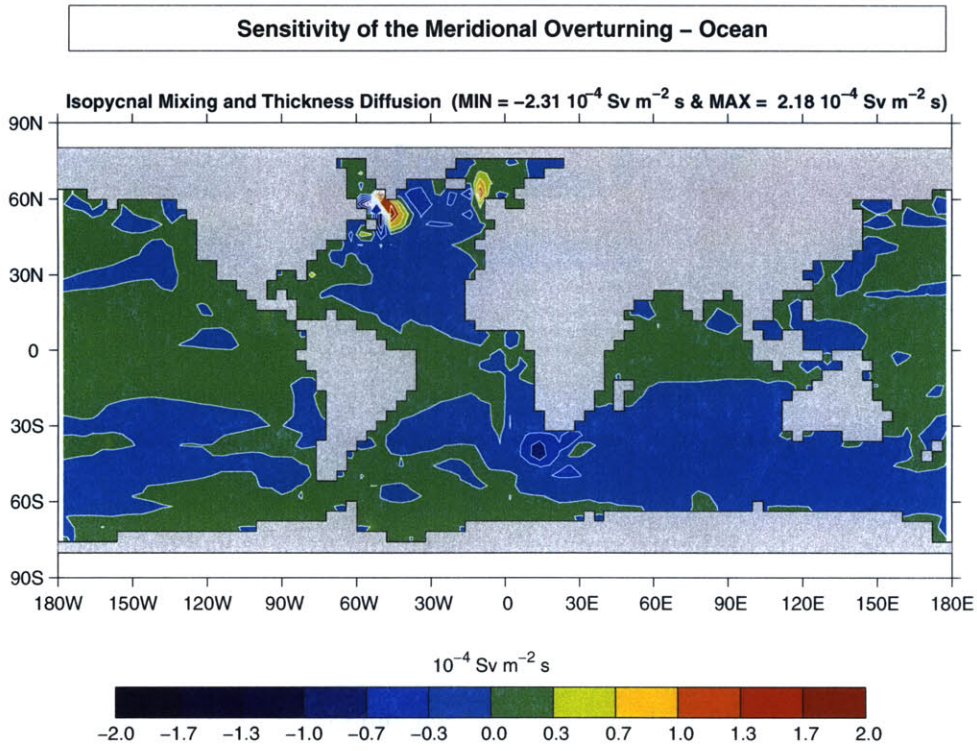

Figure 5-11: Sensitivity of the maximum value of the streamfunction ψ_{MAX} to the isopycnal mixing and thickness diffusion: $\frac{\partial \psi_{MAX}}{\partial \kappa_i, \kappa_{td}}$ in $Sv\, m^{-2}\, s$ in the ocean model. The model's boundary conditions are $F_w = (E - P - R)_{obs}$ and $Q = Q_{obs} + \lambda_s(T - T_{obs})$.

The idealized rectangular basin model described in chapters 2 and 3 is quite helpful in explaining the consistencies and discrepancies between the hypothesis of Toggweiler and Samuels (1995) and Gnanadesikan (1999) and the results of the adjoint model. This model highlights the role played by the surface boundary conditions in determining the sensitivity patterns. Fig.5-12 shows the sensitivity of the streamfunction maximum to the zonal wind stress in the region of the "Antarctic Circumpolar Channel" for the three sets of surface boundary conditions presented in Table 3.1. Mixed boundary conditions similar to the ones

used in the realistic geography model are shown in the middle panel. Restoring boundary conditions were used in the left-hand panel, and the equivalent flux boundary conditions were used on the right. All figures are plotted on the same scale. The sensitivities in the channel are three times larger under restoring boundary conditions than under flux boundary conditions, with the mixed boundary conditions presenting an intermediate case.

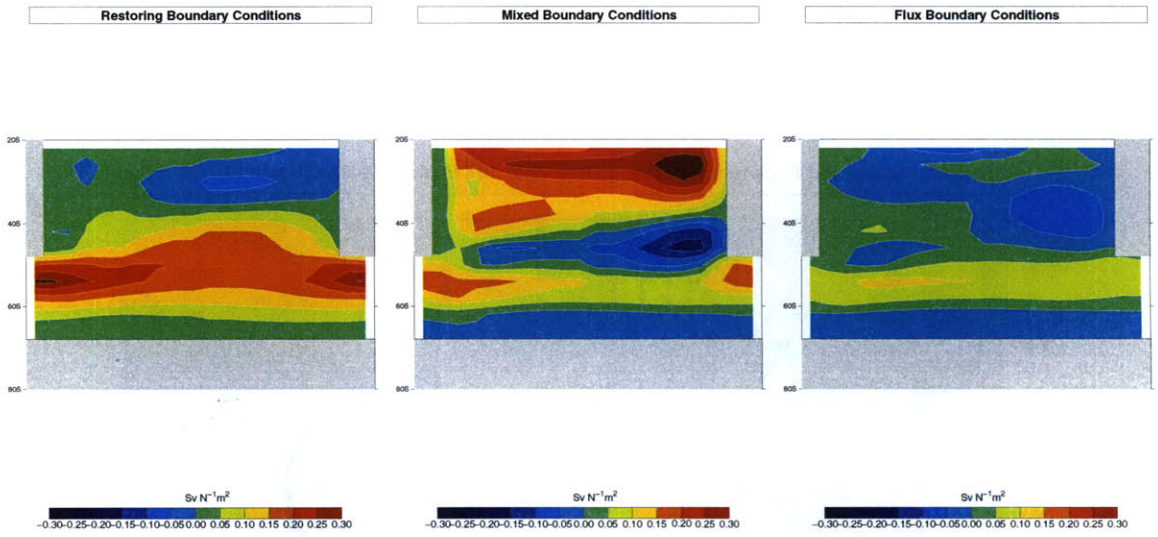

Figure 5-12: Sensitivity of the streamfunction maximum to the zonal wind stress $\left(\frac{\partial \psi_{MAX}}{\partial \tau_x}\right)$ in $Sv\, N^{-1}\, m^2$. Left: Restoring boundary conditions. Middle: Mixed boundary conditions. Right: Flux boundary conditions. The three plots are on the same scale.

The key difference between the restoring, mixed and flux simulations lies in the response of the density field to perturbations in the wind stress. The surface density is very nearly fixed under restoring boundary condition. Under mixed or flux boundary conditions, the near surface density is no longer constant.

Fig.5-13 shows the response of the near-surface temperature field to a wind stress perturbation for each of the three cases shown in Fig.5-12. A westerly wind stress anomaly was imposed at $50°\ S$ above the sill, south of the continent. The resulting perturbations in the temperature fields at $100\, m$ depth are shown in Fig.5-13, the three plots are on the same scale. The temperature and salinity perturbations decrease with depth, but the relative magnitude of the anomalies between the three cases remains similar. The wind stress anomaly induces convergence and downwelling equatowards of $50°\ S$, divergence and upwelling polewards of the perturbation. The magnitude of the perturbation in the Eulerian

upwelling velocity is similar in all three cases. The dominant temperature response shows a cooling where anomalous downwelling is taking place between 50° S and 60° S and warming polewards of the anomaly. The pattern of salinity anomaly are similar, with increased salinity where upwelling is taking place. The salinity anomalies are greater under mixed and flux boundary conditions than under restoring boundary conditions.

The perturbation bolus velocity is defined as:

$$w^{\star'} = \kappa_{td}\left(\frac{\partial S'_x}{\partial x} + \frac{\partial S'_y}{\partial y}\right) \approx \kappa_{td}\frac{\partial S'_y}{\partial y}$$

where S_x and S_y are the isopycnal slopes in the meridional and zonal directions.

The salinity and temperature anomalies induce a perturbation in the meridional slope, with isopycnals anomalies sloping upwards between "Antarctica" and 60° S, and downwards from 60° S towards the continent. The eddy transport will seek to flatten these isopycnals. This induces a perturbation flow with downwelling taking place polewards of 50° S, thereby opposing the Eulerian circulation. It is clear from the magnitude of the buoyancy perturbations, that the changes in eddy transport will compensate a larger fraction of the induced Eulerian circulation under flux boundary conditions than in the restoring case.

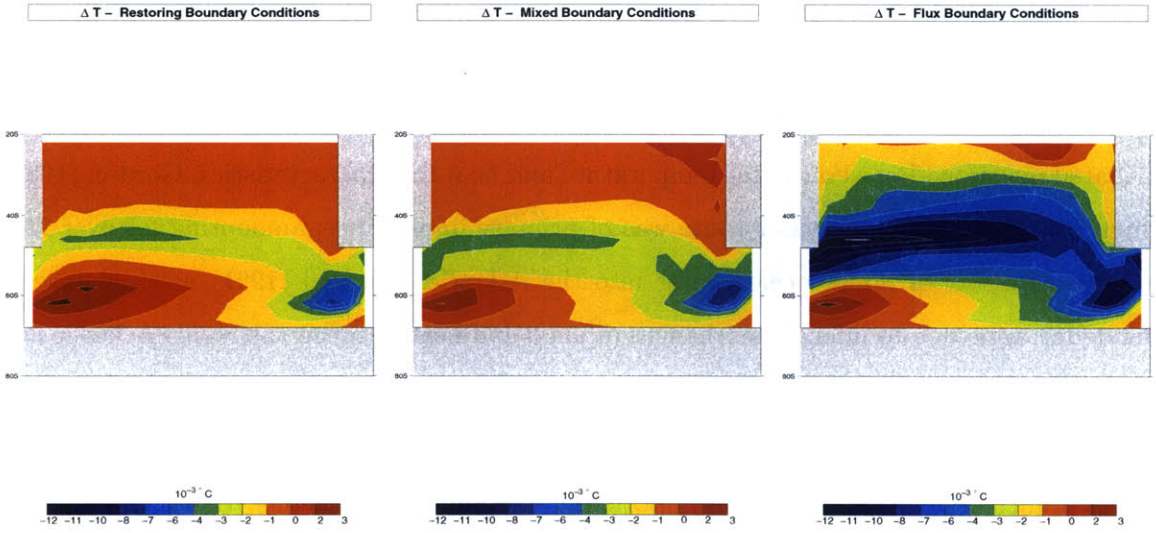

Figure 5-13: Change in temperature, in $°C$ at 100m. for a perturbation in the surface wind stress of Sensitivity of the streamfunction maximum to the zonal wind stress $\Delta\tau_x = 0.001\, Nm^{-2}$ imposed at 50° S above the sill. Left: Restoring boundary conditions. Middle: Mixed boundary conditions. Right: Flux boundary conditions.

The mechanism outlined by Toggweiler and Samuels (1995) plays a crucial role in determining the strength of the meridional overturning when the surface boundary conditions are formulated as restoring terms. This was indeed the case in the analysis of Toggweiler and Samuels (1995). This mechanism does, however, lose much of its importance when the surface fields are allowed to evolve constrained only by surface fluxes of heat and freshwater. This feature had already been noticed by Rahmstorf and England (1997) in a model without the Gent-McWilliams parameterization. These authors compared the sensitivity of the meridional overturning to changes in the wind stress south of of 30° S in a model forced with restoring boundary conditions and a model forced with boundary conditions similiar to the mixed boundary conditions used here. The difference in sensitivity was attributed to the stabilizing role of the thermal feedback effect. This effect stabilizes the overturning by allowing the ocean to cool in response to a weakening of the circulation, something that is not possible under flux boundary conditions.

A second hypothesis is therefore proposed to explain the observed sensitivity of the meridional overturning to the surface wind stress. It relies on a direct control of the properties, and in particular of the salinity, of the water allowed to enter or leave the Atlantic basin. It rests on the premise that the Atlantic is the saltiest of the world's oceans.

Relying on the hypothesis that much of the North Atlantic Deep Water upwells in the Pacific and Indian Oceans, Gordon (1986) proposed two routes for the return flow of thermocline water: a cold water route through the Drake Passage and a warm water route by a branch of the Agulhas current. Which is the dominant route has been a highly debated question. Based on water temperature and heat flux characteristics, Gordon (1986) suggested that the warm water route was of primary importance, amounting for over 75% of the transport of upper ocean water into the Atlantic. Rintoul (1991) used an inverse modeling approach to infer the exchanges of mass and heat between the South Atlantic and its neighboring basins. He concluded that most of the water entered the South Atlantic via the cold water route of the Drake Passage.

A branch of the Agulhas current imports Indo-Pacific water into the Atlantic, it coincides with the region of sensitivity minimum. The region of positive sensitivity just south of the Agulhas retroflection exports Atlantic water to the rest of the world's oceans. The surface currents in that region are notably complex, they are shown for reference in Fig.5-14. The branch of the Agulhas current, which enters the Atlantic has a salinity of approximately

34.6. The Benguela current, which follows the western coast of Africa, draws its source in fresher water in the Southern Oceans, with an approximate source at a salinity of 33.4.

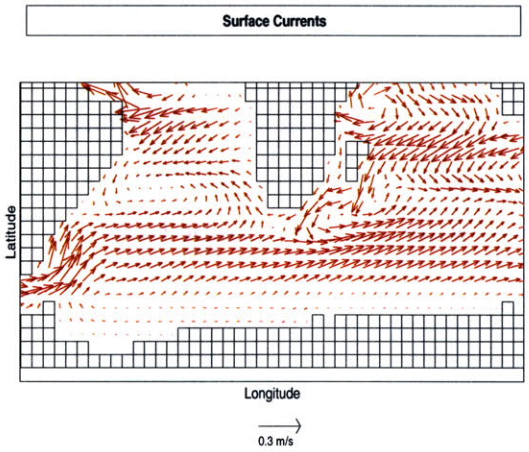

Figure 5-14: Surface currents around the African continent. Ocean model.

Complex interactions exist over the Agulhas Plateau between the surface wind stress and the ocean currents. The sensitivity analysis indicates that a westerly wind perturbation south of the Cape of Good Hope would eventually weaken the meridional overturning. South of the Agulhas Plateau, the same westerly wind perturbation would increase the overturning. The sign of the sensitivity to the wind stress north of the Indonesian throughflow is such that hindering the mass flow through that passage with a southerly or a westerly wind perturbation increases the overturning. Once out of the Indonesian throughflow, the water takes a direct route across the Indian Ocean, into the Mozambique channel and feeds into the Agulhas current. This result contradicts Macdonald and Wunsch (1996), who concluded from an inverse modeling study that the strength of the Agulhas current and retroflection were independent of factors affecting the transport in the Indonesian throughflow.

The sensitivity to the meridional wind is positive along the Chilean coastline (Fig.5-10, bottom panel), implying that a southerly flow perturbation would increase the overturning by diverting water out of the Antarctic Circumpolar Current, instead of allowing it into the Atlantic. This would favor the warm, and saltier, water route at the expense of the cold, and fresher, water route.

In the ocean-only version of the model, the Philippine and South China Seas, and the Chilean waters have some of the ocean's lowest salinities ($\sim$ 31, see figure 4-5). Those are in

fact some of the regions of largest discrepancy with the Levitus salinity climatology (Levitus and T.P.Boyer, 1994a), Fig.4-4. These features all point to the salt advection feedback as playing a key role in determining the sensitivity of the meridional overturning to wind stress in ocean-only models. The sensitivity pattern to the precipitation field over the Atlantic (Fig.5-2, bottom panel) is such that a net decrease in precipitation over the basin, and concurrent increase in its salinity increases the overturning. The sign of the sensitivity at the gateways must therefore be related to the control, which wind stress exerts on the import and export of fresher water into the Atlantic basin.

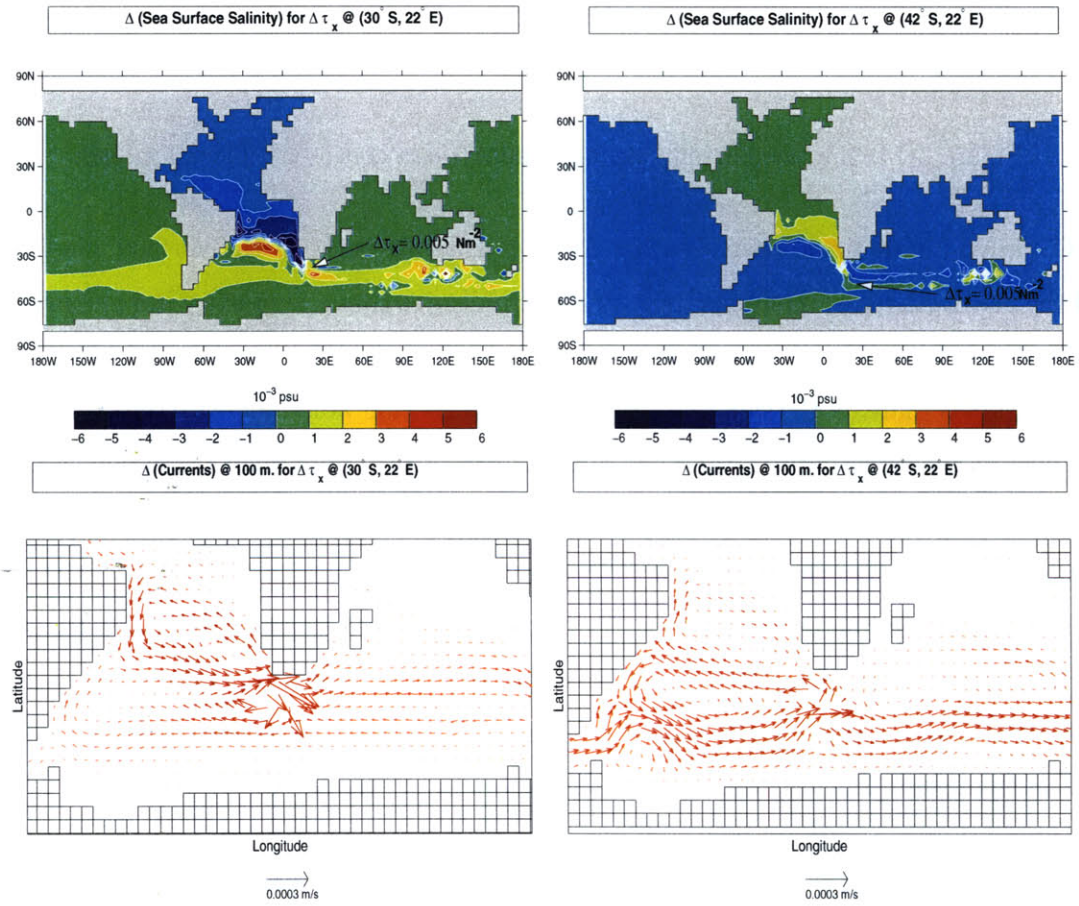

Figure 5-15: Top: Difference in salinity (in 10^{-3}) between simulations with a wind stress perturbation ($\Delta\tau_x = 0.005\,N\,m^{-2}$) imposed at $30°\ S$ (left) and $42°\ S$ (right), both at $22°\ E$, and an unperturbed simulation. Bottom: Difference in near surface currents (in $m\,s^{-1}$) between simulations with a wind stress perturbation ($\Delta\tau_x = 0.005\,N\,m^{-2}$) imposed at $30°\ S$ (left) and $42°\ S$ (right), both at $22°\ E$, and an unperturbed simulation. Ocean model.

Solid evidence for this hypothesis can be gathered through a simple perturbation analysis. A westerly wind stress perturbation of magnitude $\Delta\tau_x = 0.005\,N\,m^{-2}$ was added at $42°\,S$ and $30°\,S$, both at $22°\,E$. The resulting equilibrated response in the sea surface salinity and near surface currents is shown in Fig.5-15. The perturbation imposed at $30°\,S$ (left panels), south of the Cape of Good Hope, weakens the Agulhas current. The Benguela current increases its strength to maintain a constant import of thermocline water into the Atlantic, thereby increasing the import of very fresh Southern Ocean water into the Atlantic at the expense of the saltier Indian Ocean water. The perturbation applied at $42°\,S$ (right panels), weakens the Benguela current at the expense of the Agulhas branch, thereby allowing an increase in salinity of the Atlantic basin, and an increase in the meridional overturning's strength.

Perturbations in diapycnal mixing have a dynamical effect: in a region of positive vertical temperature gradient, increasing κ_d will induce a warming below the level of the perturbation and cooling above it. Perturbations in the flow fields are associated with these temperature anomalies. The sensitivity to diapycnal mixing at $290\,m$ and $1250\,m$ is shown in Fig.5-16 for the region of the Agulhas current, there is very little sensitivity elsewhere in the Southern Oceans or in the Indian and Pacific basins. The sensitivity is positive down to a depth of $1000\,m$. and negative below. The sign reversal takes place at the depth where the Agulhas current ceases to go in the westward direction, and the flow is eastward through the entire passage south of Africa.

The role played by the gateways is a robust feature of the meridional overturning and is not related to whether the circulation is diagnosed by its streamfunction or by the amount of heat, which it transports. The sensitivity map of the heat transport to the zonal wind stress exhibits the same dipole pattern South of the Cape of Good Hope (Fig.5-17).

These features are, however, largely absent when the interactive energy and moisture balance atmosphere is coupled to the ocean model (see Fig.5-9). The large negative sensitivity south of the Cape of Good Hope drops from $-2.5\ Sv\,N^{-1}\,m^2$ in the ocean model to $-0.6\ Sv\,N^{-1}\,m^2$ in the coupled model. By allowing feedbacks between the ocean and the atmosphere on much shorter time scales, the atmosphere effectively short-circuits the oceanic salt advection feedback. Since the stratification is greatest in the tropics, this is where wind stress perturbations can have the greatest impact on the surface buoyancy, and consequently on the atmospheric heat and moisture transport. The mechanism outlined

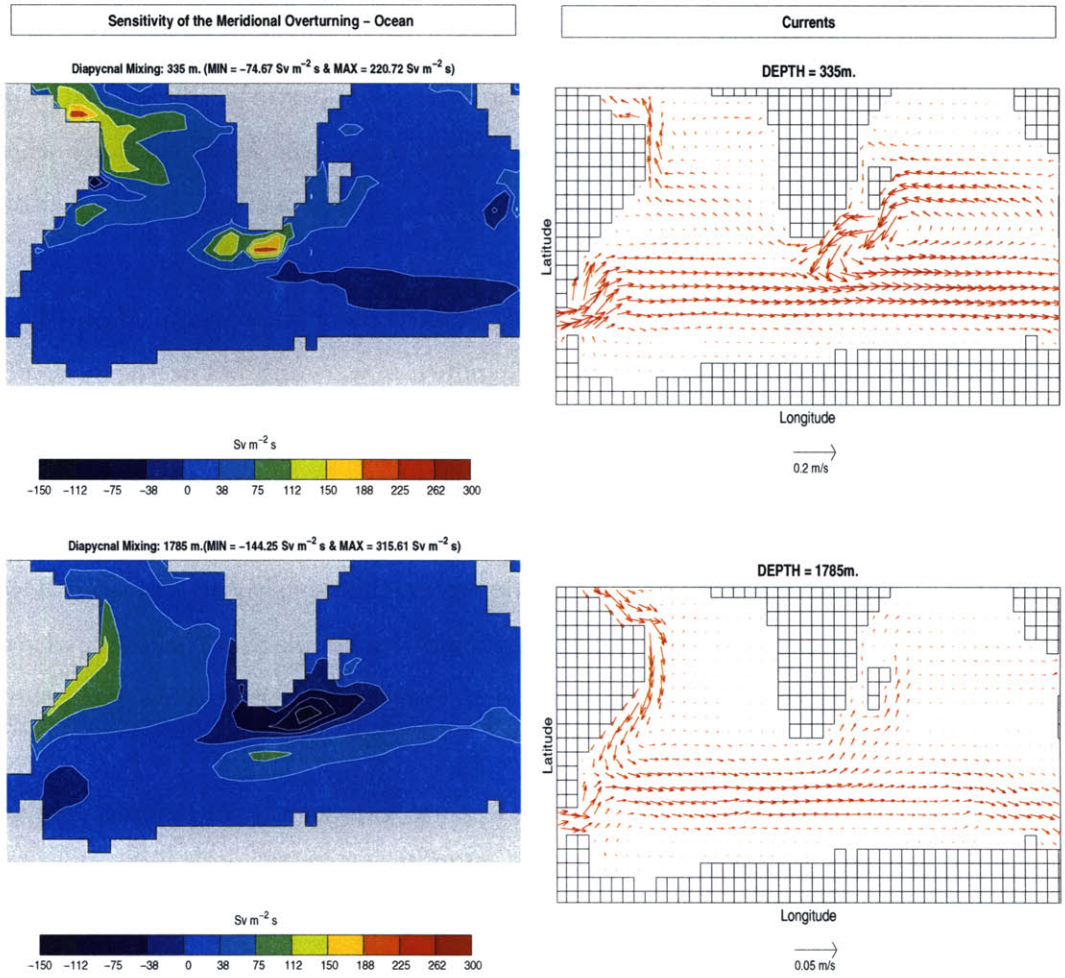

Figure 5-16: Left: Sensitivity of the overturning maximum to diapycnal mixing in the Agulhas Plateau region: $\frac{\partial \psi_{MAX}}{\partial \kappa_d}$ in $Sv\, m^{-2}\, s$. The top panel represents the sensitivity at $290\, m$, the bottom one at $1250\, m$. Right: Flow velocities at those two depths.

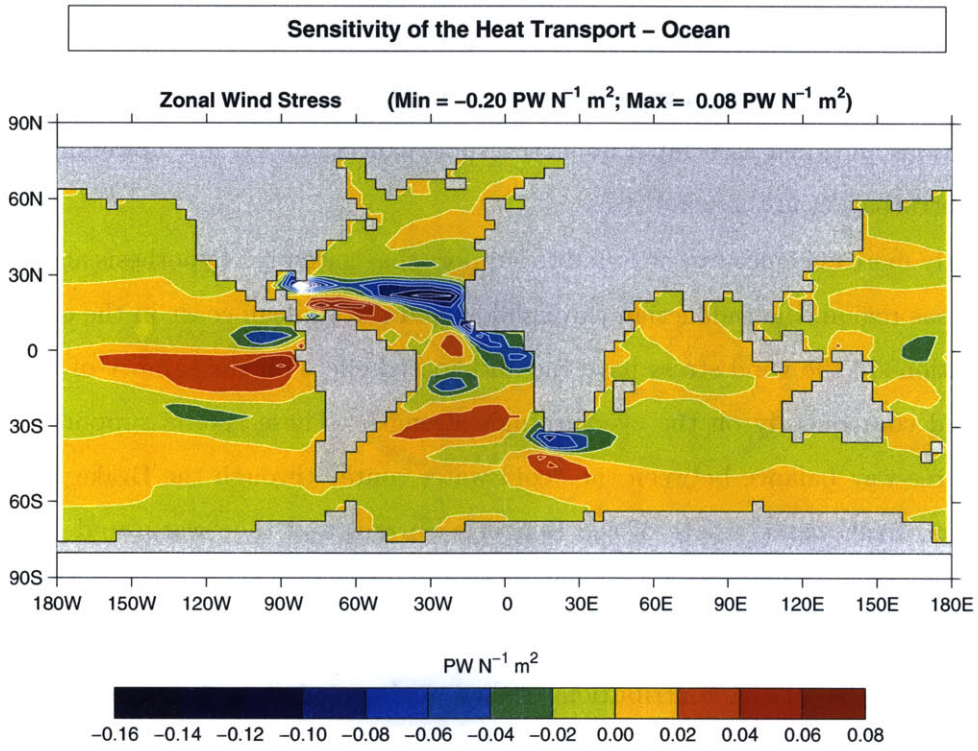

Figure 5-17: Sensitivity of the maximum value of the heat transport at $24^\circ\ N$ HT_{MAX} to the zonal wind stress: $\frac{HT_{24^\circ N}}{\partial \tau_x}$ in $PW\ N^{-1}\ m^2$ in the ocean model. The model's boundary conditions are $F_w = (E - P - R)_{obs}$ and $Q = Q_{obs} + \lambda_s(T - T_{obs})$.

above to explain the absence of sensitivity to wind stress in the open channel under flux boundary conditions can also readily be applied to the case of the coupled model, which allows the surface temperature and salinity to evolve freely forced only by fluxes calculated from the energy balance model.

5.4.2 Discussion

The hypothesis of a control of the overturning by upwelling in the Drake passage was confirmed by the adjoint analysis within the framework on pure restoring surface boundary conditions. Much less support for it exists when the sea surface temperature and salinity is less constrained, notably in the coupled model. This shift takes place because buoyancy perturbations and their associated bolus transport cancel much of the upwelling associated with a perturbation in the wind stress.

Slightly more evidence can be found to support the "gateway" hypothesis and the role of the Agulhas region, the Indonesian throughflow and the Chilean coast in the ocean model. Perturbations in the wind stress have the anticipated effect on the salinity of the Atlantic basin, and consequently on the overturning's strength. These results support the notion that a three-way balance between the "cold water route" through the Drake Passage, the "warm and fresh water" route of the Benguela current and the "warm and salty" water route of the Agulhas current plays a role in determining the salinity of the Atlantic Ocean and the intensity of the meridional overturning circulation. This model does not address the question of the relative contributions of these regions to inflow of thermocline water into the Atlantic. It merely gives an indication of the sensitivity of the meridional overturning to change in wind stress in those regions. It is unfortunate that large discrepancies exist in those regions between the Levitus climatology and that of the model's surface salinity. Only improvements in the evaporation and precipitation fields could remedy this problem, adding a term restoring surface salinities to observations has namely been shown to dramatically alter the sensitivity pattern in that region.

The importance of wind in the Southern Oceans diminishes greatly when the energy and moisture balance is coupled to the ocean model. The largest sensitivities to the zonal wind stress in Fig.5-9 are found in the tropics, where they sustain the overturning through equatorial Ekman upwelling. Although oceanic advective feedbacks are still present in the coupled model, their impact is dwarfed by the atmospheric feedback effects that link directly

the tropics and the polar region where convection takes place.

5.5 Mass and Heat Transport in the Western Boundary Current

The sensitivity of the overturning maximum and of the heat transport to perturbations in the diapycnal mixing and in the thickness diffusion in the western boundary current region are positive in the ocean model and negative in the coupled model.

The effect of a perturbation in mixing in the western boundary current in the ocean model is a surface cooling, which is advected northward, cools the convecting water and increases the overturning. The ocean model is only subject to the oceanic salinity and temperature advective feedbacks.

The coupling to the energy balance model allows the atmosphere to compensate an increase in the diffusive heat loss in the ocean. The local surface cooling induced by increased diffusion in the Western Boundary Current results in an increase in the North-South temperature gradient, which in this model is estimated by taking the difference between the temperature in the $[0-35^\circ\ N]$ and $[35-80^\circ\ N]$ latitude bands. This increase in temperature gradient has two consequences. The first is an increase in the atmospheric heat transport. The tropical ocean temperatures therefore cool slightly while the polar region sees a slight warming. Note that the cold perturbation induced by increased diffusion is also advected northwards by the ocean's circulation, which explains why high latitude temperatures warm only very slightly. The second effect is on the mid- to high latitude atmospheric freshwater transport, which increases. This results in a decrease in the salinity of the convecting water, and consequently a decrease in the overturning's strength. These processes illustrate two of the coupled atmosphere-ocean feedback mechanisms discussed in Nakamura et al. (1994), and explain why the sign of the sensitivity pattern in that region is negative.

5.6 Quantitative Comparison

One advantage of the adjoint method is that it allows a quantitative comparison of the effects of various perturbations on the diagnostic. Published estimates of the climatological uncertainty in the fields will be used to assess what impact they have on the uncertainty in

the meridional overturning.

5.6.1 Buoyancy

The uncertainty in the heat and net freshwater flux datasets was estimated at 30% of the value of the fields or $\Delta Q = \pm 30\, W m^{-2}$ and $\Delta F_w = \pm 30\, cm\, y^{-1}$. These numbers are based on the results of Schmitt et al. (1989); Wijffels et al. (1992) for the evaporation - precipitation climatology of the Atlantic Ocean and Isemer et al. (1989) for the heat flux. These authors note that the uncertainty is probably larger in the poorly sampled areas in high latitudes.

	Ocean Model	Coupled Model
$\Delta Q = \pm 30\% \cdot Q$		
North Atlantic $[58 - 66°N]$	$\pm 0.8\ Sv$	$\pm 1.5\ Sv$
Mid-Latitude, all basins $[38 - 46°N]$	$\pm 0.07\ Sv$	$\pm 1.1\ Sv$
$\Delta F_w = \pm 30\% \cdot P$		
North Atlantic $[58 - 66°N]$	$\pm 0.5\ Sv$	$\pm 0.8\ Sv$
Tropics Atlantic N. Hem. $[14 - 38°N]$	$\pm 4.2\ Sv$	$\pm 2.8\ Sv$
Tropics Atlantic S. Hem. $[22 - 6°S]$	$\pm 2.2\ Sv$	$\pm 1.5\ Sv$

Table 5.1: Uncertainty in the estimates of the overturning maximum ψ_{MAX} estimated by applying perturbations in the heat and freshwater fluxes in various regions. These perturbations are 30% of the value of the fields themselves.

	Ocean Model	Coupled Model
$\Delta Q = \pm 30\, W m^{-2}$		
North Atlantic $[58 - 66°N]$	$\pm 0.95\ Sv$	$\pm 3.8\ Sv$
Mid-Latitude, all basins $[38 - 46°N]$	$\pm 0.008\ Sv$	$\pm 4.4\ Sv$
$\Delta F_w = \pm 30\, cm\, y^{-1}$		
North Atlantic $[58 - 66°N]$	$\pm 1.3\ Sv$	$\pm 1.8\ Sv$
Tropics Atlantic N. Hem. $[14 - 38°N]$	$\pm 5.2\ Sv$	$\pm 3.6\ Sv$
Tropics Atlantic S. Hem. $[22 - 6°S]$	$\pm 2.3\ Sv$	$\pm 1.6\ Sv$

Table 5.2: Uncertainty in the estimates of the overturning maximum ψ_{MAX} estimated by applying perturbations in the heat and freshwater fluxes in various regions. These perturbations are $\Delta Q = \pm 30\, W m^{-2}$ and $\Delta F_w = \pm 30\, cm y^{-1}$

The fixed and relative perturbation approaches give similar results. The perturbations are applied locally in order to avoid adding a net input of heat or water to the basin. It is estimated that the balancing perturbation, when divided and applied uniformly over the

rest of the oceans has a very small impact on the overturning's strength. Both heat- and freshwater fluxes contribute substantial uncertainties to the value of the overturning, on the order of $1-3\ Sv$. The uncertainty associated with the heat flux stems largely from the Labrador and Norwegian Seas. Since fluxes in that region are notably poorly known, the uncertainty may in fact be greater than is indicated by these estimates.

The contribution of the net freshwater flux to the uncertainty in the overturning originates primarily in the tropical region of both hemispheres where the fluxes and sensitivities are largest.

A number of recent climate change studies have analyzed the relative importance of changes in heat- and freshwater fluxes in driving changes in the intensity of the meridional overturning. Climate models are by no means in agreement on this subject. The results of Dixon et al. (1999) and Wiebe and Weaver (1999) indicate that changes in the hydrological cycle are of prime importance in determining the changes in the overturning. The argument used by Wiebe and Weaver (1999) to support their results is that density is only weakly dependent on temperature for low temperatures, allowing salinity changes and increased freshening to have the greatest impact on the buoyancy of high latitude waters. The results of Mikolajewics and Voss (2000) and Kamenkovich et al. (2000b) show anomalous heating of the ocean's surface as the primary mechanism responsible for the slowdown of the overturning. In the former study, changes in freshwater forcing explain less than a quarter of the observed change in overturning strength. What is most surprising is that these results do not seem to depend on the formulation of the ocean model, the results of Wiebe and Weaver (1999) and Kamenkovich et al. (2000b) were both obtained with the GFDL MOM2 model. This could indicate that it is differences in the atmospheric models, which really determine the sensitivity of the overturning to surface forcing. In a recent article, Latif et al. (2001) argue that enhanced frequency of El Niño type events in climate change scenarios lead to anomalously high salinities in the tropical Atlantic. These perturbations are advected northward where they reduce the buoyancy of the water in the North Atlantic. This effect is sufficient to compensate the increase in buoyancy associated with the warming and freshening of the waters, and little change in the overturning's strength is observed.

The results presented in this chapter represent a linearization around a steady-state, they could be significantly different from a linearization about the time dependent trajectory of climate change scenario. It is, however, possible to draw some inferences from the present

results.

The high latitude sensitivity patterns will dominate on decadal and shorter time scales. Increased freshening or warming of the surface waters in a climate change scenario would then reduce the overturning. In this model, the effect of the heat flux dominates.

Beyond a few decades, the low latitude increases in salinity associated with enhanced atmospheric freshwater transport will have an important impact on the overturning's strength, which will tend to increase. This confirms Latif et al. (2001)'s observation. It also concurs with Wiebe and Weaver (1999), who did not see a continued reduction in the overturning strength past the point of CO_2 doubling, when the forcing ceased to increase beyond that stage. The circulation not only recovers, but reaches a slightly more intense new equilibrium. These authors attributed the re-establishment of the circulation to a shift from a situation where freshening in high latitudes dominates to one in which low latitude warming dominates. This warming increases the meridional steric height gradient, which is linearly proportional to the overturning's strength. The results presented in this chapter indicate that, within the context of this simple model, the strengthening of the equilibrated circulation can be attributed to increased evaporation in low latitudes, and the advection of salinity anomalies towards high latitudes.

The overall response of the meridional overturning circulation to global warming will depend on the competing effects a weakening attributed to high latitude freshening and warming, and a strengthening associated with enhanced evaporation in the tropics. The former will dominate over the first few decades, but the latter will likely be important over longer time scales.

5.6.2 Mixing

Little is known about how much mixing actually takes place in the ocean. Modeling studies often tune the diapycnal diffusion coefficient in order to obtain an overturning circulation of adequate intensity. The micro structure and tracer release measurements made by Ledwell and Hickey (1995); Ledwell and Bratkovich (1995); Polzin et al. (1997); Ledwell et al. (2000) found much higher mixing intensities directly above rough topography, and along coastlines and mid-oceanic ridges $\mathcal{O}(10^{-4}\ m^2 s^{-1})$, and much lower values elsewhere $\mathcal{O}(10^{-5}\ m^2 s^{-1})$.

The adjoint sensitivities will be used to investigate three possible scenarios. The first is the impact of a 66% increase and decrease in the global value used for diapycnal mixing

(Table 5.3). This is likely to be less than the actual uncertainty in the mean value of κ_d, but it includes the numbers used in many modeling studies ($[1 - 5 \cdot 10^{-5} m^2 s^{-1}]$). The associated uncertainty in the maximum streamfunction is substantial, $\sim 6\ Sv$, with increased overturning strength associated with increased mixing.

$\Delta\kappa_d = \pm 2 \cdot 10^{-5}\ m^2 s^{-1}$	
Ocean Model	$\Delta\psi_{MAX} = \pm 6.2\ Sv$ $\quad \Delta HT_{24^\circ N} = \pm 0.13\ PW$
Coupled Model	$\Delta\psi_{MAX} = \pm 5.7\ Sv$ $\quad \Delta HT_{24^\circ N} = \pm 0.17\ PW$

Table 5.3: Impact of a 66% increase and decrease in the value of the diapycnal mixing coefficient.

The scaling relationship between overturning strength and diapycnal mixing implied by these numbers can easily be derived. If $\psi_{MAX} \propto \kappa^N$, then N can be estimated from the present results:

$$\frac{\psi_{MAX}}{\psi_{MAX} + \Delta\psi_{MAX}} = \left(\frac{\kappa}{\kappa + \Delta\kappa}\right)^N \tag{5.7}$$

$$N = \ln\left(\frac{29}{35.2}\right) / \ln\left(\frac{3 \cdot 10^{-5}}{5 \cdot 10^{-5}}\right) \approx 0.4 \tag{5.8}$$

This is smaller than the numbers usually predicted by scaling analysis. The "classical" scaling of Bryan (1987) predicts a power law with a two-thirds power. This scaling has, however, been shown to depend on the surface boundary conditions (Park and Bryan, 2000), with a smaller power law applicable under mixed boundary conditions (Zhang et al., 1999). Vallis (2000) has also shown that the appropriate scaling law when wind and Ekman pumping are included goes as $\kappa_d^{1/2}$, closer to what is observed here.

The second scenario concentrates the mixing along coastlines and eliminates it elsewhere. Assuming $\Delta\kappa_d = 7 \cdot 10^{-5}\ m^2 s^{-1}$ along the coast and $\Delta\kappa_d = -3 \cdot 10^{-5}\ m^2 s^{-1}$ everywhere else, the changes in the overturning's strength and in the heat transport are summarized in table 5.4. The magnitude of the perturbations that were used in this analysis clearly go beyond the small perturbation range where the adjoint sensitivities can be expected to be accurate. The result is, however, surprisingly consistent with those of Marotzke (1997) and Scott (2000) who saw little change in the intensity of the overturning when the mixing was concentrated along the boundaries.

$\Delta\kappa_d = +7 \cdot 10^{-5} / -3 \cdot 10^{-5}\ m^2 s^{-1}$		
Ocean Model	$\Delta\psi_{MAX} = -1.15\ Sv$	$\Delta HT_{24^\circ N} = -0.06\ PW$
Coupled Model	$\Delta\psi_{MAX} = -1.74\ Sv$	$\Delta HT_{24^\circ N} = -0.06\ PW$

Table 5.4: Boundary mixing hypothesis. $\Delta\kappa_d = 7 \cdot 10^{-5}\ m^2 s^{-1}$ along coastlines, $\Delta\kappa_d = -3 \cdot 10^{-5}\ m^2 s^{-1}$ elsewhere.

The third scenario concentrates the mixing in the tropical thermocline and eliminates it elsewhere, where the sensitivities are the greatest. There is no observational evidence to support this case (Ledwell et al., 1993), although Emanuel (2001) has suggested that tropical cyclones could provide a source of energy for mixing in that region. Assuming that $\Delta\kappa_d = 7 \cdot 10^{-5}\ m^2 s^{-1}$ between $22 - 6^\circ S$ and $6 - 22^\circ N$ and above $1000\,m$ and $\Delta\kappa_d = -3 \cdot 10^{-5}\ m^2 s^{-1}$ everywhere else, the changes in the overturning's strength and in the heat transport are summarized in table 5.5. The observational evidence that no hurricanes are found in the southern Atlantic was neglected in this simplified calculation. The near equatorial band where hurricanes cannot form was, however, excluded. Table 5.5 shows relatively minor changes in the overturning's strength in this scenario. This indicates that the overturning could be maintained solely through mixing in the tropical thermocline. The maximum overturning is in fact enhanced in the coupled model, which has high sensitivities throughout the tropics in all basins.

$\Delta\kappa_d = +7 \cdot 10^{-5} / -3 \cdot 10^{-5}\ m^2 s^{-1}$		
Ocean Model	$\Delta\psi_{MAX} = -2.1\ Sv$	$\Delta HT_{24^\circ N} = +0.18\ PW$
Coupled Model	$\Delta\psi_{MAX} = +6.2\ Sv$	$\Delta HT_{24^\circ N} = +0.34\ PW$

Table 5.5: Tropical mixing hypothesis. $\Delta\kappa_d = 7 \cdot 10^{-5}\ m^2 s^{-1}$ between $22 - 6^\circ S$ and $6 - 22^\circ N$ and above $1000\,m$, $\Delta\kappa_d = -3 \cdot 10^{-5}\ m^2 s^{-1}$ elsewhere.

5.6.3 Wind Stress

The impact of uncertainty in the climatological value of the zonal wind stress on the meridional overturning is estimated by assuming that the data are accurate to within 30% (Isemer and Hasse, 1991) or $\pm 0.03\,N m^{-2}$. This may underestimate the uncertainty in the wind stress in poorly sampled regions such as the Southern Oceans. The results are summarized in table 5.6 for the $\pm 30\%$ perturbation and table 5.7 for the $\pm 0.03\,N m^{-2}$ perturbation.

	Ocean Model	Coupled Model
$\Delta\tau_x = \pm 30\% \cdot \tau_x$		
ACC $[6 - 42°E]; [50 - 38°S]$	$\pm 0.70\ Sv$	$\pm 0.06\ Sv$
ACC $[6 - 42°E]; [38 - 26°S]$	$\pm 0.33\ Sv$	$\pm 0.08\ Sv$
Tropics Atlantic $[6 - 26°N]$	$\pm 0.13\ Sv$	$\pm 1.1\ Sv$
Mid-Latitude Atlantic $[42 - 50°S]$	$\pm 0.21\ Sv$	$\pm 0.1\ Sv$

Table 5.6: Uncertainty in the estimates of the overturning maximum ψ_{MAX} estimated by applying perturbations in the zonal wind stress. These perturbations are 30% of the value of the field.

	Ocean Model	Coupled Model
$\Delta\tau_x = \pm 0.03\, Nm^{-2}$		
ACC $[6 - 42°E]; [50 - 38°S]$	$\pm 0.57\ Sv$	$\pm 0.04\ Sv$
ACC $[6 - 42°E]; [38 - 26°S]$	$\pm 0.88\ Sv$	$\pm 0.12\ Sv$
Tropics Atlantic $[6 - 26°N]$	$\pm 0.25\ Sv$	$\pm 1.78\ Sv$
Mid-Latitude Atlantic $[42 - 50°N]$	$\pm 0.42\ Sv$	$\pm 0.18\ Sv$

Table 5.7: Uncertainty in the estimates of the overturning maximum ψ_{MAX} estimated by applying perturbations in the zonal wind stress. These perturbations are $\pm 0.03\, Nm^{-2}$ of the value of the field.

Although highly localized features, the high sensitivities observed in the Antarctic Circumpolar Channel South of Africa are sufficient to add a $\pm 0.5\ Sv$ uncertainty bound on the climatological value of the overturning maximum. This is, for example, noticeably larger than the contribution of the uncertainty in the mid-latitude wind field in the Atlantic. Possible changes in the position of the subtropical convergence zone on glacial-interglacial time scales could alter the composition of the water entering the Atlantic basin (Gordon, 1986), thereby influencing the overturning's strength. The pattern of sensitivity changes substantially once the model is coupled to the energy and moisture balance model. The dominant source of uncertainty then stems from the tropical region of the Atlantic. It is of the same order of magnitude as the contribution of the Agulhas region in the uncoupled case.

5.7 Discussion

Only weak evidence was found in support of the Drake Passage hypothesis. The role played by gateways should be re-examined within the framework of a more complex coupled

atmosphere-ocean model. It is potentially important, but can be short-circuited by the rapid transfer of energy and moisture in the atmosphere. The role of wind in the coupled model is associated with equatorial Ekman upwelling and the efficiency of the diapycnal mixing process. It therefore compounds the already dominant effect of mixing in determining the uncertainty in the overturning's strength.

The coupling to the energy and moisture balance model allows the development of global sensitivity patterns to the heat flux, diapycnal mixing and wind stress. These maps are related to the effect of perturbations in the sea surface temperature on the atmospheric transport of heat and freshwater.

The relative importance of heat and freshwater fluxes in sustaining the meridional overturning is clarified by this analysis, in particular the geographic distribution of these contributions. In steady-state, the dominant source of uncertainty stems from poor precipitation and evaporation data in the tropics. It is, however, likely that over shorter time scales, changes in the heat flux in high latitudes would cause an important portion of the observed changes in the overturning's strength.

Flux adjustments have often been used in coupled atmosphere - ocean modeling to correct the discrepancies between the surface fluxes provided by the atmospheric model and those required by the ocean to maintain a realistic circulation (Cubasch et al., 1992; Manabe and Stouffer, 1994; Houghton et al., 1996). These flux adjustments prevent a drift of the coupled model (Washington and Meehl, 1989), which often resulted in a collapse of the meridional overturning circulation (Manabe and Stouffer, 1988). A number of recent results have been obtained without flux adjustments (Wood et al., 1999; Bryan, 1998; Gordon et al., 2000), but a drift in some important model variables, usually in the deep ocean, often persists. Flux adjustments can lead to spurious multiple equilibria in the meridional overturning circulation (Dijkstra and Neelin, 1999), and they do not correct errors in the atmosphere - ocean feedbacks which control the climate change response (Marotzke and Stone, 1995). Flux adjustments have most often been applied as additive terms. The results of the adjoint analysis can therefore be interpreted as a map, which predicts the impact of flux adjustments on the overturning and its heat transport. In a coupled system, heat flux adjustments must have a global distribution, but the greatest impact will stem from corrections located in the proximity of the convection sites. Freshwater flux adjustments can be confined to the Atlantic basin, with the tropics playing a role as important as the high

latitudes. A rigorous analysis of the role of flux adjustments could be performed with the adjoint method. Fixed surface "corrective" fields, set to a nominal value of zero, would be added to the fluxes of heat, freshwater and momentum at the ocean - atmosphere interface. The sensitivity of the cost function to these fixed fields would give an indication of the impact of flux adjustments on the diagnostic over the time scale of the adjoint integration.

Chapter 6

Conclusion

This thesis has demonstrated that it is possible to calculate adjoint sensitivities on climatological time scales in coarse resolution ocean and coupled models.

The modeling framework designed for this project reproduced reasonably well the large scale features of the ocean's circulation. It was, however, deficient in a number of respects, which will briefly be discussed. There are several issues related to the resolution of the model, which remain to be addressed.

- Very large sensitivities are observed in the near surface layers, notably in relation to Ekman up- and downwelling in the tropics. This highlights the necessity to resolve adequately the ocean's mixed layer. This can be achieved in ocean models by including the so-called KPP scheme. Future versions of the adjoint of the ocean model will include the KPP scheme (Heimbach, personal communication).

- Another region, which exhibited large sensitivities to a number of key factors, is the western boundary current. The model dynamics are discretized on a grid, which requires two points to resolve the western boundary current. The current is therefore close to 800 km wide, while in reality it does not exceed 100 km. It could, therefore, be worthwhile to repeat these calculations with an increased resolution along the western boundary following the model of Kamenkovich et al. (2000a). While this represents a simple implementation in idealized geometry models, it can present major issues in realistic geography basins.

- The third issue related to resolution is the representation and resolution of eddies. The

role of eddies in transporting tracers was parameterized with the Gent Mc-Williams scheme in the present model. Deriving the adjoint of eddy resolving models presents a number of new issues related to the rapid loss of information in shedding and re-absorbing eddies, and the chaotic nature of these processes (Lea et al., 2000; Köhl and Willebrand, 2001). The spatial resolution, at which adjoint solutions cease to asymptote steadily towards a constant pattern and grow exponentially is poorly known, but can be expected to be on the order of the Rossby radius of deformation, which is close to 30 km in ocean models in mid-latitudes (Gill, 1982). Since the Rossby radius is closer to 1000 km in the atmosphere and synoptic scale disturbances are resolved even in coarse resolution models, similar issues will inevitably be present in any three-dimensional atmospheric model.

The limits to the linearity assumption underlying the adjoint analysis have not been explored in any detail, primarily because the answer is unlikely to be homogeneous in space for steady state problems, or space and time when linearizing about non-linear trajectories.

A number of physical processes that could be important are not represented in this simplified framework.

- Amongst them is the role played by the Arctic Ocean and the import of fresher water into the Atlantic through the Bering Strait. Gateways have been shown to play a key role in the ocean model, and the large sensitivities to buoyancy forcing in the high latitudes of the Atlantic basin all point to a potentially very important role for the exchange of water with the Arctic Ocean.

- The role of boundary mixing has only been explored very superficially. It is conceivable that the sensitivity pattern to diapycnal mixing would change significantly if the mixing was concentrated along the boundaries, a scenario supported by tracer and dye release data.

- Parameterizing the diapycnal mixing in function of the wind stress would allow a more complete picture of the effect of changes in wind forcing on the meridional overturning circulation.

- The energy and moisture balance model, which was coupled to the ocean model, was amongst the simplest of its category. It did not, for example, allow for any changes

in the forcing of the momentum terms and omitted the feedbacks associated with the Hadley cell in the tropics.

The adjoint method is extremely efficient in providing the sensitivity of a diagnostic to a number of parameters and initial conditions on climatological time scales in a single integration of the model. This allows useful insights into the relative importance of these parameters. The relative contributions of the various forcings to uncertainty in the meridional streamfunction's maximum are summarized in Fig.6-1. The area of each circle is proportional to the uncertainty that it contributes to the overturning's maximum. The geographic areas over which the contributions were calculated are outlined by solid lines. These regions are the North Atlantic, the tropics in both hemispheres and the equatorial region. These regions are confined to the Atlantic basin in the case of the ocean model, they extend to the other basins in the coupled model. The contribution of the diapycnal mixing is calculated for a global perturbation.

Assuming that the uncertainty in the forcing fields and parameters are not correlated, our current knowledge of the surface data and diapycnal mixing does not allow a reduction of the uncertainty in the model's estimate of the overturning maximum below 29 ± 8 Sv for the ocean model and 25 ± 7 Sv for the coupled model. In the present calculations, no parameter stands out as dominant. It is, however, clear that the large uncertainty in the global value of the diapycnal mixing coefficient limits our ability to know the overturning streamfunction's maximum to within less than 6 Sv of any precise value. The role of advection in transporting buoyancy perturbations, in particular salinity anomalies, from the tropics towards high latitudes where they influence the density of abyssal waters is also quite important. The direct role played by the heat flux forcing in high latitudes and the indirect effects of wind stress are slightly less important, but by no means second order effects.

The time dependence of the contributions of the heat-, freshwater fluxes and diapycnal mixing to uncertainty in the meridional overturning circulation in the ocean model is summarized in Fig.6-2. The effect of uncertainty in the heat flux, in red, is split into two parts; the contribution of the tropical region (22° S to 22° N) is the dashed line while that of high latitudes (54° N to 74° N)is the dash-dotted line. Both lines represent the response to a 30% increase in the heat flux over observations. A cooling of the ocean in the North Atlantic (dash-dotted red line) will have the greatest influence on the overturning's strength over

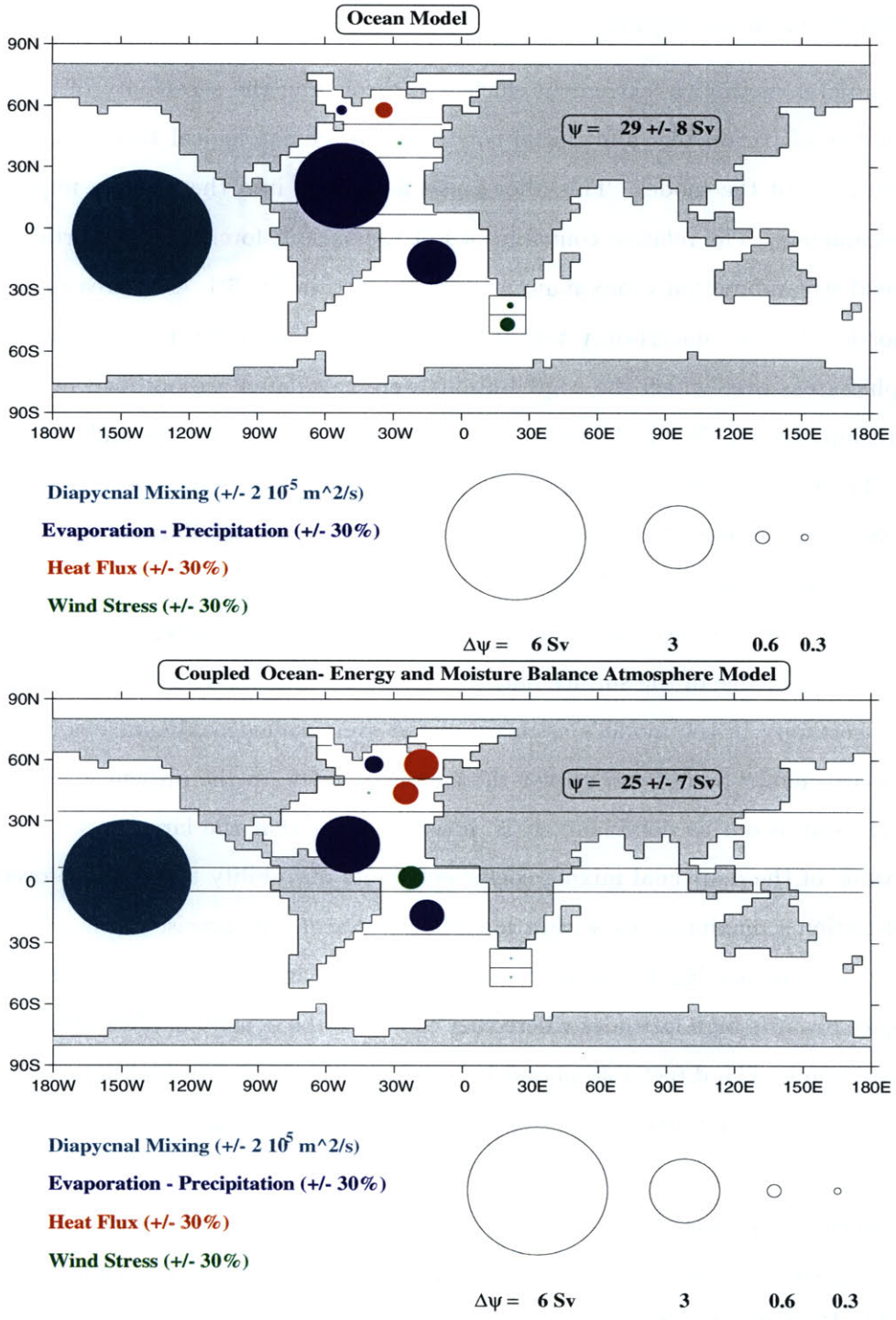

Figure 6-1: Estimates of the effect of uncertainty in the heat and freshwater fluxes, wind stress and diapycnal mixing on the meridional overturning's strength. The area of each circle is proportional to its contribution to the uncertainty in ψ_{MAX}, in Sv. Top: Ocean model. Bottom: Coupled model.

time scales up to twenty years. The effect peaks after a few years and has a magnitude of $2\,Sv$ at that point. Heat flux perturbations in the tropics (dashed red line) have a negligible impact. The effect of a 30% increase in the freshwater flux is shown in blue. An increase in rainfall in high latitudes (dash-dotted blue line) will also have a relatively rapid impact on the overturning; the effect peaks after ten to twenty years. Increasing evaporation in the tropics will only have an impact on the meridional overturning once the induced salinity anomalies have been advected towards high latitudes. It takes close to a century for this effect to reach its full strength, $3\,Sv$. The effect of increased diapycnal mixing is the slowest to be develop; it dominates for time scales of a century or more and has not fully equilibrated after 400 years.

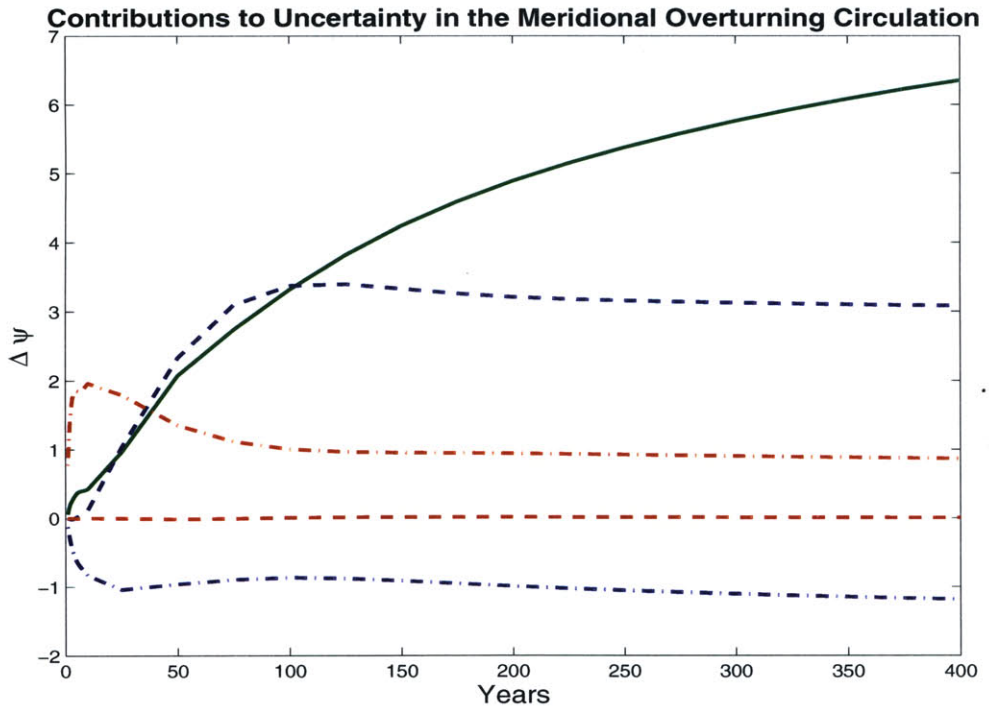

Figure 6-2: Estimates of the effect of uncertainty in the heat, freshwater fluxes and diapycnal mixing on the meridional overturning's strength for the ocean model. Solid green line: Effect of a 66% increase in diapycnal mixing, worldwide. Dash-dotted blue line: Effect of a 30% increase in freshwater flux (increased rainfall) between $54°\,N$ and $74°\,N$ in the Atlantic. Dashed blue line: Effect of a 30% increase in freshwater flux (increased evaporation) between $22°\,S$ and $22°\,N$ in the Atlantic. Dash-dotted red line: Effect of a 30% increase in heat flux (cooling of the ocean) between $54°\,N$ and $74°\,N$ in the Atlantic. Dashed red line: Effect of a 30% increase in heat flux (warming of the ocean) between $22°\,S$ and $22°\,N$ in the Atlantic.

Another advantage of the adjoint method is that it provides complete two or three-dimensional map of sensitivity to parameters such as wind stress, buoyancy or mixing. The adjoint method allows to identify the sites or regions that have a key influence on the diagnostic. The present analysis has shown that the meridional overturning streamfunction is most sensitive to direct heat flux forcing in the region where convection takes place, in the Labrador and Greenland Seas. The sensitivity to evaporation and precipitation is, however, concentrated in the tropics of both hemispheres. The tropics, and the near surface equatorial upwelling region in particular, determine much of the sensitivity to diapycnal mixing and wind stress in the coupled model. The important role played by the tropics in setting the overturning's strength seems to confirm the thermodynamic principles outlined by Sandström (1908), Jeffreys (1925) and Munk and Wunsch (1998): upward advection of heat is balanced by downward diffusion. The strength of the meridional overturning is then determined by the power available to return the fluid to the surface across the ocean's stratification. Because the ocean is most strongly stratified in the tropics, the mixing process is most efficient in that region.

Only weak evidence was found in support of the Drake Passage hypothesis. The Agulhas Plateau, the Chilean coastline and the Indonesian throughflow play an important role in setting the overturning's strength. These "gateways" act as regulators of the salinity of the Atlantic basin in the ocean model forced by mixed boundary conditions. The wind stress determines the balance between the inflow of relatively salty Indian Ocean water through the Agulhas current, the flux of fresher Benguela current water southwest of Africa and the flow of very cold and fresh water through the Drake Passage. The role played by gateways should be re-examined within the framework of a more complex coupled atmosphere-ocean model. It is potentially important, but can be short-circuited by the rapid transfer of energy and moisture in the atmosphere. The role of wind in the coupled model is associated with equatorial Ekman upwelling and the efficiency of the diapycnal mixing process. It therefore compounds the already dominant effect of mixing in determining the uncertainty in the overturning's strength.

The most important conclusion of this thesis is the critical influence which the formulation of the surface boundary conditions has on the model's sensitivity. The sensitivity to wind stress in the Southern Oceans has proven this point quite dramatically. Circulation patterns, which may appear equally consistent with observations when forced with restoring

terms or flux boundary conditions, can respond in very different ways to perturbations and changes in forcing.

The most striking difference between the sensitivity maps obtained under relaxation boundary conditions and those obtained under mixed or flux boundary conditions is the generally greater sensitivities in the latter cases. This is not surprising, relaxation terms are constraints imposed onto the circulation, which make it much less sensitive to perturbations than a system with more freedom. It is the ability of the flow to advect buoyancy perturbations towards high latitudes under flux boundary conditions, which allows high sensitivities to heat and freshwater fluxes to extend throughout the basin. Both high and low latitudes play an important role under mixed boundary conditions, the case thought to be the most realistic. The coupling to the energy and moisture balance model allows the development of global sensitivity patterns to the heat flux, diapycnal mixing and wind stress. These maps are related to the effect of perturbations in the sea surface temperature on the atmospheric transport of heat and freshwater.

The extreme sensitivity to the formulation of the boundary conditions limits the inferences, which can be drawn from sensitivity analyses performed with models forced with unphysical boundary conditions, such as salinity restoring terms, and highlights the necessity to provide physically meaningful boundary conditions to ocean models. The differences between the sensitivity patterns obtained with the ocean and coupled models also points to limitations in the former category of models, and suggests that this analysis be repeated with an atmospheric model with more complete physics and dynamics. The climatology of the forward ocean model is credible and quite similar in both the ocean and coupled models. However, including interactive atmospheric transports of heat and moisture changes the manner in which the ocean model state adjusts to changes in wind stress, heat flux and diapycnal mixing. Considering the role of both the atmosphere and the ocean when studying the climatological behavior of the meridional overturning is, therefore, clearly important.

This thesis has focused primarily on the sensitivity of the steady-state meridional overturning and its associated heat transport to a range of parameters and boundary conditions. This allows an assessment of the impact of climatological uncertainties in fields and parameters on our ability to model the meridional overturning. The analysis could be repeated with annual, decadal and centennial patterns to gauge how inter-annual and inter-decadal variability patterns such as the Arctic Oscillation or the North Atlantic Oscillation translate

into changes in the overturning and its heat transport. Figure 6-3 illustrates the changing balance between the influence of heat and freshwater fluxes and that of mixing on the decadal time scale. For periods of a decade or less, uncertainty and variability in the heat flux in high latitudes is likely to dominate the variability in the overturning's strength. Changes in the freshwater flux in the tropics begin to play a role after twenty-five years. When compared to Fig.6-1, the role of diapycnal mixing in determining the uncertainty in the meridional streamfunction is relatively minor for periods of a couple decades or less; it does, however, dominate the uncertainty after a few hundred years.

The number of questions, which can be addressed with the adjoint method is in fact virtually unlimited. Possibilities include the sensitivity of the atmospheric temperature change in a global warming scenario to the model's parameters or the sensitivity of carbon dioxide exchange between the ocean and the atmosphere to a source of carbon dioxide placed in the ocean in a carbon sequestration scenario.

An important avenue, which this method should lead to, is developing an understanding of the predictability of the atmosphere-ocean system on climatological time scales. By sampling the singular vectors of the sensitivity patterns and building a set of initial conditions, an ensemble of forward trajectories can be calculated. The predictability of the evolution of the system can then be gauged from the convergence or divergence of these trajectories over time. This approach does, however, require a coupled model, which has the appropriate variability on climatic time scales. Diverging trajectories also require bifurcation points, such as a collapse of the meridional overturning circulation, and instability in the evolution of the forced system. Many interesting questions could be addressed with this approach. For example, on the time scale of global warming, the predictability of the behavior of the meridional overturning when convection comes close to collapsing could be examined. On longer time scales, one could study the predictability of the meridional overturning's response to large pulses of freshwater, such as those thought to have taken place at the end of the last ice age.

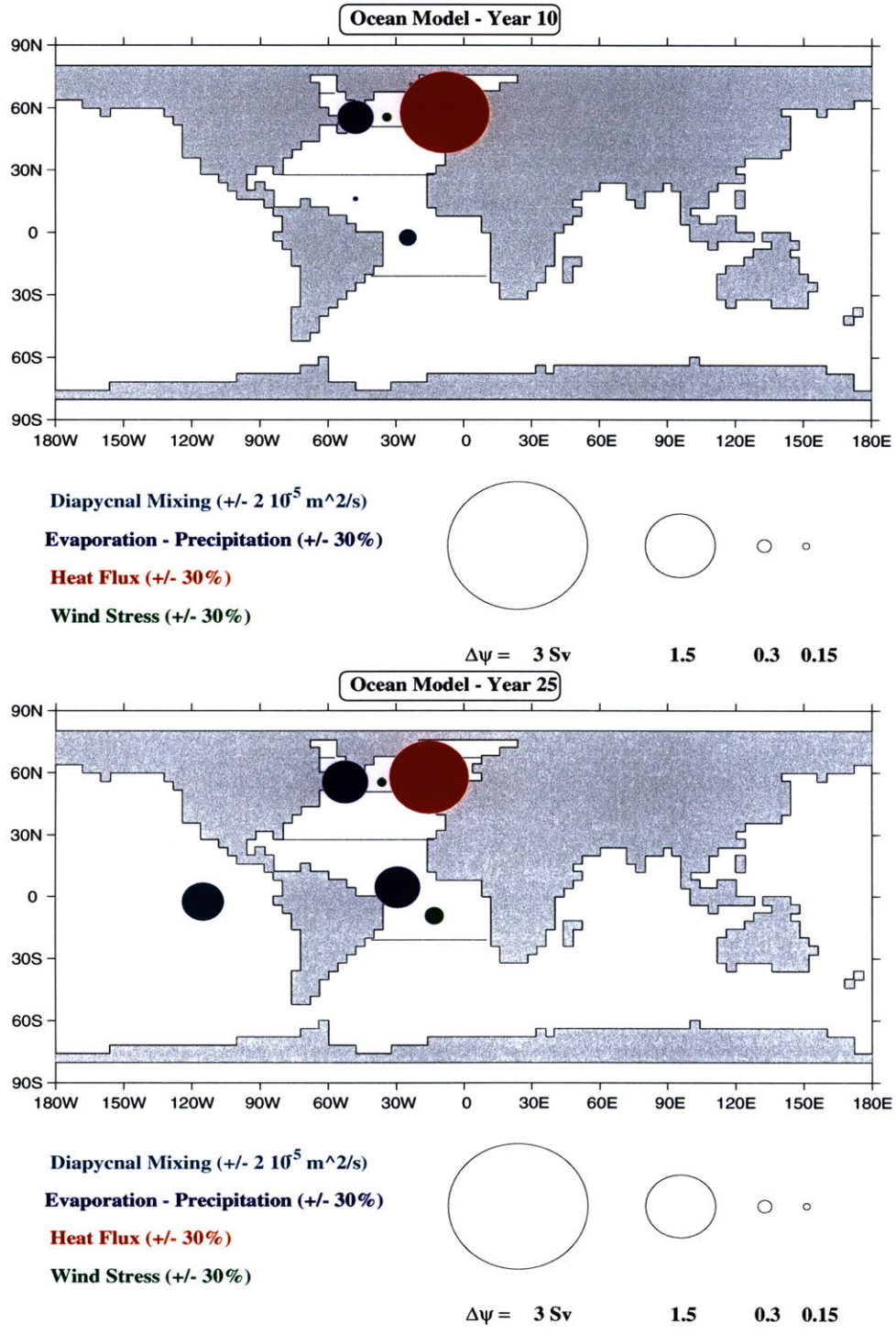

Figure 6-3: Estimates of the effect of uncertainty in the heat and freshwater fluxes, wind stress and diapycnal mixing on the meridional overturning's strength. The area of each circle is proportional to its contribution to the uncertainty in ψ_{MAX}, in Sv. Top: The perturbations are maintained during ten years. Bottom: The perturbations are maintained during 25 years.

Appendix A

Model parameters:

Vertical viscosity	ν_v	$10^{-3}\,\mathrm{m^2 s^{-1}}$
Horizontal viscosity	ν_h	$5 \cdot 10^{5}\,\mathrm{m^2 s^{-1}}$
Diapycnal diffusivity	κ_d	$3 \cdot 10^{-5}\,\mathrm{m^2 s^{-1}}$
Isopycnal diffusivity	κ_i	$10^{3}\,\mathrm{m^2 s^{-1}}$
Thickness diffusivity	κ_{td}	$10^{3}\,\mathrm{m^2 s^{-1}}$
Maximum slope (GM)		10^{-3}
Momentum timestep	$\Delta t_{u,v}$	3600 s
Tracer timestep	$\Delta t_{T;S}$	24 hours

Bibliography

A. Adcroft and C. Hill. Implementation of the gm/redi/griffies schemes in the mit ogcm. MIT, July 2000.

C.W. Böning, W. R. Holland, F.O. Bryan, G. Danabasoglu, and J.C. McWilliams. An overlooked problem in model simulations of the thermohaline circulation and heat transport in the atlantic ocean. *J. Climate*, 8:515–523, 1995.

W. Broecker, D. Peteet, and D. Rind. Does the ocean-atmosphere system have more than one stable mode of operation. *Nature*, 315:21–26, 1985.

W. Broecker, T-H. Peng, J. Jouzel, and G. Russell. The magnitude of global fresh-water transports of importance to ocean circulation. *Clim. Dyn.*, 4:73–79, 1990.

K. Bryan. Accelerating the convergence to equilibrium of ocean-climate models. *J. Phys. Oceanogr.*, 14:666–673, 1984.

F. Bryan. High latitude salinity effects and interhemispheric thermohaline circulation. *Nature*, 323:301–304, 1986.

F. Bryan. Parameter sensitivity of primitive equation ocean general circulation models. *J. Phys. Oceanogr.*, 17:970–985, 1987.

F.O. Bryan. Climate drift in a multicentury integration of the ncar climate system model. *J. Climate*, 11(6):1455–1471, 1998.

H. Bryden, D. Roemmich, and J Church. Ocean heat transport across $24°N$ in the pacific. *Deep Sea Research*, 38(3):297–324, 1991.

R. Buizza and T.N. Palmer. The singular-vector structure of the atmospheric global circulation. *J. of the Atmospheric Sciences*, 52(9):1434–1456, 1995.

R. Buizza, J. Tribbia, F. Molteni, and T. Palmer. Computation of optimal unstable structures for a numerical weather prediction model. *Tellus*, 45A:388–407, 1993.

A. Colin De Verdière. Buoyancy driven planetary flows. *J. Mar. Res.*, 46:215–265, 1988.

U. Cubasch et al. Time-dependant greenhouse warming computations with a coupled ocean-atmosphere model. *Clim. Dyn.*, 8:55–69, 1992.

G. Danabasoglu and J.C. McWilliams. Sensitivity of the global ocean circulation to parameterizations of mesoscale tracer transports. *J. Climate*, 8:2967–2987, 1995.

G. Danabasoglu, J.C. McWilliams, and W.G. Large. Approach to equilibrium in acelerated global oceanic models. *J. Climate*, 9(5):1092–1110, 1996.

M.K. Davey, W.W. Hsieh, and R. C. Wajsowicz. The free Kelvin wave with lateral and vertical viscosity. *J. Phys. Oceanogr.*, 13:2182–2191, 1983.

H.A. Dijkstra and J.D. Neelin. 1999. *J. Climate*, 12:1382–1392, 1999.

K.W. Dixon, T.L. Delworth, M.J. Spelman, and R.J. Stouffer. The influence of transient surface fluxes on north atlantic overturing in a coupled gcm climate change experiment. *Geophys. Res. Lett.*, 26(17):2749–2752, 1999.

K. Emanuel. The contribution of tropical cyclones to the ocean's meridional heat transport. *J. Geophys. Res. in press*, 2001.

J. Frøyland and K.H. Alfsen. Lyapunov-exponent spectra for the lorenz model. *Phys. Rev A*, 29:2928–2931, 1984.

A. Ganachaud and C. Wunsch. Improved estimates of global circulation, heat transport and mixing from hydrographic data. *Nature*, 408:453–456, 2000.

P.R. Gent and J.C. McWilliams. Isopycnal mixing in ocean circulation models. *J. Phys. Oceanogr.*, 20:150–155, 1990.

R. Giering. *Tangent linear and Adjoint Model Compiler.* Center for Global Science - MIT, Cambridge, MA, manual version 1.2 edition, 1997.

Adrian E. Gill. *Atmosphere-Ocean Dynamics*, volume 31 of *International Geophysics Series.* Academic Press, 1982.

A. Gnanadesikan. A simple predictive model for the structure of the oceanic pycnocline. *Science*, 283:2077–2079, 1999.

C. Gordon, C. Cooper, C.A. Senior, H. Banks, J.M Gregory, T.C. Johns, J.F.B. Mitchell, and R.A. Wood. The simulation of sst, sea ice extents and ocean heat transports in a version of the hadley centre coupled model without flux adjustments. *Clim. Dyn.*, 16:147–168, 2000.

A.L. Gordon. Interocean exchange of thermocline water. *J. Geophys. Res.*, 91:5037–5046, 1986.

M.C. Gregg. Diapycnal mixing in the thermocline: A review. *J. Geophys. Res.*, 92(C5):5249–5286, 1987.

A. Griewank and G.F. Corliss, editors. *Automatic Differentiation of Algorithms: Theory, Implementation and Application.* SIAM, Philadelphia, PA, 1991.

M. Hall and H. Bryden. Direct estimates and mechanisms of ocean heat transport. *Deep Sea Research*, 3A:339–359, 1982.

M.C.G. Hall and D.G. Cacuci. Physical interpretation of the adjoint functions for sensitivity analysis of atmospheric models. *J. of the Atmospheric Sciences*, 40:2537–2546, 1983.

M.C.G. Hall, D.G. Cacuci, and M.E. Schlesinger. Sensitivity analysis of a radiative-convective model by the adjoint method. *J. of the Atmospheric Sciences*, 1982.

M.C.G. Hall. Application of adjoint sensitivity to an atmospheric general circulation model. *J. of the Atmospheric Sciences*, 1986.

R.L. Haney. Surface thermal boundary conditions for ocean circulation models. *J. Phys. Oceanogr.*, 1:241–248, 1971.

I.M. Held. The vertical scale of an unstable baroclinic wave and its importance for eddy heat flux parameterizations. *J. of the Atmospheric Sciences*, 35:572–576, 1978.

J.T. Houghton, L.G.M. Filho, B.A. Callander, N. Harris, A. Kattenberg, and K. maskell, editors. *Climate Change 1995: The Science of Climate Change.* Cambridge University Press, 1996.

R.X. Huang, M.A. Cane, N. Naik, and P. Goodman. Global adjustment of the thermocline in response to deepwater formation. *Geophys. Res. Lett.*, 27(6):759–762, 2000.

R.X. Huang. Mixing and energetics of the oceanic thermohaline circulation. *J. Phys. Oceanogr.*, 29:727–746, 1999.

T. Huck, A.J. Weaver, and A. Colin de Verdière. On the influence of the parameterization of lateral boundary layers on the thermohaline circulation in coarse-resolution models. *J. Mar. Res.*, 57:387–426, 1999.

H.J. Isemer and L. Hasse. The scientific beaufort equivalent scale: Effects on wind statistics and climatological air-sea flux estimates in the north atlantic ocean. *J. Climate*, 4:819–836, 1991.

H.J. Isemer, J. Willebrand, and L. Hasse. Fine adjustment of large scale air-sea energy flux parameterizations by direct estimates of ocean heat transport. *J. Climate*, 2:1173–1184, 1989.

H. Jeffreys. On fluid motions produced by differences of temperature and humidity. *Q.J.R. Meteorol. Soc*, 1925.

S. Jiang, P.H. Stone, and P. Malanotte-Rizzoli. An assessment of the gfdl ocean model with coarse resolution: Annual-mean climatology. *J. Geophys. Res.*, 104(C11):25623–25645, 1999.

H. Jones and J.C. Marshall. Convection with rotation in a neutral ocean; a study of open-ocean deep convection. *J. Phys. Oceanogr.*, 23:1009–1039, 1993.

I. Kamenkovich, J. Marotzke, and P.H. Stone. Factors affecting heat transport in an ocean general circulation model. *J. Phys. Oceanogr.*, 30(1):175–194, 2000a.

I.V. Kamenkovich, A. Sokolov, and P.H. Stone. A coupled atmosphere-ocean model of intermediate complexity for climate change study. Technical Report 60, MIT Joint Program on the Science and Policy of Climate Change, Cambridge, USA, 2000b.

M. Kawase. Establishment of deep ocean circulation driven by deep-water production. *J. Phys. Oceanogr.*, 17:2294–2311, 1987.

L.D. Keigwin, G. A. G.A. Jones, S. J. S.J. Lehman, and E.A. Boyle. Deglacial meltwater discharge, north atlantic deep circulation, and abrupt climate change. *J. Geophys. Res.*, 96(C9):16811–16826, 1992.

B.A. Klinger and J. Marotzke. Behavior of double-hemisphere thermohaline flows in a single basin. *J. Phys. Oceanogr.*, 29:382–400, 1999.

A. Köhl and J. Willebrand. An adjoint method for the assimilation of statistical characteristics into eddy-resolving ocean models. *in preparation*, 2001.

Cornelius Lanczos. *Linear Differential Operators.* D. Van Nostrand Company, 1961.

W.G. Large, G. Danabasoglu, and S.C. Doney. Sensitivity to surface forcing and boundary layer mixing in a global ocean model: Annual-mean climatology. *J. Phys. Oceanogr.*, 27(11):2418–2447, 1997.

M. Latif, E. Roeckner, U. Mikolajewicz, and R. Voss. Tropical stabilization of the thermohaline circulation in a greenhouse warming simulation. *J. Climate*, 13:1809–1813, 2001.

D.J. Lea, M.R. Allen, and T.W.N. Haine. Sensitivity analysis of the climate of a chaotic system. *Tellus*, 52A:523–532, 2000.

J.R. Ledwell and A. Bratkovich. A tracer study of mixing in the Santa Cruz Basin. *J. Geophys. Res.*, 100:20681–20704, 1995.

J.R. Ledwell and B.M. Hickey. Evidence for enhanced boundary mixing in the Santa Monica Basin. *J. Geophys. Res.*, 100:20665–20679, 1995.

J.R. Ledwell, A.J. Watson, and C.S. Law. Evidence for slow mixing across the pycnocline from an open-ocean tracer release experiment. *Nature*, 364:701–703, 1993.

J.R. Ledwell, E.T. Montgomery, K.L. Polzin, L.C. St. Laurent, R.W. Schmitt, and J.M Toole. Evidence for enhanced mixing over rough topography in the abyssal ocean. *Nature*, 403:179–182, 2000.

S. J. Lehman and L. D. Keigwin. Deep circulation revisited. *Nature*, 358:197–198, 1992.

S. Levitus and T.P.Boyer. World Ocean Atlas 1994 Volume 3: Salinity. Technical report, NOAA Atlas NESDIS 3, 1994a.

S. Levitus and T.P.Boyer. World Ocean Atlas 1994 Volume 4: Temperature. Technical report, NOAA Atlas NESDIS 4, 1994b.

A. Macdonald and C. Wunsch. An estimation of global ocean circulation and heat fluxes. *Nature*, 382:436–440, 1996.

S. Manabe and R. J. Stouffer. Two stable equilibria of a coupled ocean-atmosphere model. *J. Climate*, 1:841–865, 1988.

S. Manabe and R. J. Stouffer. Multiple-century response of a coupled ocean-atmosphere model to an increase of atmospheric carbon dioxide. *J. Climate*, 7:5–23, 1994.

S. Manabe and R. J. Stouffer. Simulation of abrupt climate change induced by fresh water input. *Nature*, 378:165–167, 1995.

J. Marotzke and B.A. Klinger. The dynamics of equatorially asymmetric thermohaline circulations. *J. Phys. Oceanogr.*, 30:955–970, 2000.

J. Marotzke and J.R. Scott. On convective mixing and the thermohaline circulation. *J. Phys. Oceanogr.*, 29:2962–2970, 1999.

J. Marotzke and P.H. Stone. Atmospheric transports, the thermohaline circulation, and flux adjustments in a simple coupled model. *J. Phys. Oceanogr.*, 25:1350–1364, 1995.

J. Marotzke and J. Willebrand. Multiple equilibria of the global thermohaline circulation. *J. Phys. Oceanogr.*, 21(9):1372–1385, 1991.

J. Marotzke, R. Giering, K.Q. Zhang, D. Stammer, C. Hill, and T. Lee. Construction of the Adjoint MIT Ocean General Circulation Model and Application to Atlantic Heat Transport Sensitivity. *J. Geophys. Res.*, 104(C12):29529–29547, 1999.

J. Marotzke. *Decadal Climate Variability: Dynamics and Predictability*, chapter Analysis of Thermohaline Feedbacks. Springer-Verlag, 1995.

J. Marotzke. Boundary mixing and the dynamics of the three-dimensional thermohaline circulation. *J. Phys. Oceanogr.*, 27:1713–1727, 1997.

J. Marshall and F. Schott. Open ocean deep convection: observations, models and theory. *Rev. of Geophysics*, 37(1):1–64, 1999.

J. Marshall, A. Adcroft, C. Hill, and L. Perelman. Hydrostatic, quasi-hydrostatic and non-hydrostatic ocean modeling. *J. Geophys. Res.*, 102(C3):5733–5752, 1997a.

J. Marshall, A. Adcroft, C. Hill, L. Perelman, and C. Heisey. A finite-volume, incompressible Navier Stokes model for studies of the ocean on parallel computers. *J. Geophys. Res.*, 102(C3):5753–5766, 1997b.

D.A. McDermott. The regulation of northern overturning by southern hemisphere winds. *J. Phys. Oceanogr.*, 26:1234–1255, 1996.

U. Mikolajewics and R. Voss. The role of the individual air-sea flux components in co2-induced changes of the ocean's circulation and climate. *Clim. Dyn.*, 16(8):627–642, 2000.

Uwe Mikolajewicz, Thomas J. Crowley, Andreas Schiller, and Reinhard Voss. Modelling teleconnections between the North Atlantic and North Paciric during the Younger Dryas. *Nature*, 387:384–387, 1997.

F. Molteni and T.N. Palmer. Predictability and finite-time instability of the northern winter circulation. *Q.J.R. Meteorol. Soc*, 119:269–298, 1993.

F. Molteni, R. Buizza, T.N. Palmer, and T. Petroliagis. The ECMWF ensemble preciction system: Methodology and validation. *Q.J.R. Meteorol. Soc*, 122:73–119, 1996.

Philip M. Morse and Herman Feshbach. *Methods of Theoretical Physics.* McGraw-Hill, Inc., 1953.

W. Munk and C. Wunsch. Abyssal Receipes II: Energetics of tidal and wind mixing. *Deep Sea Research*, 45:1977–2010, 1998.

R. Mureau, F. Molteni, and T.N. Palmer. Ensemble prediction using dynamically conditioned perturbations. *Q.J.R. Meteorol. Soc*, 119:299–323, 1993.

M. Nakamura, P. H. Stone, and J. Marotzke. Destabilization of the thermohaline circulation by atmospheric eddy transports. *J. Climate*, 7(12):1870–1882, 1994.

G.R. North, R.F. Calahan, and J.A. Coakley. Energy balance climate models. *Rev. Geophys. Space Phys.*, 19:91–121, 1981.

T.N. Palmer, R. Buizza, F. Molteni, Y.-Q. Chen, and S. Corti. Singular vectors and the predictability of weather and climate. *Phil. Trans. R. Soc. Lond. A*, 348:459–475, 1994.

T.N. Palmer. Extended-range atmospheric prediction and the Lorenz model. *Bulletin of the American Meteorological Society*, 74(1):49–65, 1993a.

T.N. Palmer. A nonlinear dynamical perspective on climate change. *Weather*, 48:313–348, 1993b.

T.N. Palmer. *Decadal Climate Variability*, volume 44 of *NATO ASI Series*, chapter Predictability of the Atmosphere and Oceans: From Days to Decades. Springer-Verlag, Berline Heidelberg, 1996.

T.N. Palmer. A nonlinear dynamical perspective on climate prediction. *J. Climate*, 12:575–591, 1999.

Y.-G. Park and K. Bryan. Comparison of thermally driven circulations from a depth coordinate model and an isopycnal layer model: Part i. a scaling law - sensitivity to vertical diffusivity. *J. Phys. Oceanogr.*, 30(3):590–605, 2000.

José P. Peixoto and Abraham H. Oort. *Physics of Climate.* American Institute of Physics, 1992.

G. D. Perry, P. B. Duffy, and N. Miller. An extended data set of river discharges for validation of general circulation models. *J. Geophys. Res.*, 101(D16):21339–21349, 1996.

K.L. Polzin, J.M. Toole, J.R. Ledwell, and R.W. Schmitt. Spatial variability of turbulent mixing in the abyssal ocean. *Science*, 276:93–96, 1997.

Stephen Pond and George L. Pickard. *Introductory Dynamical Oceanography.* Butterworth-Heinemann, 2 edition, 1983.

S. Rahmstorf and M.H. England. Influence of southern hemisphere winds on north atlantic deep water flow. *J. Phys. Oceanogr.*, 27:2040–2054, 1997.

S. Rahmstorf. Rapid climate transitions in a coupled ocean-atmosphere model. *Nature*, 372:82–85, 1994.

S. Rahmstorf. Bifurcation of the Atlantic thermohaline circulation in response to changes in the hydrological cycle. *Nature*, 378:145–149, 1995.

S. Rahmstorf. On the freshwater forcing and transport of the atlantic thermohaline circulation. *Clim. Dyn.*, 12:799–811, 1996.

M.H. Redi. Oceanic isopycnal mixing by coordinate rotation. *J. Phys. Oceanogr.*, 12:1154–1158, 1982.

N. Reeh. *Proceedings of the Workshop on the Calving Rate of West Greenland Glaciers in Response to Climate Change*, chapter Calving from Greenland glaciers: Observations, balance estimates of calving rate, calving laws, page 171. Danish Polar Center, 1994.

S.R. Rintoul. South atlantic interbasin exchange. *J. Geophys. Res.*, 96:2675–2692, 1991.

D. Roemmich and C. Wunsch. Two transatlantic sections: meridional circulation and heat flux in the subtropical North Atlantic Ocean. *Deep Sea Research*, 32:619–664, 1985.

C. Rooth. Hydrology and ocean circulation. *Prog. Oceanogr.*, 11:131–149, 1982.

R.M. Samelson and G.K. Vallis. Large-scale ciculation with small diapycnal diffusion: The two-thermocline limit. *J. Mar. Res.*, 55:223–275, 1997.

J.W. Sandström. Dynamische Versuche mit Meerwasser. *Annalen der Hydrographie und Maritimen Meteorologie*, 36:6–23, 1908.

R.W. Schmitt, P.S. Bogden, and C. E. Dorman. Evaporation minus precipitation and density fluxes for the north atlantic. *J. Phys. Oceanogr.*, 19:1208–1221, 1989.

J.R. Scott and J. Marotzke. Diapycnal stirring and the meridional overturning circulation: Does it matter where the mixing occurs? *submitted to Journal of Physical Oceanography*, 2001.

J.R. Scott, J. Marotzke, and P.H. Stone. Interhemispheric Thermohaline Circulation in a Coupled Box Model. *J. Phys. Oceanogr.*, 29:351–365, 1999.

Jeffrey R. Scott. *The Roles of Diapycnal Mixing, Geothermal Heating and Surface Buoyancy Forcing in Ocean Meridional Overturning Dynamics.* PhD thesis, Massachusetts Institute of Technology, September 2000.

Z. Sirkes and E. Tziperman. Finite difference of adjoint of adjoint of finite difference? *Monthly Weather Review*, 125:3373–3378, 1997.

D. Stammer and C. Wunsch. The determination of large-scale circulation of the pacific ocean from satellite altimetry using model green's functions. *J. Geophys. Res.*, 101:18409–18432, 1996.

T. Stocker and A. Schmittner. Influence of co_2 emission rates on the stability of the thermohaline circulation. *Nature*, 388:862–865, 1997.

H. Stommel. Thermohaline convection with two stable regimes of flow. *Tellus*, 13(2):224–230, 1961.

P.H. Stone and D.A. Miller. Empirical relations between seasonal changes in meridional temperature gradients and meridional fluxes of heat. *J. of the Atmospheric Sciences*, 37:1708–1721, 1980.

P. H. Stone and M.-S. Yao. Development of a two-dimensional zonally averaged statistical-dynamical model. III. The parametrization of the eddy fluxes of heat and moisture. *J. Climate*, 3:726–740, 1990.

O. Talagrand. Assimilation of Observations, an Introduction. *Journal of the Meteorological Society of Japan*, 75(1B):191–209, 1997.

M. Tanguay, P. Bartello, and P. Gauthier. Four-dimensional data assimilation with a wide range of scales. *Tellus*, 47A:974–997, 1995.

J.R. Toggweiler and B. Samuels. Effect of Drake Passage on the global thermohaline circulation. *Deep Sea Research*, 42(4):477–500, 1995.

J.R. Toggweiler and B. Samuels. On the ocean's large-scale circulation near the limit of no vertical mixing. *J. Phys. Oceanogr.*, 28(9):1832–1852, 1998.

K. Trenberth and A. Solomon. The global heat balance: Heat transport in the atmosphere and ocean. *Clim. Dyn.*, 10:107–134, 1994.

K. E. Trenberth, J. G. Olson, and W. G. Large. A global ocean wind stress climatology based on ECMWF analysis. Technical report, NCAR Tech Nota, 1989.

H. Tsujino and N. Suginohara. Thermohaline circulation enhanced by wind forcing. *J. Phys. Oceanogr.*, 29:1506–1516, 1999.

G.K. Vallis. Large-scale circulation and production of stratification: Effects of wind, geometry, and diffusion. *J. Phys. Oceanogr.*, 30:933–954, 2000.

X. Wang, P.H. Stone, and J. Marotzke. Global thermohaline circulation. Part I: Sensitivity to atmospheric moisture transport. *J. Climate*, 12(1):71–82, 1999a.

X. Wang, P.H. Stone, and J. Marotzke. Global thermohaline circulation. Part II: Sensitivity with interactive atmospheric transports. *J. Climate*, 12(1):83–91, 1999b.

X. Wang. *Global Thermohaline Circulation and Ocean-Atmosphere Coupling.* PhD thesis, M.I.T., Cambridge, MA, 1997.

W.M. Washington and G.A. Meehl. Climate sensitivity due to increased co_2: experiments with a coupled atmosphere and ocean general circulation model. *Clim. Dyn.*, 4:1–38, 1989.

A. Weaver. Driving the ocean conveyor. *Nature*, 378:135–136, 1995.

E.C. Wiebe and A.J. Weaver. On the sensitivity of global warming experiments to the parametrisation of sub-grid scale ocean mixing. *Clim. Dyn.*, 15:875–893, 1999.

S.E. Wijffels, R.W. Schmitt, H.L. Bryden, and A. Stigebrandt. Transport of freshwater by the oceans. *J. Phys. Oceanogr.*, 22:155–162, 1992.

R.A. Wood, A.B. Keen, J. F.B. Mitchell, and J.M. Gregory. Changing spatial structure of the thermohaline circulation in response to atmospheric co_2 forcing in a climate model. *Nature*, 399:572–575, 1999.

Carl Wunsch. *The ocean circulation inverse problem.* Cambridge University Press, 1996.

F. Zaucker, T.F. Stocker, and W.S. Broecker. Atmospheric freshwater fluxes and their effect on the global thermohaline circulation. *J. Geophys. Res.*, 99(C6):12443–12457, 1994.

J. Zhang, R.W. Schmitt, and R.X. Huang. The relative influence of diapycnal mixing and hydrologic forcing on the stability of the thermohaline circulation. *J. Phys. Oceanogr.*, 29:1096–1108, 1999.